The Influence of Coronal Radiation on Solar Prominence Plasma

Gerrard Martyn Brown, MPhys

Astronomy and Astrophysics Group
SUPA School of Physics and Astronomy
Kelvin Building
University of Glasgow
Glasgow, G12 8QQ
Scotland, U.K.

Presented for the degree of
Doctor of Philosophy
The University of Glasgow
September 2015

This thesis is my own composition except where indicated in the text. No part of this thesis has been submitted elsewhere for any other degree or qualification.

30th September 2015

Abstract

Solar prominences are structures located within the solar corona. The flow of energy within them is through radiative processes and this needs to be studied using radiative transfer, which is dependent upon the radiation entering the prominence. For a full understanding of the radiative processes within the prominence we need to fully account for all the radiation that originates outwith the prominence but still influences it. Previous studies have only looked at the radiation from the disc, this thesis will add to this the radiation from the corona and investigate the effects of this. Chapter 1 introduces the Sun and prominences, to explain the conditions prominences occur in. In chapter 2 radiative transfer is discussed, it is shown where the 1-D form of the radiative transfer equation and the statistical equilibrium equation comes from. Previous studies of prominences using radiative transfer are discussed, and we explain the radiative transfer code which will be modified to include the coronal radiation. To add the radiation from the corona it is necessary to know what the coronal radiation would be visible to the prominence as spectra observed from outside the corona would not be suitable for the light an object within the corona receives and so in chapter 3 the radiation that a prominence within the corona would receive is calculated. The methods for determining the radiation from the corona which would be visible to the prominence are explained. The results for this at various heights are shown, and this shows that there would be sufficient difference between the radiation recevied by prominencies at different heights to justify recalculating the coronal radiation for different heights. The coronal radiation is added to the incident radiation below 912Å in chapter 4. The radiative transfer code is modified so that it can receive the light from either individual lines or from many lines averaged over a wavelength range. It is demonstrated that different lines will have different degrees of influence over the ionisation of the prominence by moving an individual test line and so when we add

radiation from lines average over wavelength ranges we take this into account. It is shown that the effects of coronal radiation on the hydrogen in the prominence for iso-thermal iso-baric slabs, and for slabs with a PCTR (Prominence to Corona Transition Region). The coronal radiation is then added to the helium continua in chapter 5. The effects of the coronal radiation on the helium in the prominence for iso-thermal iso-baric slabs and for slabs with a PCTR are shown. The coronal radiation has a significant effect on the condition and emissions of a prominence, and must be taken into account to fully understand the radiative processes of a prominence.

Contents

List of Tables

List of Figures

Chapter 1

Introduction

1.1 Solar Properties

The star known as "the Sun" is a G2 type main sequence star located at the centre of the Solar System. Being a main sequence star means that the nuclear fusion processes going on in its core primarily involve the fusion of hydrogen to produce helium. The surface temperature of the Sun is about 6000 K. For comparison at the hottest end of the main sequence, the massive O-type stars have surface temperatures of over 30,000 K whilst the coolest M-type red dwarf stars are less than 4000 K and at a third of the mass of the Sun are only barely large enough to count as a star.

The Sun is a population I star which means that it has a high metalicity. The metalicity is a measure of how much of the star is composed of "metals" which in astronomy refers to elements other than hydrogen and helium. The death of the earlier population II and III stars is what produced and scattered the metals which find themselves in population I stars. The Sun being rich in these elements means that the spectrum of the Sun will not be simply a hydrogen continuum with a few hydrogen

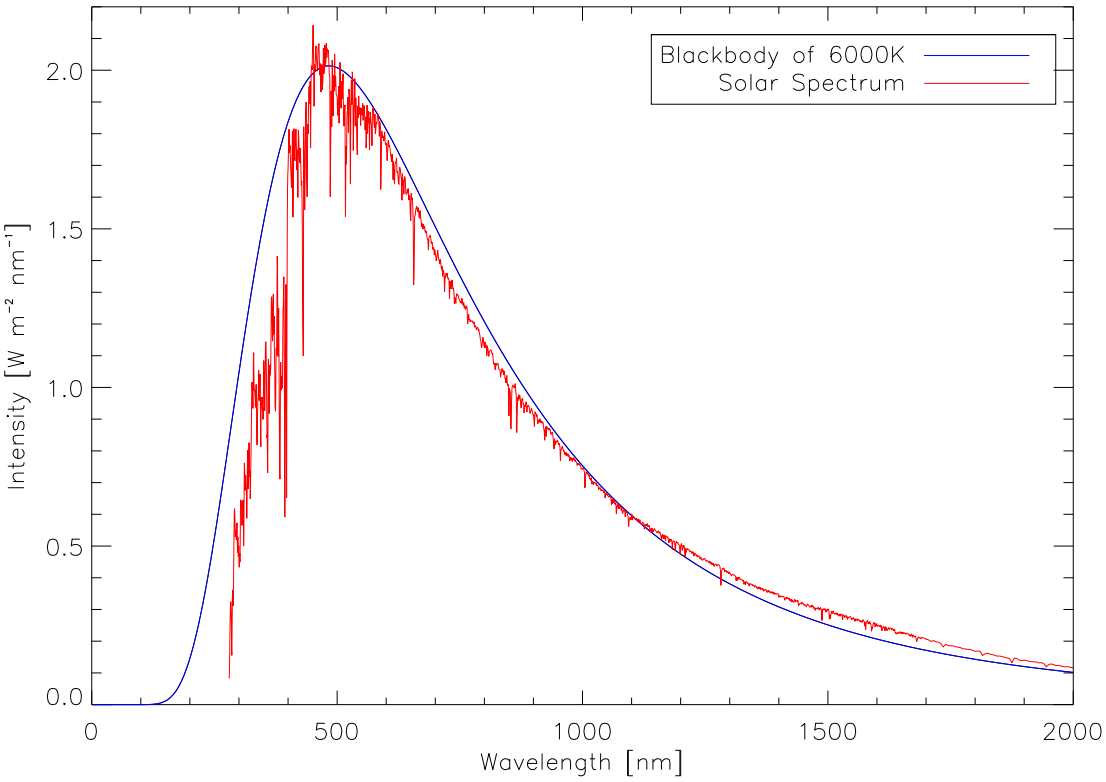

Figure 1.1: A comparison of a plain black body spectrum and the solar spectrum as observed outside the Earth's atmosphere, taken from the ASTM G173-03 Reference Spectra.

lines. The Solar spectrum will feature many emission and absorption lines as a result of these elements being present. Heavier elements having more ions, energy levels, and electron transitions means they have more lines than hydrogen. Figure 1.1 shows the effects on the solar spectrum.

The energy released from the nuclear fusion in the core travels outwards first through the radiative zone, where the energy is transferred through radiative processes, then through the convective zone, where densities are low enough to permit convective currents. This internal structure can be seen in figure 1.2. Also shown in this figure is the visible surface of the Sun, the photosphere meaning sphere of light, which lies above the convective zone and is where most of the light seen from the Sun originates.

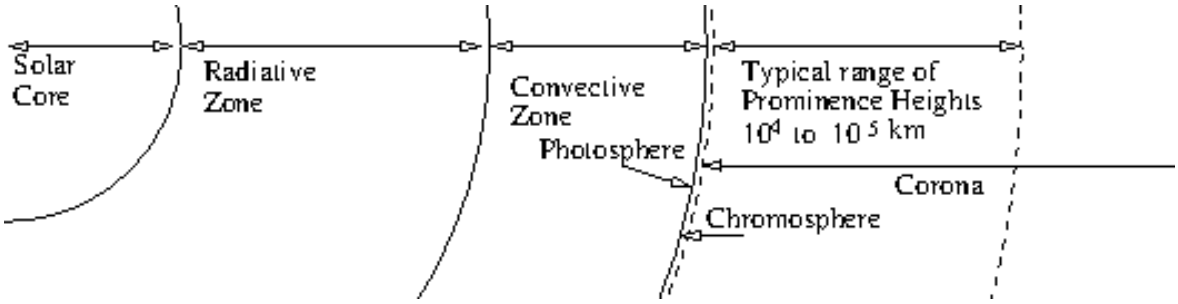

Figure 1.2: A diagram of the structure of the Sun, showing the typical heights above the Solar surface, the photosphere, at which prominences are found.

The atmosphere above the photosphere is optically thin at most wavelengths so most radiation from the photosphere will not be absorbed. The bottom of the photosphere is where the optical depth, τ, approaches 1 and so the Sun below the photosphere is opaque to an observer.

The chromosphere above the photosphere is hotter than the photosphere, at about 10^5K, but even though the chromosphere is above the photosphere the Sun does not appear to be this temperature, the solar spectrum is close to a blackbody of about 6000K, the photosphere temperature. This is because at most wavelengths the chromosphere is optically thin, and so the light from the photosphere passes straight through. It is not optically thin at all wavelengths, and the exceptions such as Hα are what allow it to be studied. Above the chromosphere is the corona. It is much hotter than the chromosphere, but also less dense. The corona is also optically thin at most wavelengths. Being much less bright than the solar disc the corona is not ordinarily observable in visible wavelengths, however it can be observed when the light from the disc is blocked out. This happens naturally on Earth during an eclipse, but telescopes can be fitted with a coronograph which achieves the same effect.

The Sun is not a static arrangement of layers which emit light; the Sun's magnetic field varies over time and in doing so creates many interesting features. One of the most well known are sunspots, dark patches on the disc which appear in areas of high

magnetic field strength. Near the sunspots form plages which differ from sunspots in that they are bright patches and longer lasting. A feature of the magnetic field which is much shorter lasting is flares, ejections of energy which occur when tangled magnetic field lines untangle themselves through reconnection.

Another feature is solar prominences.

1.2 Prominence Properties

A solar prominence is a structure located in the solar corona. They were first observed during eclipses as far back as during the 13th century and were thought to be either clouds, flames or mountains. Given that they were observed during eclipses it was not initially clear to observers whether they were features of the Sun or the Moon but in the mid 19th century observers, including most notably Angelo Secchi, were able to notice that they changed in altitude as the Moon moved across the Sun and so were not connected to the Moon (Vial 2015).

The prominence plasma is cooler and denser than the surrounding corona and is confined by magnetic fields in the boundary between different polarities of the magnetic field (Babcock & Babcock 1955). Temperatures inside the prominence are on the order of 10^4 K compared to coronal temperatures which are on the order of 10^6 K. Prominence internal number densities are about 10^9-10^{11} cm^{-3}, compared to coronal number densities of about 10^9 cm^{-3} (Hirayama 1985; Labrosse et al. 2010). With a hundredfold difference between it and the surroundings in temperature and density and a density and pressure more comparable to the chromosphere, origins of the plasma material are unknown with it either being lifted from the chromosphere or gathered in situ both being possible explanations (Mackay et al. 2010; Labrosse et al. 2010). Observations of a prominence disappearing and then reforming from in situ material have been made

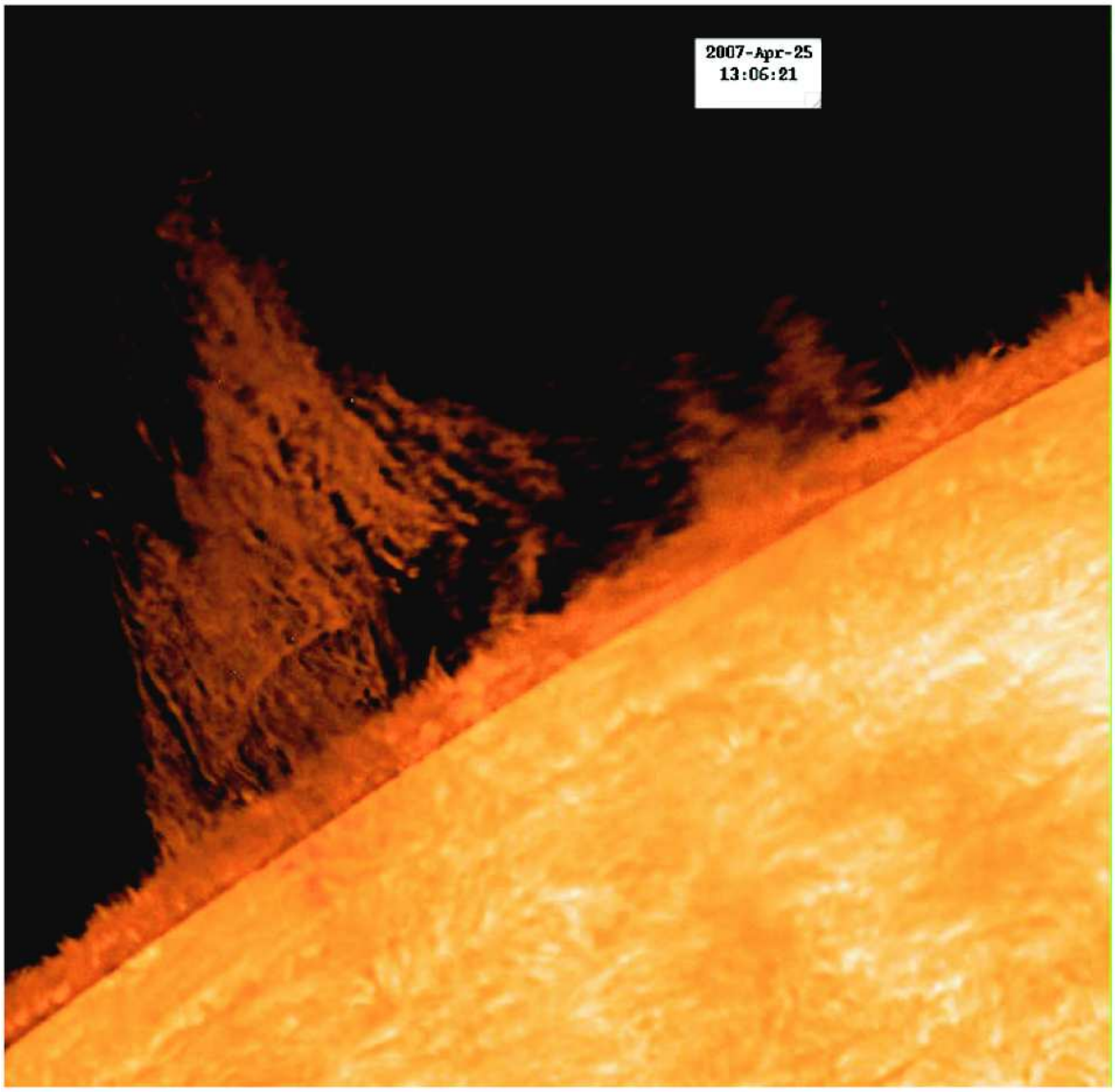

Figure 1.3: A quiescent solar prominence observed above the limb in Hα visible as a bright structure above the solar surface (Heinzel et al. 2008).

(Berger et al. 2012), however this is not the initial formation of the prominence. On the other hand magnetic field modelling has produced results showing how a magnetic flux rope rising from the chromosphere may explain the material within a prominence (Rust & Kumar 1994)

A prominence is referred to as a prominence when it is observed above the solar

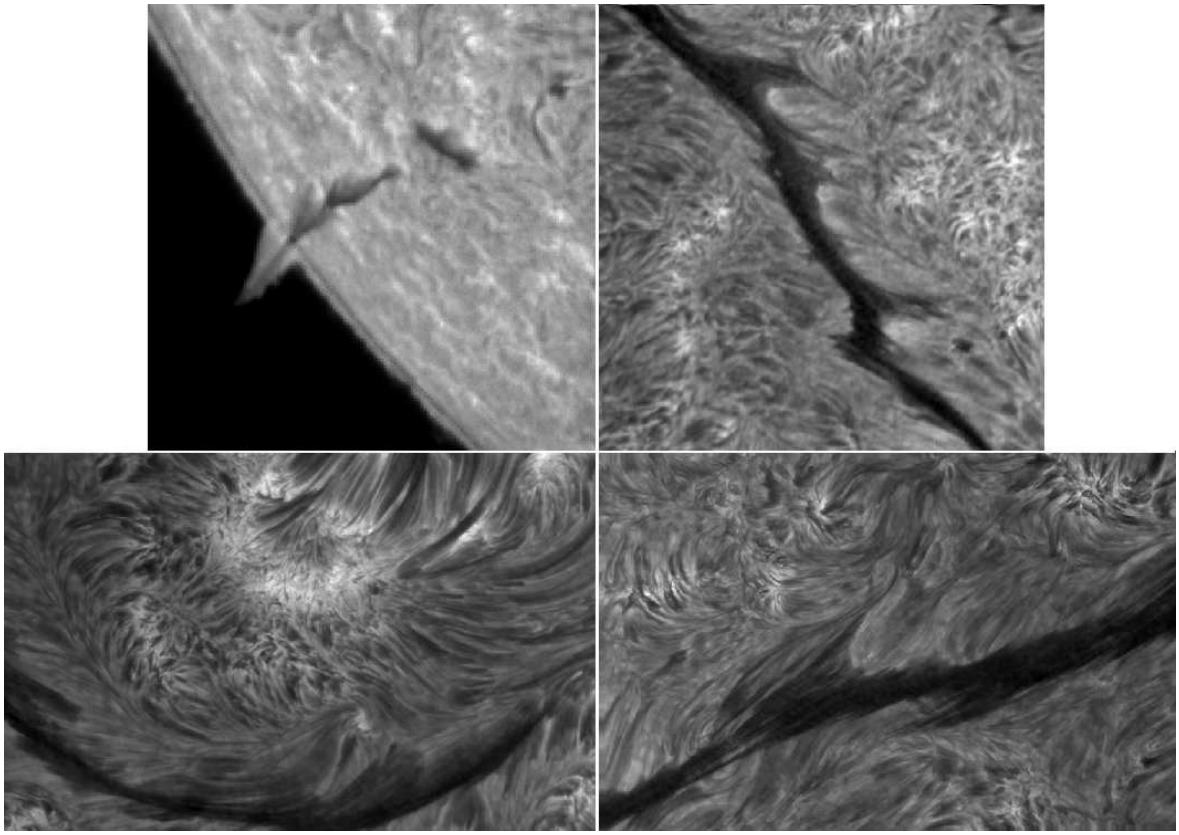

Figure 1.4: Four different solar filaments shown against the solar disc visible as dark structures. The structure of a central spine with barbs coming out of the sides is clear in the second and fourth images (Lin et al. 2008).

limb as seen in figure 1.3, however when observed against the solar disk it is refered to as a filament as seen in figure 1.4. Depending on where it is seen the observed spectrum differs; as a prominence its lines are emission lines but when it is a filament its lines are in absorption. In this work the object shall be mainly referred to as a prominence, only being referred to as a filament when the distinction is worthy of note although it is mostly prominences above the limb which are considered (Labrosse et al. 2010).

Another relevant distinction is that between active and quiescent prominences. The former forms in active regions on the Sun, while the latter forms in the quiet regions of the Sun and are longer lived. That there is a distinction between quiet long lasting prominences and prominences which don't last as long is something which has been

noted about prominences from when they were first determined to be Solar features. Given that the two prominences are in different regions of the sun, they will experience different external conditions which means that their final equilibrium state will be different in each case. So if one is concerned with the effect of the external conditions on the prominence, as is the case in this work, then one needs to consider whether the prominence is active or quiescent (Hirayama 1985; Labrosse et al. 2010; Engvold 2015).

The prominence suspended by magnetic fields is not just an amorphous cloud of plasma, it has a structure made up of a spine with barbs coming out of the sides which extend down to the chromosphere with legs at the ends of the prominence. A central spine with barbs coming from the sides is clear in the second and fourth images of figure 1.4. The alignment of the barbs, whether they bear to the right or left when viewed from above, depends on the chirality of the magnetic field, the direction of the field along the prominence when viewed from the side with positive polarity (Martin et al. 1992; Mackay et al. 2010). Rotating structures within prominences refereed to as solar tornadoes have been observed, these form in the legs of the prominence (Levens et al. 2015; Wedemeyer et al. 2013).

Observations of prominences, especially of their spectra, are performed by space based instruments. The SOHO space based observatory operated by ESA/NASA contains a number of such instruments which have applicability to prominence science and were outlined by Patsourakos & Vial (2002). For example the range of temperatures obtained using its SUMER instrument were 5000 to 15000 K which was obtained from examination of the Lyman continuum, whose edge of 912 Å falls within SUMER's 500-1600 Å range.

Illumination from the Sun is a large net flow of energy into the prominence. To a large degree the prominence can be considered as being optically thick at many wavelengths. Therefore the large amount of external energy from the solar illumination

is important to the internal energy structure of the prominence; the transport of energy within the prominence happens through the emission and absorption of radiation inside the prominence, so any external light which enters the prominence will have an effect on the absorption and emission of radiation in the plasma. These considerations result in departure from local thermodynamic equilibrium for solar prominences as they are constantly receiving energy from an external source, so any modelling methods which assume thermodynamic equilibrium will produce false results (Labrosse et al. 2010).

1.3 Aims

Prominences are illuminated by the rest of the Sun and are highly influenced by it. The energy flow within a prominence is modelled through NLTE (Non-Local Thermodynamic Equilibrium) radiative transfer modelling, which has to take into account the radiation incident to the prominence as boundary conditions. Previous attempts at modelling only took into account the radiation which originates from the solar disc, but the prominence will also be illuminates by other solar sources of radiation, the corona.

This work will investigate the effects of the corona radiation on the prominence plasma. To do this a 1-D NLTE radiative transfer code will be modified to add to the incident radiation it considers the coronal radiation. This will allow us to study the state of the hydrogen and helium of the prominence. The coronal radiation however will have to be carefully considered to ensure that what is being added is appropriate.

Chapter 2

Radiative Transfer

Energy can be transferred through a medium by various means, however in a prominence the most significant is where particles interact with each other through radiation. This radiation is conveyed through the medium by absorption, emission, scattering and collisional processes. Such radiative processes are studied through radiative transfer (Labrosse et al. 2010; Heinzel 2015).

2.1 Radiative Transfer Basics

Radiative transfer describes the transfer of energy through radiative processes, that is through the absorption and emission of electromagnetic radiation. The equation of radiative transfer describes the change in the specific intensity I_ν due to these processes along a path ds.

$$\frac{dI_\nu}{ds} = -\chi_\nu I_\nu + \eta_\nu \tag{2.1}$$

where χ_ν is the absorption coefficient and η_ν is the emission coefficient (Hubeny & Mihalas 2014; Labrosse et al. 2010; Heinzel 2015; Rutten 2003; Böhm-Vitense 1989)

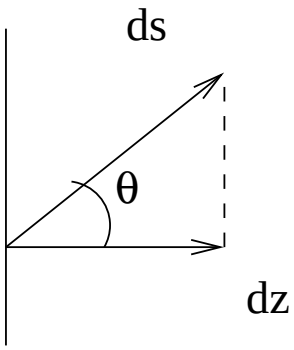

Figure 2.1: The depth dz which is normal to the surface, the path ds which is not and the angle θ which lies in between.

It is often more useful to talk about position in terms of the optical depth, which is defined as the integrated opacity to a depth z into the material

$$\tau_\nu(z) = -\int_{z_{max}}^{z} \chi_\nu(z')dz' \tag{2.2}$$

where $\tau_\nu(z)$ is the optical depth for the frequency ν at the geometrical position z and $\chi_\nu(z')$ is the absorption coefficient at geometrical position z'. τ_ν is zero at the surface z_{max}, and increases inwards, as it is the number of photon mean free paths to the depth z (Hubeny & Mihalas 2014).

So then the change $d\tau_\nu$ in optical depth along a distance dz is

$$d\tau_\nu = -\chi_\nu dz \tag{2.3}$$

A path ds is not necessarily parallel to the normal to the surface, so the length along the path is not always the depth as can be seen in figure 2.1. When the angle between the path and the normal to the surface is θ then the viewing angle μ is given by (Heinzel 2015)

$$\frac{dz}{ds} = cos(\theta) = \mu \tag{2.4}$$

The source function is another important part of radiative transfer. The source function of a medium is defined as being the ratio of the emissivity η_ν to the opacity χ_ν of the medium (Hubeny & Mihalas 2014).

$$S_\nu = \frac{\eta_\nu}{\chi_\nu} \tag{2.5}$$

Taking equations 2.3, 2.4 and 2.5 and putting them in equation 2.1 gives the standard 1-D form of the radiative transfer equation.

Combining equations 2.3 and 2.4 gives

$$\frac{1}{-\chi_\nu}\frac{d\tau_\nu}{ds} = \mu \tag{2.6}$$

and so for $\frac{1}{ds}$ this is

$$\frac{1}{ds} = \frac{-\chi_\nu \mu}{d\tau_\nu} \tag{2.7}$$

and rearranging equation 2.5 gives η_ν as $\eta_\nu = S_\nu \chi_\nu$. Now these can be placed into equation 2.1

$$-\chi_\nu \mu \frac{dI_\nu}{d\tau_\nu} = -\chi_\nu I_\nu + \chi_\nu S_\nu \tag{2.8}$$

and simplifying this gives the standard 1-D form of the radiative transfer equation.

$$\mu \frac{dI_\nu}{d\tau_\nu} = I_\nu - S_\nu \tag{2.9}$$

The 1-D form of the radiative transfer equation is useful when the medium being considered can be treated as having no variations in directions parallel to its surface and so only varies in depth. An example of such a situation is plane parallel geometry, where the medium is considered as a series of parallel homogeneous planes.

In the case of local thermodynamic equilibrium (LTE), where the level populations are given by the Boltzmann distribution, the source function is equivalent to the Planck function B_ν (Böhm-Vitense 1989)

$$\mu \frac{dI_\nu}{d\tau_\nu} = I_\nu - B_\nu \tag{2.10}$$

However when the atmosphere in question is not in a state of LTE and is in a state of non-LTE (NLTE) the source function has to be solved.

2.2 Radiative transfer in 1-D NLTE

A prominence is not in a state of LTE due to the strong influence of the incident radiation (Labrosse et al. 2010). The density of a prominence is low enough that scattering of the incident radiation is a significant factor in determining the source function. (Labrosse et al. 2007; Gontikakis et al. 1997)

The emission coefficient is

$$\eta_\nu = n_j A_{ji} \frac{h\nu}{4\pi} \psi_\nu \tag{2.11}$$

and the absorption coefficient, corrected for stimulated emission, is

$$\chi_\nu = n_i B_{ij} \frac{h\nu_{ij}}{4\pi} \phi_\nu - n_j B_{ji} \frac{h\nu_{ij}}{4\pi} \psi_\nu \tag{2.12}$$

where A_{ji}, B_{ji} and B_{ij} are the Einstein coefficients for spontaneous emission, stimulated emission and absorption. ψ_ν is the emission profile and ϕ_ν is the absorption profile. n_i is the number density of the ith state and n_j is the number density of the jth state. The absorption profile is normalised so that the integral of it across all frequencies is 1 (Heinzel 2015; Labrosse et al. 2010).

Putting these into equation 2.5 gives

$$S_\nu = \frac{n_j A_{ji} \psi_\nu}{n_i B_{ij} \phi_\nu - n_j B_{ji} \psi_\nu} \tag{2.13}$$

For the case of complete redistribution in frequency, where the re-emitted photons have no dependence on their previous frequency, the emission and absorption profiles ψ_ν and ϕ_ν are equal and so equation 2.13 becomes

$$S_\nu = \frac{n_j A_{ji}}{n_i B_{ij} - n_j B_{ji}} \tag{2.14}$$

For partial redistribution the stimulated emission term in equation 2.12 can be considered with an absorption profile ϕ_ν when the stimulated emission is much smaller

than the stimulated absorption (Hubeny & Mihalas 2014; Labrosse et al. 2010). So equation 2.12 becomes

$$\chi_\nu = n_i B_{ij} \frac{h\nu_{ij}}{4\pi} \phi_\nu - n_j B_{ji} \frac{h\nu_{ij}}{4\pi} \phi_\nu \tag{2.15}$$

which results in equation 2.13 becoming

$$S_\nu = \frac{n_j A_{ji} \psi_\nu}{n_i B_{ij} \phi_\nu - n_j B_{ji} \phi_\nu} = \frac{n_j A_{ji}}{n_i B_{ij} - n_j B_{ji}} \rho_{ij}(\nu) \tag{2.16}$$

where $\rho_{ij}(\nu)$ is the ratio of the emission and absorption profiles $\rho_{ij}(\nu) = \psi_\nu / \phi_\nu$. For complete redistribution where the emission and absorption profiles are equal $\rho_{ij}(\nu) = 1$ and so equations 2.14 and 2.16 would be equal. For partial redistribution, the emission profile can be expressed in terms of the scattering integral $\bar{J}$

$$\bar{J} = \int_0^\infty J_{\nu'} \phi_{\nu'} d\nu' \tag{2.17}$$

$$\psi_\nu = \frac{1}{\bar{J}} \int_0^\infty R_{\nu',\nu} d\nu' \tag{2.18}$$

where $J_{\nu'}$ is the mean intensity at the frequency ν' and $R_{\nu'\nu}$ is the redistribution function.

The redistribution function is the probability that a photon absorbed at the frequency ν' will be emitted at the frequency ν. For complete redistribution, the redistribution function is $R_{\nu'\nu} = \phi_{\nu'} \phi_\nu$. The opposite case to complete redistribution is purely coherent scattering where the absorbed and emitted photons have the same frequency. Here $R_{\nu'\nu}$ is one for where $\nu' = \nu$ and zero for all other cases.

The situation between the two extremes is partial redistribution, where some of the scattered photons retain the frequency of the absorbed photon and the rest gain a new frequency. The redistribution function for the case of resonance lines, which are transitions involving the ground state, for partial redistribution is

$$R_{\nu'\nu} = \gamma R_{II} + (1 - \gamma) R_{III} \tag{2.19}$$

where R_{II} is the redistribution function for the coherent scattering and R_{III} is the redistribution function for the complete redistribution. γ is the branching ratio, the proportion of photons which undergo coherent scattering instead of redistribution.

$$\gamma = \frac{A_{jg}}{A_{jg} + Q_E} \tag{2.20}$$

where Q_E is the rate of elastic collisions, which are transitions to another sub-level of the same level. Partial redistribution is not applicable to the non-resonance lines, such as Hα (Heinzel 2015).

So now a finite 1-D slab can be considered. This 1-D slab can be oriented either vertically above the solar surface or oriented horizontally above the solar surface. In the vertical case, this represents a prominence viewed above the limb and in the horizontal case a filament viewed against the solar disc.

Integrating equation 2.9 with respect to τ_ν gives the emergent intensity at the slab surface, where $\tau_\nu = 0$, for a direction μ as

$$I(0, \mu) = I_0(\tau, \mu)\mathrm{e}^{-\tau/\mu} + \int_0^\tau S(\tau')\mathrm{e}^{-\tau'/\mu} d\tau'/\mu \tag{2.21}$$

where $I_0(\tau, \mu)$ is the incident radiation on the other side of the slab.

The solution to the source function relies on the atomic level populations being known, for it is on these that the absorption and emission coefficients depend. These populations are found from the equations of statistical equilibrium, which fulfil the role for the NLTE case that the Boltzman equation does for the LTE case.

The statistical equilibrium equations have the general form

$$\frac{dn_i}{dt} = \sum_j n_j(R_{ji} + C_{ji}) - n_i \sum_j (R_{ij} + C_{ij}) \tag{2.22}$$

where R_{ji} and R_{ij} are the radiative rates between levels i and j, C_{ji} and C_{ij} are the collisional rates between the two levels, and n_i and n_j are the population levels of the

energy levels i and j (Heinzel 2015). In the case where there is no net transfer between energy levels, such as in a quiescent prominence, $dn_i/dt = 0$ and so

$$\sum_j n_j(R_{ji} + C_{ji}) = n_i \sum_j (R_{ij} + C_{ij}) \tag{2.23}$$

The radiative rate for absorption is $R_{ij} = B_{ij}\bar{J}_{ij}$ while the radiative rate for emission is $R_{ji} = A_{ji} + B_{ji}\bar{J}_{ij}$ where A_{ji} pertains to the spontaneous emission and $B_{ji}\bar{J}_{ij}$ pertains to the stimulated emission. In the case of the "two-level atom" where the atom is considered as having only a upper level 2 and a lower level 1 then using these radiative rates equation 2.23 can be written as

$$n_1 B_{12}\bar{J}_{12} + n_1 C_{12} = n_2 A_{21} + n_2 B_{21}\bar{J}_{12} + n_2 C_{21} \tag{2.24}$$

For the two level case it is possible to solve the radiative transfer and statistical equilibrium equations numerically.

2.3 Multilevel NLTE Modelling

The two level atom is not sufficient for modelling of realistic situations, a real atom does not simply have the ground state and one excited state, there are multiple excited states approaching infinity and for accuracy many of these levels will have to be modelled. Fortunately a infinite number of modelled energy levels are not required given that diminishing returns in increased accuracy are reached with a reasonable number of modelled levels (Gouttebroze et al. 1993). In addition to the actual levels of the atoms, also required is a "ionised level" for although the ionised form of an atom is not strictly speaking a energy level of the atom it is convenient in these radiative transfer calculations to treat it as such.

As the two level approach will not work, some multilevel approach must be used.

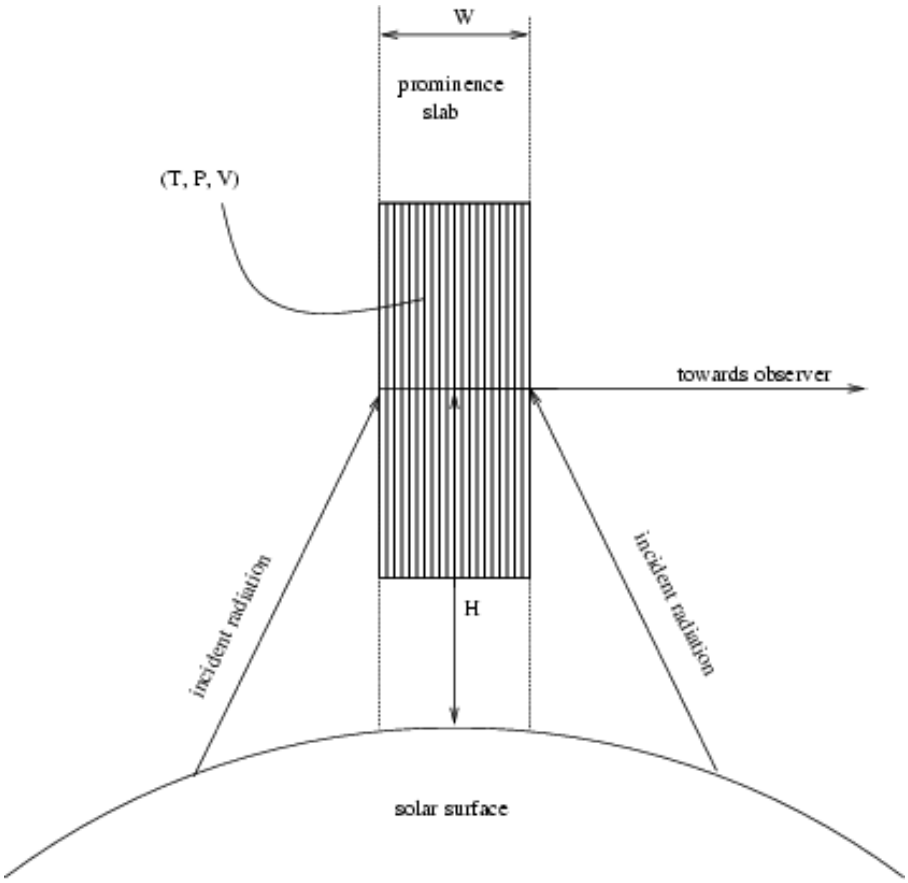

Figure 2.2: A 1D slab as a method of modelling a prominence (Labrosse & Gouttebroze 1999).

For Prominence NLTE modelling there are two primary methods which have been used, the complete linearisation method (Auer & Mihalas 1969) and the equivalent two level atom method (ETLA) (Avrett & Loeser 1987). The ETLA method requires that each separate transition between two levels be treated as though they were the only levels in the atom. An initial estimate of the populations for all levels are made and this is used to make initial estimates of the radiative rates. In each iteration new estimates of the occupation levels and radiative rates are obtained and used in the next iteration. Once convergence is reached the source function for all transitions is known (Hubeny & Mihalas 2014).

2.4 Previous NLTE Radiative Modeling

Computational studies of the non-local thermodynamic equilibrium radiative transfer problem have been applied to the solar atmosphere since the 1960s in studies such as that of Auer & Mihalas (1969) who used NLTE methods to probe the structure of the solar atmosphere. Computational techniques applied to the solar atmosphere can then be applied to specific objects located within the solar atmosphere.

Such computational work was applied to studies of prominences such as Heasley et al. (1974). In this work the authors investigated prominences of various temperatures and hydrogen densities, which were kept constant for all depths in the prominence.

Studies then largely considered fairly uniform prominence slabs; properties such as temperature, pressure and density were considered to be constant through the prominence. The slab of material was given boundary conditions by considering the radiation incident to the slab, the incident radiation being the main way in which the surroundings interact with the prominence. This radiation plays a larger role in determining quiescent prominence emissions than the internal processes of the prominence, such as collisions (Hirayama 1963).

It is convenient when dealing with prominences to treat them as a one dimensional plane parallel slab, as seen in figure 2.2. Each point along the prominence slab has values such as temperature and pressure defined. One could either consider these values to be the same for every plane or to vary through the prominence, being different for each successive plane. In this figure the prominence is a prominence above the limb and its planes are perpendicular to the solar surface, which is important when considering the directions from which the prominence is illuminated by the incident radiation from the solar surface. The prominence here is illuminated on both sides by the solar surface; for a filament the plane parallel slab would be lying parallel to the solar surface and hence only the bottom surface of the filament would receive illumination from the

solar surface. A side of the object can only be illuminated by the solar surface if there is a clear path from that side of the object to the solar surface. The height of the prominence above the solar surface is also important when considering the incident radiation. The higher the prominence is above the solar surface the smaller the angular size the prominence sees the solar surface to be, so the less it is illuminated by the solar surface (Gouttebroze et al. 1993; Heasley et al. 1974). Plane parallel modelling does not require that the fine structure of the prominence be ignored, Fontenla et al. (1996) treated threads within a prominence as separate plane parallel slabs.

Parallel planes in a slab is not the only geometry which the 1-D case can deal with, for example it is also possible to deal with cylindrical problems when the incident radiation in uniform over all angles. If the incident radiation is not the same in all directions then two dimensional cylinders are used, that is the dimensions used are the radius and azimuth, the angle dependent incident radiation will result in angle dependent emergent radiation (Gouttebroze & Labrosse 2009). The 2 dimensional extension of 1-D parallel planes are parallel threads which can be used to investigate variations in line profile with viewing angle relative to magnetic field lines (Heinzel et al. 2001), and there will also be changes visible emergent continua (Gunár et al. 2007).

In two dimensional problems there is a technique called the Short Characteristic method which reduces the computational resources needed for complete redistribution in frequency by an order of magnitude (Auer & Paletou 1994). This differs from the alternative, the long characteristic method in that the long characteristic method requires solving the transfer problem for each grid point across the entire slab, but the short characteristic method only requires solving it across the neighbouring cells (Kunasz & Auer 1988). The use of 1-D vs 2-D models may have an effect on the line profiles, for example Vial (1982) compared line profiles from both, and in some lines found changes to the profile such as the Lyman α line developing a reversal in a 2-D case where the authors did not find on in a 1-D case.

The temperature and pressure structure of the prominence was considered in studies such as Heasley & Mihalas (1976) in which these parameters of the prominence plasma were considered by considering various models of different variations as a function of depth of temperature and density through the slab so that the results of the calculations could be compared to observations to judge which model best matched the observations. By comparing their different models they found a model featuring diffuse penetration of the incident ultraviolet radiation to give better results than non-radiative source of energy input.

Eruptive prominences require slightly different considerations than non-moving prominences. Eruptive prominences move away from the sun in a radial direction and so the radiation the prominence receives from the Sun will be Doppler shifted. This Doppler shift results in the absorption profile of the radiative transition between the two levels responsible for a line dominated by scattering being out of resonance with the incident radiation for the line from the disc which results in Doppler brightening for a line in absorption and Doppler dimming for a line in emission (Hyder & Lites 1970). It is not just the intensity of the lines which change but also their profile, as the incident line shifts more towards the red the emergent line profile gets more distorted (Labrosse et al. 2007), which can result in the double peak in lines such as Lymanα disappearing at high velocities (Gontikakis et al. 1997). Lines can be distorted in models with a PCTR as well as in iso-thermal models (Labrosse et al. 2008).

The Prominence, being cooler and denser than the surrounding corona, is not going to have an abrupt cut off between it and the corona in spite of its confining magnetic fields which has necessitated studies such as Labrosse et al. (2002) and Heinzel et al. (2001) which define the structure of the prominence to corona transition region for the code to study. The structure of the prominence to corona transition region to be used in such works needs to be first determined from something similar to the results of Anzer & Heinzel (1999) which provides two expressions dependent on the column mass

of the prominence which can be used for the temperature and the pressure structure.

$$p(m) = 4p_c \frac{m}{M}(1 - \frac{m}{M}) \tag{2.25}$$

$$T = T_{cen} + (T_{tr} - T_{cen})(1 - 4\frac{m}{M}(1 - \frac{m}{M}))^{\gamma} \tag{2.26}$$

$p(m)$ is the pressure at a column mass of m, M is the total column mass, p_o is the pressure at the outer boundary, p_c is the difference between the central pressure and p_o, T is the temperature at a column mass of m, T_{cen} is the central temperature and T_{tr} is the temperature at the outer boundary. γ describes the temperature profile, and is at least 2.

Improvements in other, related fields may require updates to be done to the work done on NLTE prominence modelling. New understandings of atomic physics and of the structure of the radiation incident to the prominence are two such things which may invalidate previously obtained results. (Gouttebroze et al. 1993)

Improvements in technology can also necessitate a revisiting of previously done work. Gouttebroze & Labrosse (2000) updated work which was previously performed on supercomputers to be run on more modest machines which as technology improves become more suitable for such computational work.

The results of radiative transfer calculations can be published as a catalogue of results for various prominence models, such as in Gouttebroze et al. (1993). Such a list of results is a useful diagnostic tool when examining prominence observations and the authors' subsequent paper, Heinzel et al. (1994) details the correlations between prominence plasma parameters and the emissions of the prominence in the hydrogen lines and the Lyman continuum which can be used for this. These methods were used in Heinzel et al. (1996) to determine the geometrical thickness of 18 prominence measurements and found the thicknesses to range from a few hundred km to a few tens of thousands of km.

2.5 The Radiative Transfer Code used

The radiative transfer code used in this work is a 1-D NLTE plane parallel code first outlined in Gouttebroze et al. (1993) and Gouttebroze & Labrosse (2000). It solves the radiative transfer and statistical equilibrium equations through a equivalent two level atom approach. The prominence is treated as a 1-D slab made of plane parallel planes.

The calculations start by setting up the structure of the prominence, where the temperature, pressure and unresolved velocities of each plane in the slab are defined. This slab can be considered either standing vertically above the solar surface, in which case it is a prominence above the limb, or horizontally above the surface, in which case it is a filament. The vertical slab can be considered as being symmetric as it will receive the same incident radiation on both surfaces and so only half of the slab needs to be modelled. The horizontal slab is only illuminated by the solar surface on its lower surface and so the entire slab has to be modelled.

The parameters in the statistical equilibrium equation are given initial values based on hydrostatic equilibrium which will be used at the start of the iterative loop. The incident radiation from the solar surface to be used it set up. The hydrogen lines from the solar surface are read in from a external file, whilst the continuum from the solar surface is treated as a Planck function, with a frequency dependent effective temperature which defines the shape of ionisation edges in the continuum, such as the hydrogen Lyman edge at 912Å. The radiation from the solar surface is multiplied by a dilution factor which represents two factors. The first is the fact that the higher the prominence is above the solar surface the less of the prominence's field of view the solar surface takes up, just as the Earth takes up more of your field of view than it did for the Apollo astronauts. The second thing the dilution factor represents is the presence of limb darkening where the edges of the visible disk of a star such as the Sun appear

darker than the centre of the visible disk.

The initial density of hydrogen at each point in the slab is set based off hydrostatic equilibrium using the equation

$$p = Nk_BT + \frac{\rho v_{turb}^2}{2} \tag{2.27}$$

The electron density is then based off this initial hydrogen density, and from this the initial collisional rates and photoionisation probabilities are set, with the incident radiation also used for the photoionisation. From this an initial solution of the statistical equilibrium equations is reached, and the electron densities and population levels are recalculated using the Saha equation.

The calculations can now begin the main iterative loop. Each step of the iterative loop first solves the statistical equilibrium equations, then moves on to finding the source function. First the source function is found for the bound-free transitions and then for the bound-bound transitions. The iteration continues until convergence in the internal radiation field is reached. After convergence is reached the radiative transfer equations are solved again for each transition in order to produce the emergent line profiles.

This is repeated for the other elements the calculations are performed for, helium and calcium, though in addition to their own internal radiation field, they also use the radiation field from hydrogen.

Chapter 3

Incident Radiation

3.1 Context

Previous NLTE modelling of solar prominences only considered radiation originating from the solar disc in the boundary conditions for the radiative transfer modelling. The prominence is located in the solar corona, which itself emits a rich spectrum of radiation. The prominence is bathed in radiation which was not previously considered. In order to asses the contribution from this surrounding radiation to the prominence boundary conditions it is necessary to first obtain accurate values for the coronal radiation.

Spectral atlases for the solar corona are available which detail the lines present in the solar corona. One such atlas is W. Curdt et al. (2004) which uses the SUMER instrument on the SOHO spacecraft. A coronal spectral atlas requires the spectrograph to be pointed above the solar limb. A spectral atlas of on disk observations, such as Curdt et al. (2001) which was also produced using the SUMER instrument, is dominated by the spectra of the photosphere and chromosphere. SUMER is a high

resolution telescope and spectrograph which produces spectra in the range 465 to 1610 Å, although this full range is not available all at once. SUMER has two detectors which work over different overlapping ranges. This wavelength range would be an issue given the wavelength of the upper ranges of the helium ground state continua, 504Å for HeI and 228Å for HeII. Only radiation below these wavelengths can ionise ground state helium and so there is the issue of a SUMER based spectrum having no lines which fall below 228Å and so cannot ionise ground state HeII. Other instruments would have a different operational range, such as the CDS instrument on SOHO which has a range of 150Å to 800Å (Harrison et al. 1995).

However there is an issue that any spectral atlas would have no matter what instrument it is based on. Instruments such as SUMER and CDS can only observe the spectrum as seen from the location of the spacecraft they are on. These spacecraft are not located inside the solar corona and so they cannot provide the coronal spectrum as it appears from within the corona.

Calculations from empirical data also provide information on the solar corona. Fontenla et al. (2011) uses semi-empirical models of the solar corona to calculate high resolution irradiance spectra of the corona as an extension of their work on other levels of the Sun (Fontenla et al. 2009). However, these are not suitable for the needs of this work. Such studies have considered the corona as it appears from outside the corona. The prominence is located within the corona and so its vantage point must be considered.

The solution to this problem then is to calculate the intensity of coronal lines as they would be seen from within the corona.

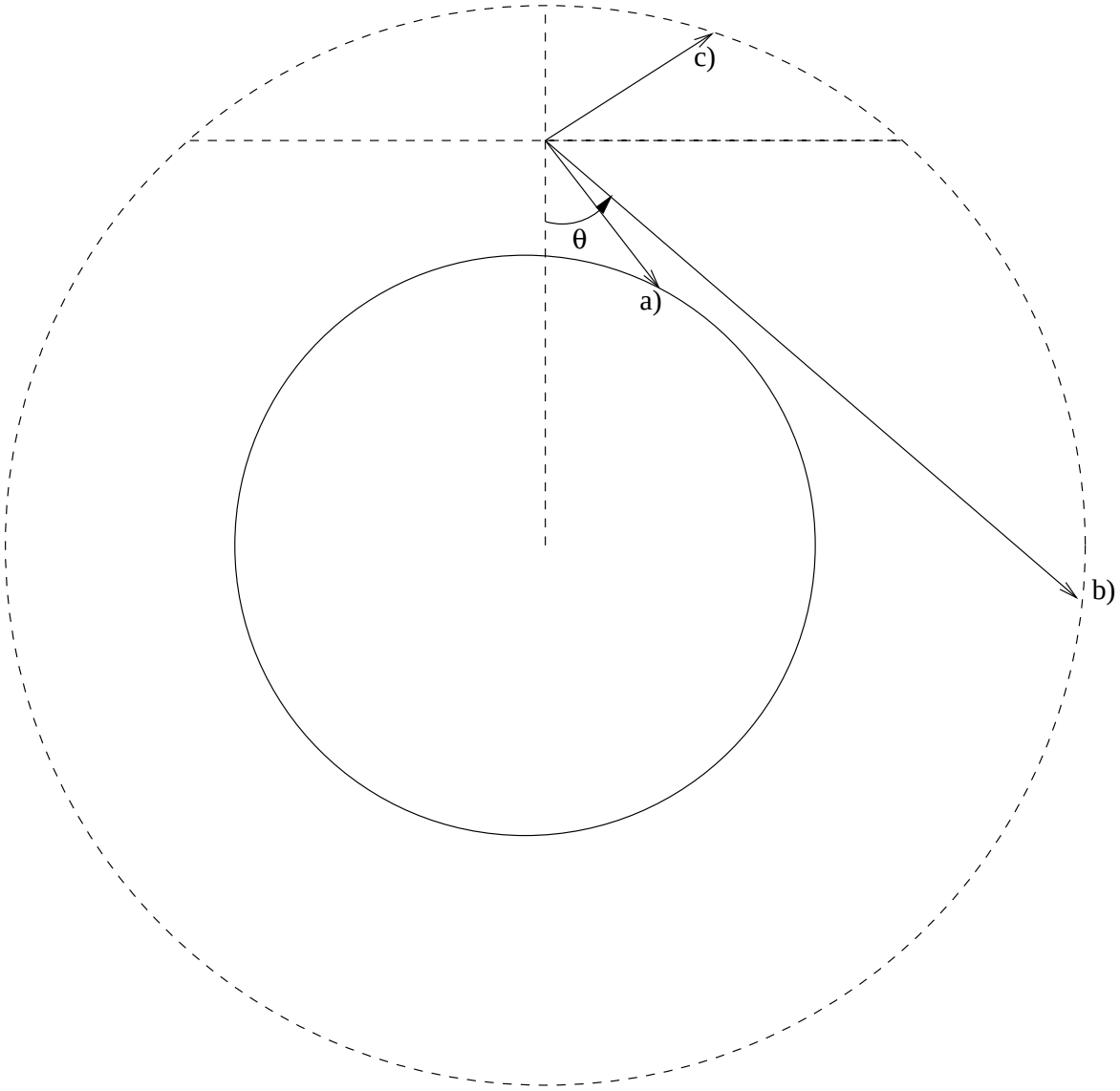

Figure 3.1: An illustration of the three types of paths through the corona which have to be handled differently. Path a) decreases in height from the inital point until it terminates on the solar surface, path b) decreases in height from the inital point until it reaches a point where the path is parallel to the solar surface after which it increases in height until it terminates at the highest considered point in the corona, path c) increases in height from the inital point until it terminates at the highest considered point in the corona. θ is the angle between the normal to the solar surface and the path.

3.2 Methodology

The intensity at a frequency λ along one path through a medium can be given as:

$$I(\lambda) = \int_{r=0}^{l} j_\nu dr \tag{3.1}$$

where j_ν is the emissivity along the path, l is the total length of the path and r is the distance along the path. As the emissivity is $j_\nu = \frac{hc}{4\pi\lambda_{ji}} n_j A_{ji}$ then the intensity is

$$I(\lambda) = \int_{r=0}^{l} \frac{hc}{4\pi\lambda_{ji}} n_j A_{ji} dr \tag{3.2}$$

Where n_j is the number density for excited level j and A_{ji} is the spontaneous decay rate from level j to level i. As the intensity from the corona is being considered the coronal approximation can be used. The coronal approximation, which applies for electron densities below 10^{10} cm^{-2}, is that the atoms and ions can be treated as though they are all in the ground state. Under this condition transitions between energy levels will all involve the ground state. The statistical equilibrium equation, in the case where only the ground level g and the excited level j are responsible for the lines, is $n_e n_g C_{gj} = n_j A_{ji}$ with n_e as the electron number density and C_{gj} as the collisional excitation rate

$$I(\lambda) = \int_{r=0}^{l} \frac{hc}{4\pi\lambda_{ji}} n_e n_g C_{gi} dr \tag{3.3}$$

The population of the ground state can be related to the electron number density by a series of ratios:

$$n_g = \frac{n_g}{N_{ion}} \frac{N_{ion}}{N_{el}} \frac{N_{el}}{N_H} \frac{N_H}{n_e} n_e \tag{3.4}$$

$\frac{n_g}{N_{ion}}$ is the ratio of the number density for the ground state compared to that for all energy levels of the same ion, $\frac{N_{ion}}{N_{el}}$ is the ratio of the ion's number density to the number density for all ions of this element, $\frac{N_{el}}{N_H}$ is the ratio of this element's number density compared to hydrogen's, and $\frac{N_H}{n_e}$ is the ratio of the number density of hydrogen to the electron density (Dere et al. 1997; Labrosse et al. 2010). Then putting equation 3.4 into 3.3 gives:

$$I(\lambda) = \int_{r=0}^{l} \frac{hc}{4\pi\lambda_{ji}} n_e \left(\frac{n_g}{N_{ion}} \frac{N_{ion}}{N_{el}} \frac{N_{el}}{N_H} \frac{N_H}{n_e} n_e\right) C_{gi} dr \tag{3.5}$$

$$I(\lambda) = \int_{r=0}^{l} \frac{hc}{4\pi\lambda_{ji}} n_e^2 (\frac{n_g}{N_{ion}} \frac{N_{ion}}{N_{el}} \frac{N_{el}}{N_H} \frac{N_H}{n_e}) C_{gi} dr \tag{3.6}$$

This can be slightly simplified by looking at a few of these number density ratios. Under the coronal approximation $\frac{n_g}{N_{ion}} = 1$ as if the electrons of each ion are being treated as all being in the ground state then the total number density for this ion is the same as the number density of the ground state. The ratio of the number densities of an element and hydrogen, $\frac{N_{el}}{N_H}$, is the abundance Ab of the element relative to hydrogen. Using these two ratios, 3.6 can be further simplified to:

$$I(\lambda) = \int_{r=0}^{l} \frac{hc}{4\pi\lambda_{ji}} n_e^2 (\frac{N_{ion}}{N_{el}} Ab \frac{N_H}{n_e}) C_{gi} dr \tag{3.7}$$

The atomic physics parameters in this can be combined into one parameter, the contribution function $G(T)$:

$$G(T) = \frac{hc}{\lambda_{ji}} \frac{N_{ion}}{N_{el}} \frac{N_H}{n_e} C_{gi} \tag{3.8}$$

Placing the contribution function of equation 3.8 into 3.7 gives:

$$I(\lambda) = \int_{r=0}^{l} \frac{G(T) Ab n_e^2}{4\pi} dr \tag{3.9}$$

Of course this is the expression for just one path through the corona, the prominence does not receive radiation from just one path through the corona, the prominence receives radiation from all directions in the corona and this radiation will be different for different directions. The length of the path will be different for different directions through the corona, as seen in figure 3.1, which is one of the reasons why the intensity is different for different directions through the corona. The other reason is the intensity depends on temperature and density and the profile of temperatures and electron densities along each path will be different for each path. The path length which must be considered is the length $l(\theta)$ which can be determined using sine and cosine rules by considering the triangles in figure 3.2. The average intensity coming from all directions when the intensity is different for different directions is

$$J(\lambda) = \frac{1}{4\pi} \int_{\phi=0}^{2\pi} \int_{\theta=0}^{\pi} I(\lambda) sin(\theta) d\theta d\phi \tag{3.10}$$

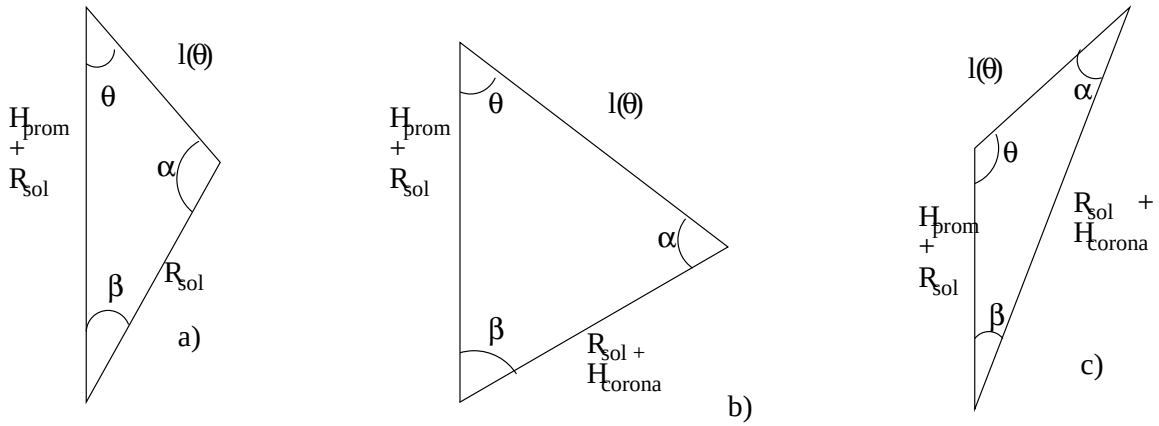

Figure 3.2: An illustration of the trigonometric determination of the length of path $l(\theta)$ for the three cases in figure 3.1 from the height of the prominence H_{prom}, the radius of the Sun R_{sol}, the height of the considered corona H_{corona} and the angle θ between the path and the normal to the solar surface. The angles α and β can be determined from the known angles and lengths to assist in determining $l(\theta)$.

So then the average intensity for the line of wavelength λ received by the prominence from all directions in the corona is.

$$J(\lambda) = \frac{1}{16\pi^2} \int_{\phi=0}^{2\pi} \int_{\theta=0}^{\pi} \int_{r=0}^{l(\theta)} AbG(T) n_e^2 dr sin(\theta) d\theta d\phi \tag{3.11}$$

The contribution function for each of the lines in the wavelength range being considered is obtained from the CHIANTI atomic database. The contribution function for a line contains the atomic information for a line, necessary to get that line's intensity.

The CHIANTI atomic database is a package of IDL procedures which can be used to obtain spectral information. It can provide the intensity of spectral lines over a desired wavelength range from atmospheric information. However as the spectrum of emitted coronal radiation is required to be as it would be observed from within the corona rather than as it would be outwith it CHIANTI can only be used to provide the contribution function to be used in 3.11 rather than the intensity itself. When used to obtain intensity it will provide an intensity for a single path through the entire

atmosphere. (Dere et al. 1997) (Landi et al. 2012)

The corona varies in density and temperature at different heights. A temperature and density profile of the corona is obtained from Fontenla et al. (2011). The contribution function depends on the density and temperature so the contribution function for each density and temperature needs to be obtained to be used in equation 3.11 for each line to be calculated. Fontenla et al. (2011) provides profiles of the temperature and density through the corona for different solar conditions. The profile which will be used to obtain intensities from within the corona is the profile provided for the quiet Sun inter-network. This represents the conditions of the majority of the Solar atmosphere for periods of low solar activity. The temperature and density variations of this profile with height can be seen in figure 3.3 The coronal lines which result from this for a height of 10,000km can be seen in figure 3.4.

3.3 Verification

With values for the intensity of coronal lines as observed at a given height obtained, these values now have to be verified to ensure that these are actually the correct values for these coronal lines. There is no atlas they can be compared to directly, for if there were easy to obtain values for the coronal radiation as it appears inside the corona it would be possible to simply use those instead of calculating the values. So an indirect comparison is necessary.

They are to be compared to intensities from Chianti as this is where the contribution functions used come from. It stands to reason that if calculations here and Chianti both use the same contribution functions and are both made to calculate intensities for the same conditions then they should provide intensities which are very similar.

A direct comparison is still not possible, so some slight changes to these calculations

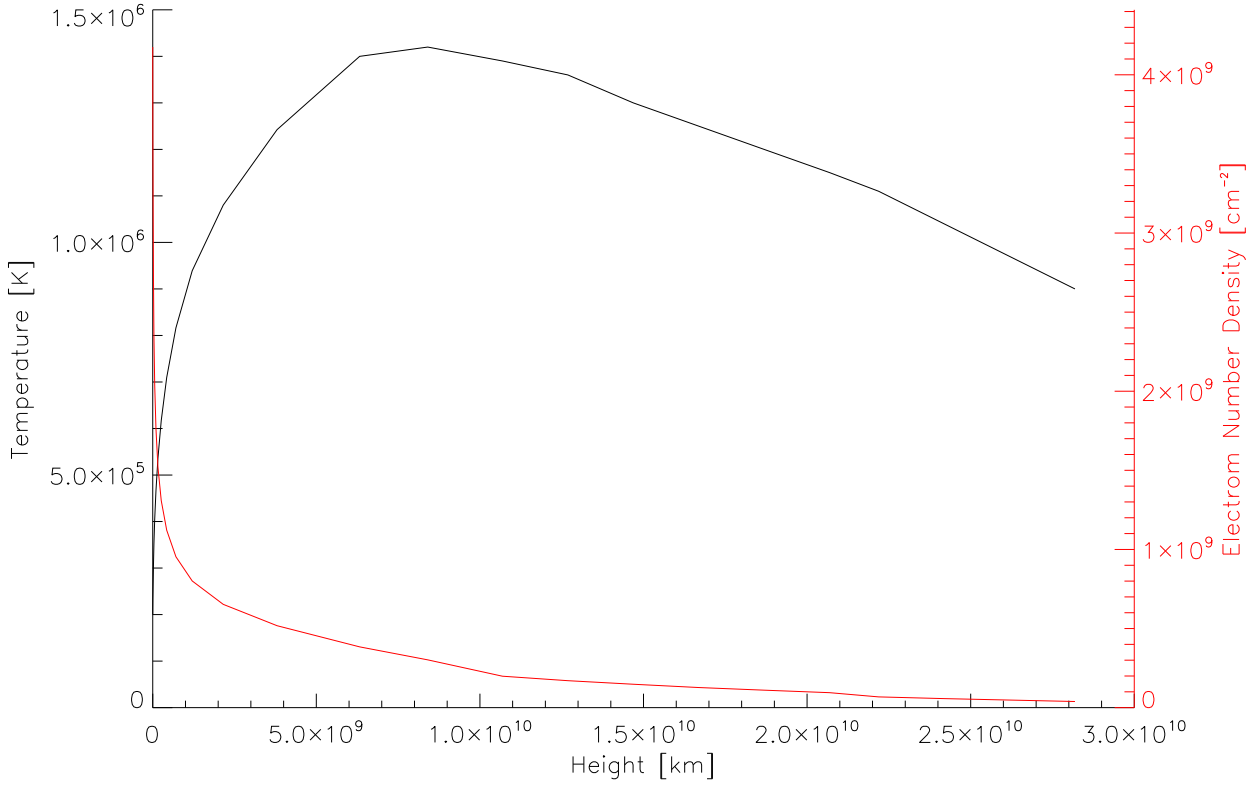

Figure 3.3: The variation of temperature and electron density through the quiet sun corona model taken from Fontenla et al. (2011).

are necessary. In order to explain what changes are necessary for a comparison the relevant part of Chianti is examined.

3.3.1 Chianti review

The Chianti procedure previously used to provide the contribution function of various lines for a given density and range of wavelengths can also provide the intensity of these lines with more information. It only requires the density to provide contribution functions for all lines within a given wavelength range.

To create intensities for the wavelength range it requires a list of the densities and

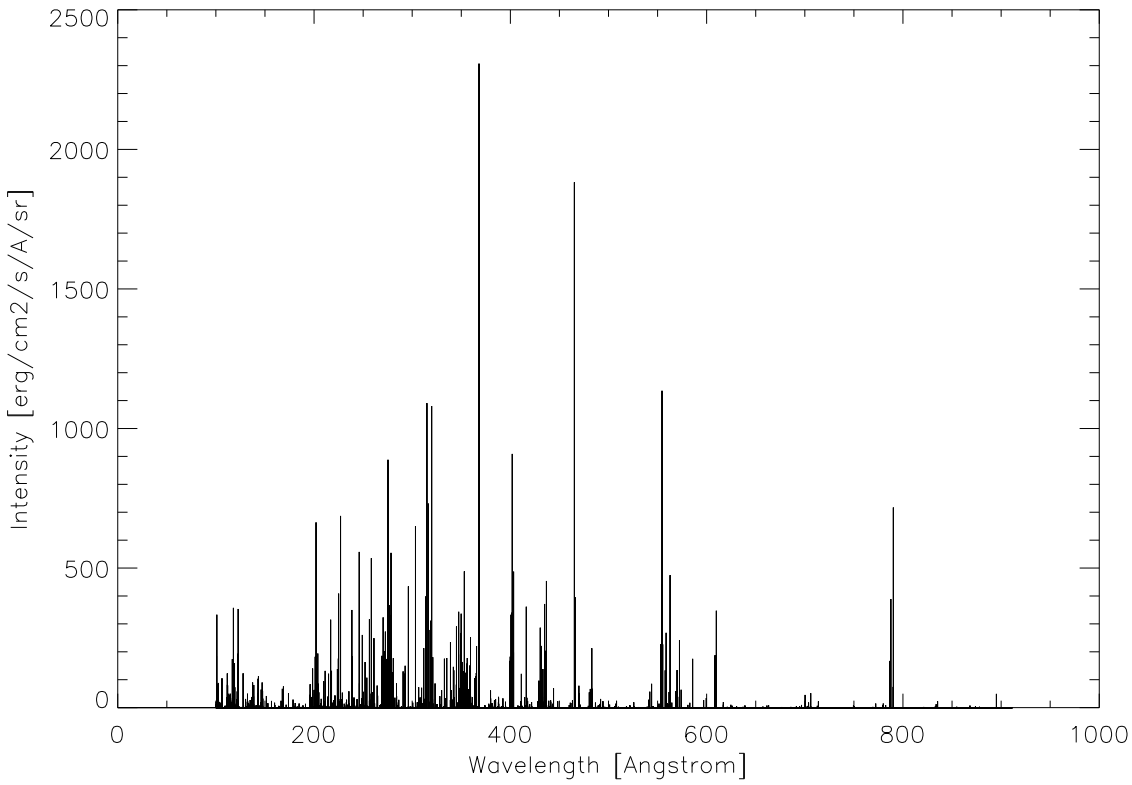

Figure 3.4: The spectrum of coronal lines received at a height of 10000 km in the corona.

temperatures in the model atmosphere, a list of ionisation fractions and the DEM, differential emission measure.

$$DEM = n_e^2 \frac{dr}{dT} \tag{3.12}$$

A DEM can be used to obtain an intensity through the equation

$$I(\lambda) = \int_{T=T_A}^{T_B} \frac{G(T)AbDEM}{4\pi} dT \tag{3.13}$$

which is integrated from the lowest temperature value of the model atmosphere, T_A, to the highest value of the model atmosphere, T_B.

An atmosphere of constant density can be used in place of a list of densities and temperatures, this requires one temperature, one density, the list of ionisation fractions and an emission measure (Dere et al. 1997) (Labrosse et al. 2010).

These parameters describe a single path through the atmosphere, where as the calculations of this work consider all directions. Rather than an integration over all directions as in equation 3.11 an integration over only one path as in equation 3.9 will be performed as this is identical to what Chianti provides intensities for. Equation 3.12 can be rearranged to

$$DEMdT = n_e^2 dr \tag{3.14}$$

and so adding in the other terms present in the integration , $\frac{G(T)Ab}{4\pi}$, shows that the integrations in equations 3.9 and 3.13 are equivalent

$$\frac{G(T)AbDEM}{4\pi}dT = \frac{G(T)Abn_e^2}{4\pi}dr \tag{3.15}$$

3.3.2 Comparisons

The calculations are set up to calculate one path through the corona, from 2.8×10^{10} km above the solar surface down to the solar surface. This is compared to the values for line intensities provided by CHIANTI. Although only one path through the corona from section 3.2 calculations is being considred in these comparisons, if the correct intensity along this path is calcualted then the intensity is correctly calculated for all the other paths. In the following comparisons it is necessary to ensure that what is being compared is the intensity from the same path through the same model corona for both methods as if paths with different variations in temperature and density are compared then it would not be expected that the same results would be produced.

3.3.2.1 Iso-thermal comparison

The next step in comparing section 3.2's calculations and CHIANTI's intensities is to make them both represent the same isothermal atmosphere. To accomplish this in section 3.2 calculations the considered atmosphere is an atmosphere of a given height of

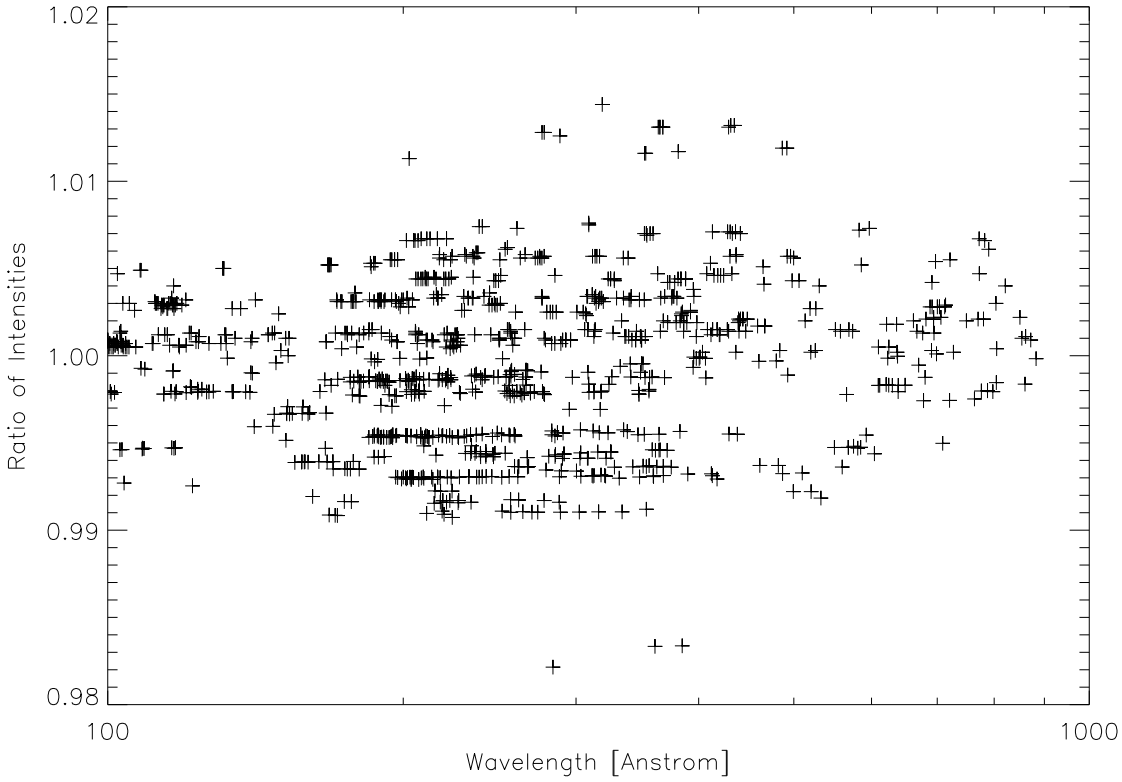

Figure 3.5: The ratio between the intensity calculated by Chianti and the intensity calculated by my code for the 1000 strongest lines in the iso-thermal case.

1×10^{10} km which has a temperature of 1.24×10^{6} K and a electron number density of 5.47×10^{8} cm^{-2} at all points and the integration of equation 3.9 is performed across the full height. CHIANTI was made to consider an atmosphere of the same temperature and density, but it also requires an emission measure corresponding to the scale of the atmosphere considered.

The ratio between the CHIANTI intensities and the intensities produced by section 3.2's calculations as seen in figure 3.5, shows ratios of intensities between the two methods which are close to one. So the intensities produced by the calculations in this test case are similar to the intensities produced by Chianti and we should be able to use the calculations to obtain the required intensities.

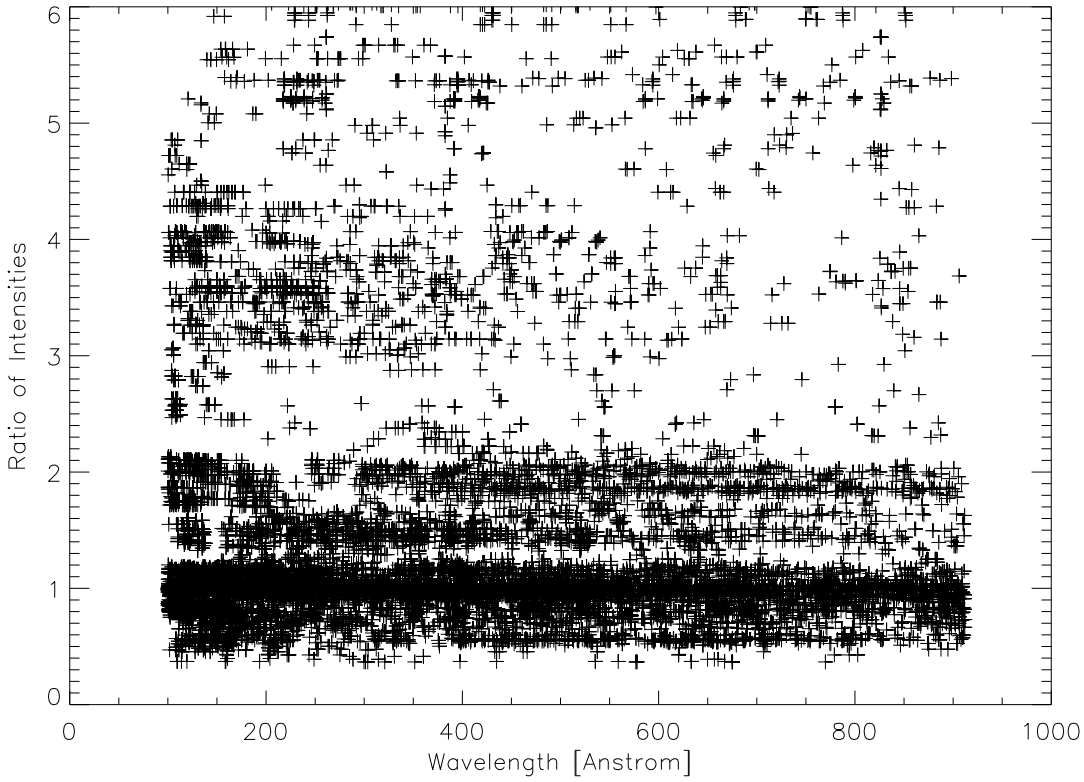

Figure 3.6: The ratio between the intensity calculated by Chianti and the intensity derived from the calculations presented here over all lines for the case of the Fontenla et al. (2011) quiet sun atmosphere.

However this test case does not accurately represent the solar corona. The corona is not of the same temperature and density through its entire depth. So it must be compared to a more realistic description of the atmosphere which features variations in temperature and density.

3.3.2.2 Comparing to a realistic atmosphere

So section 3.2's calculations and CHIANTI are both made to calculate intensities for the same corona model, the Fontenla et al. (2011) quiet sun atmosphere, by making a DEM for CHIANTI for this corona. This comparison is done over a small range in

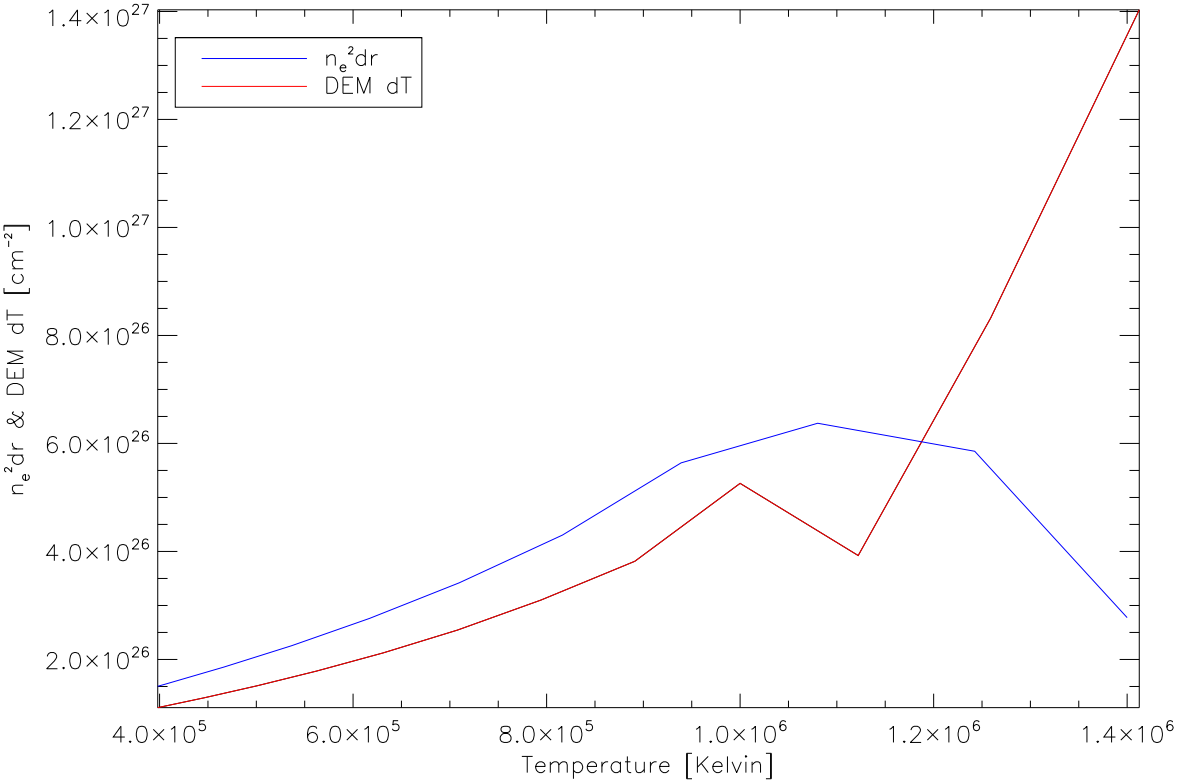

Figure 3.7: A comparison between $n_e^2 dr$ and $DEMdT$ for where the calculations presented here use the Fontenla et al. (2011) quiet sun atmosphere.

wavelength of the spectra to make it easier to look at the effects on individual lines as there are a smaller number of lines to look at than when looking over the entire range in wavlength . The intensities for the two do not match, the ratio between the CHIANTI intensities and the intensities from section 3.2 calculations is in figure 3.6. The intensities do not match, there is a wide spread in ratios between the two so they are not modelling the same atmosphere in a way that is both computationally and mathematically equivalent. Also, all lines of the same ion of the same element have the same ratio between their values as calculated by CHIANTI and their values as calculated here . Mathematically the methods used in both are equivalent as shown with equations 3.14 and 3.15. So parts of the two equations were plotted to compare to see where the difference arises. The disagreement was found between $n_e^2 dr$ and

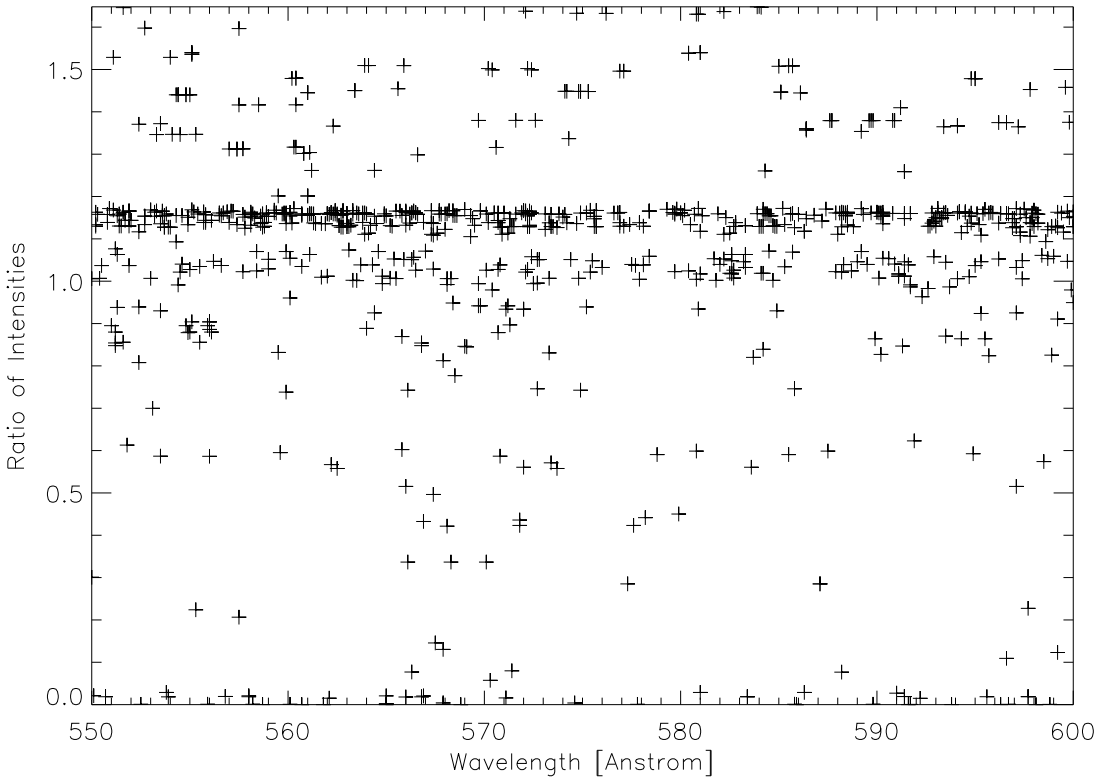

Figure 3.8: The ratio between the intensity calculated by Chianti and the intensity calculated by the calculations presented here for all lines for the case of the Fontenla atmosphere with the modified data points.

$DEMdT$, which should be the same as shown with equation 3.14. This disagreement is visible in figure 3.7.

The lines for $n_e^2 dr$ and $DEMdT$ in this graph have different curves, which should not be the case if they are equivalent. The fact that they are mathematically equivalent has been established so the disagreement comes from the numerical values used in the computations. The DEM calculated from the coronal profile is calculated with the values of temperature in this profile. CHIANTI in its calculations uses logarithmic temperatures at 0.05 intervals from 4.35 to 5.15. The temperatures used to calculate the DEM are different from the temperatures used by CHIANTI to integrate equation 3.13. So $DEMdT$ will give different values than $n_e^2 dr$ because of the two different values

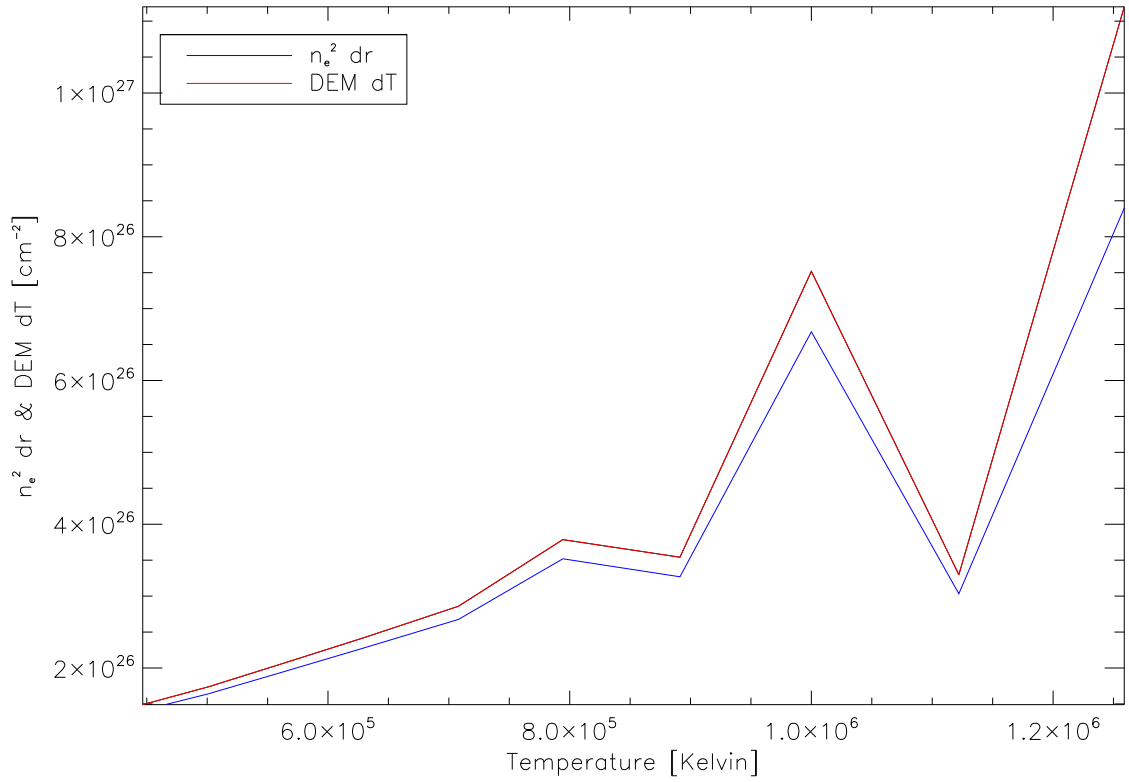

Figure 3.9: A comparison between $n_e^2 dr$ and $DEMdT$ for cases where the calculations presented here use the new profile.

for dT being used. The two different values for dT mean that rather than equation 3.14 what is had is

$$DEMdT = n_e^2 \frac{dT_{CHIANTI}}{dT_{coronaprofile}} dr \tag{3.16}$$

The solution to this is to create a new coronal profile to be used in section 3.2's calculations and in obtaining a DEM. The points in this new coronal profile will have heights and densities interpolated such that the temperatures of this new profile are the same as the temperatures used by CHIANTI.

After this change, there was still a discrepancy. Figure 3.8 shows that there is still a noticeable spread in the ratio of the CHIANTI intensity to the intensities computed from section 3.2, although it is much improved to before. In figure 3.9 the cause of this

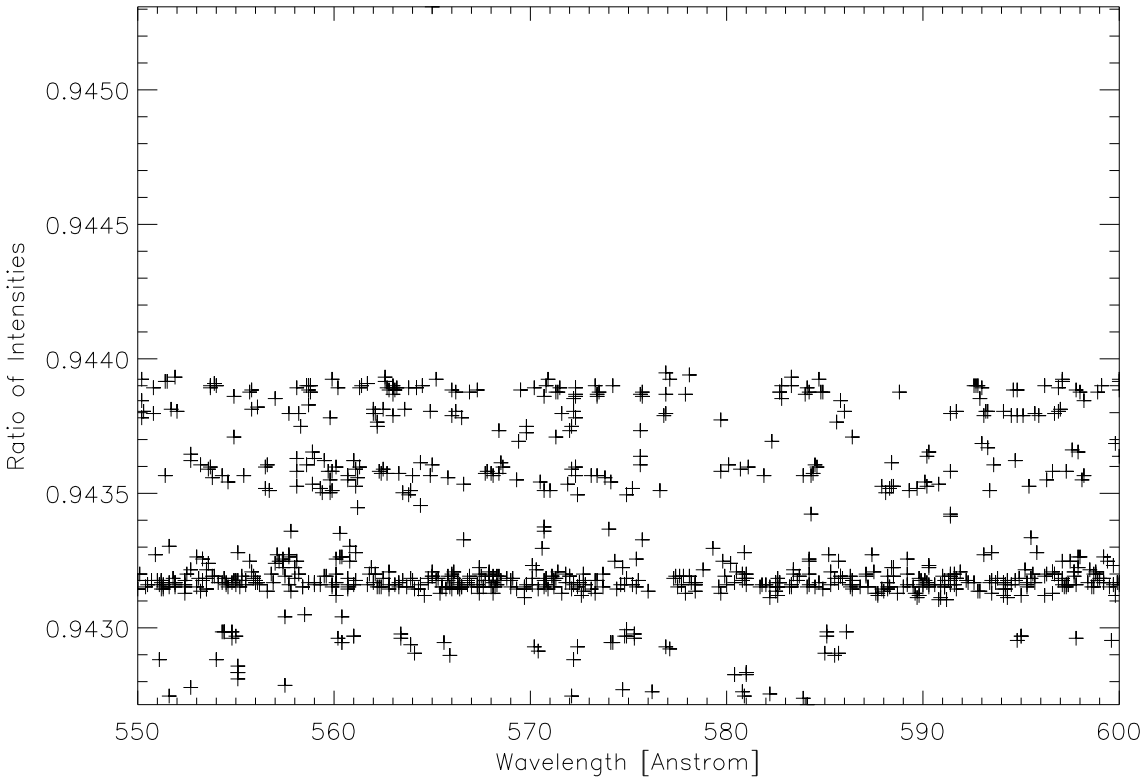

Figure 3.10: The ratio between the intensity calculated by Chianti and the intensity calculated by the calculations presented here over all lines for the case of the atmosphere with the modified data points and with the integration modified to use the rectangular method of numerical integration.

is seen. Although the $n_e^2 dr$ and $DEMdT$ curves are now the same shape, they still differ slightly in value. There must therefore be still a source of computational error.

This source was found to be how the two codes handle the numerical integration of the intensity. CHIANTI uses the rectangle method of numerical integration, whilst the calculations of section 3.2 so far use the trapezoidal rule. The rectangle method approximates the area under the curve as a series of rectangles with their bases on the x-axis and one of their top corners on the curve, whereas the trapezoidal rule uses trapezoids instead which differ from the rectangles in that both of the upper corners lie on the curve. The use of two different approximations of the area under

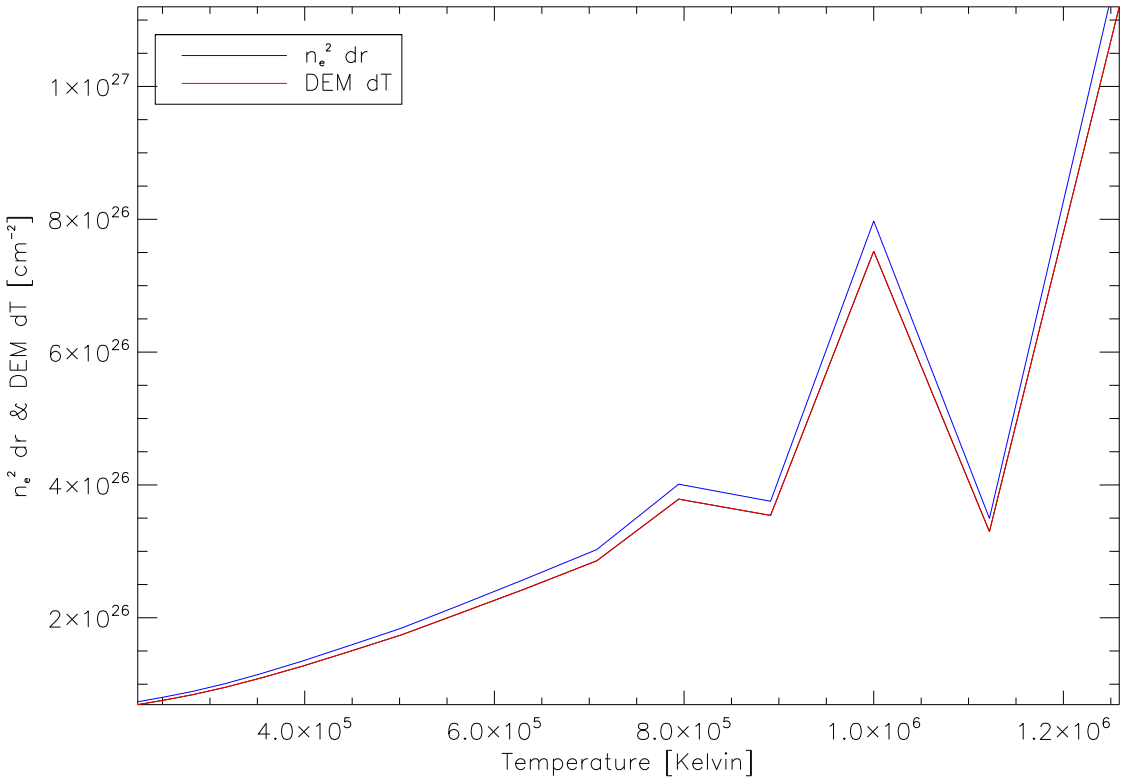

Figure 3.11: A comparison between $n_e^2 dr$ and $DEMdT$ where the calculations presented here use the new profile and with the integration modified to use the rectangular method of numerical integration.

a curve gives two different values. The check for whether or not this computational difference accounted for the remaining discrepancy between the two sets of intensities was to change the calculations fo section 3.2 to use the rectangle method of numerical integration for this test and compare the resulting intensities to CHIANTI's intensities. The agreement between the results and CHIANTI were significantly improved by this. There is now much less of a difference between n_e^2 and $DEMdT$ as shown in figure 3.11. This reduced the remaining spread of ratios, as seen in figure 3.10. The ratio between the calculations and CHIANTI is still not 1, as there is still not total agreement between n_e^2 and $DEMdT$ however the agreement is now close enough that there can be confidence in the calculations.

Going forward the calculations revert back to using the trapezoidal rule of numerical integration, for the trapezoidal rule is more accurate than the rectangle method, and to using the original heights of the data points in the model atmosphere.

3.4 Results

3.4.1 Variation with Height

	Height (km)	Local Coronal Temperature (log T(K))
1	10,000	5.948
2	20,000	6.024
3	30,000	6.066
4	40,000	6.099
5	50,000	6.120
6	60,000	6.140
7	70,000	6.148
8	80,000	6.151

Table 3.1: Temperature of the corona at the heights considered.

The spectrum needs to be recalculated for different heights. The proportion of the corona which is visible from within it depends upon the height within the corona from which it is being observed. If you are on a ship and are looking at another ship whose hull is just below the horizon, you can see more of the other ship from the top of your ship's masts than you can from the deck. So it is that the higher you are in the corona the more of the corona you can see. There will also be a stronger influence from regions of the corona closer to the vantage point.

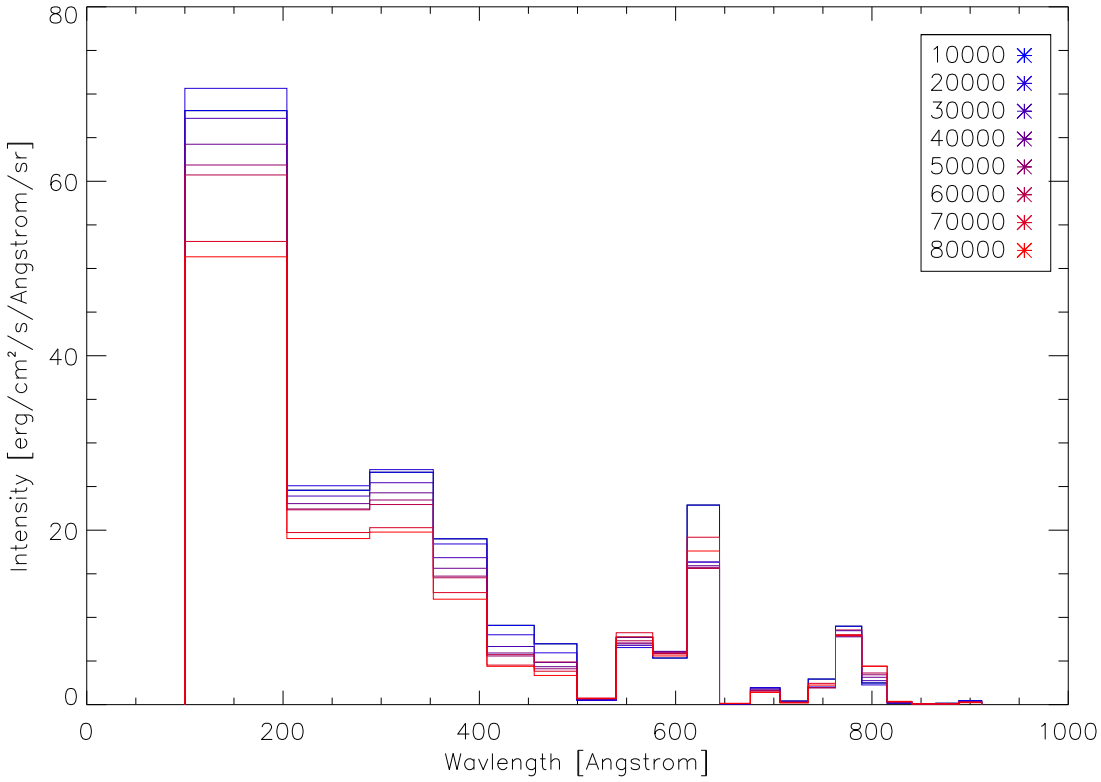

Figure 3.12: The spectrum summed into bins for eight different heights.

The effect of these two considerations on the incident intensity can be seen in figure 3.12 which shows the binned spectrum as seen at 8 different heights from 10000km to 80000km. The total intensity for each bin varies in a different way for each bin, while one bin may be at its most intense for the highest height another may be at its most intense for the lowest height. Different bins are dominated by lines for different ions. If a bin is dominated by lines of a certain ion the total intensity of the bin will be at its greatest when lines for that ion peak.

Looking at some individual lines shows how changing the height impacts the value of individual lines, how some lines are more intense at higher heights and some are more intense at lower heights. This is connected to the temperature of the corona at that height, the temperatures for these heights are seen in table 3.1. The He II 304 line in figure 3.13 is cooler than any of the coronal temperatures with a formation

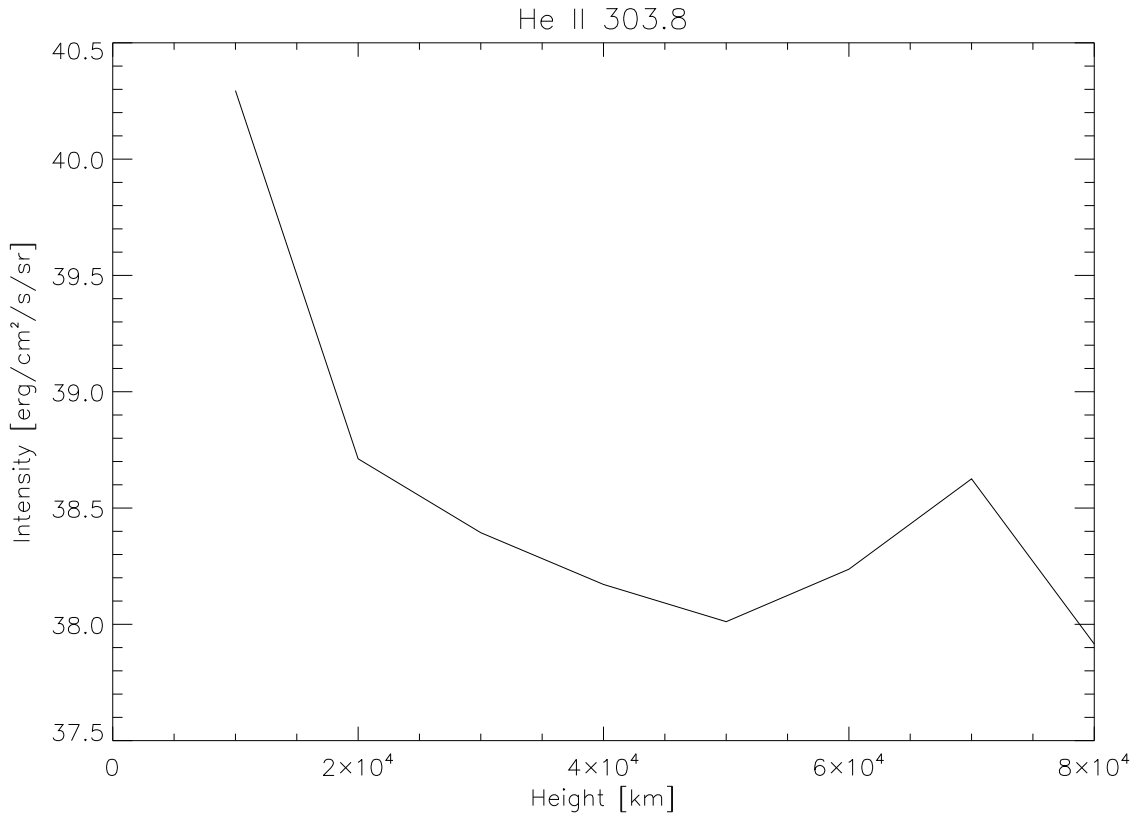

Figure 3.13: The variation of the Helium II 304 Angstrom line in total intensity with height.

logarithmic temperature given by CHIANTI of 4.95 and is at its greatest value for the lowest height in the corona, which has the lowest local temperature and so closest to 4.95. However the decrease in temperature is not as great as seen in other lines.

The variation of the Magnesium IX 368Å line's total intensity with height is shown in figure 3.14. The formation logarithmic temperature of magnesium given by CHIANTI is $log(T) = 6$ which is closest to the temperature of the corona as the second height, and this shows in figure 3.14 for the highest intensity of this line is at 20,000km, the second height. At greater heights where the local temperature is further from the formation temperature of Mg IX the total intensity of the line decreases.

Shown in figure 3.15 is the variation in total intensity against height for the Fe

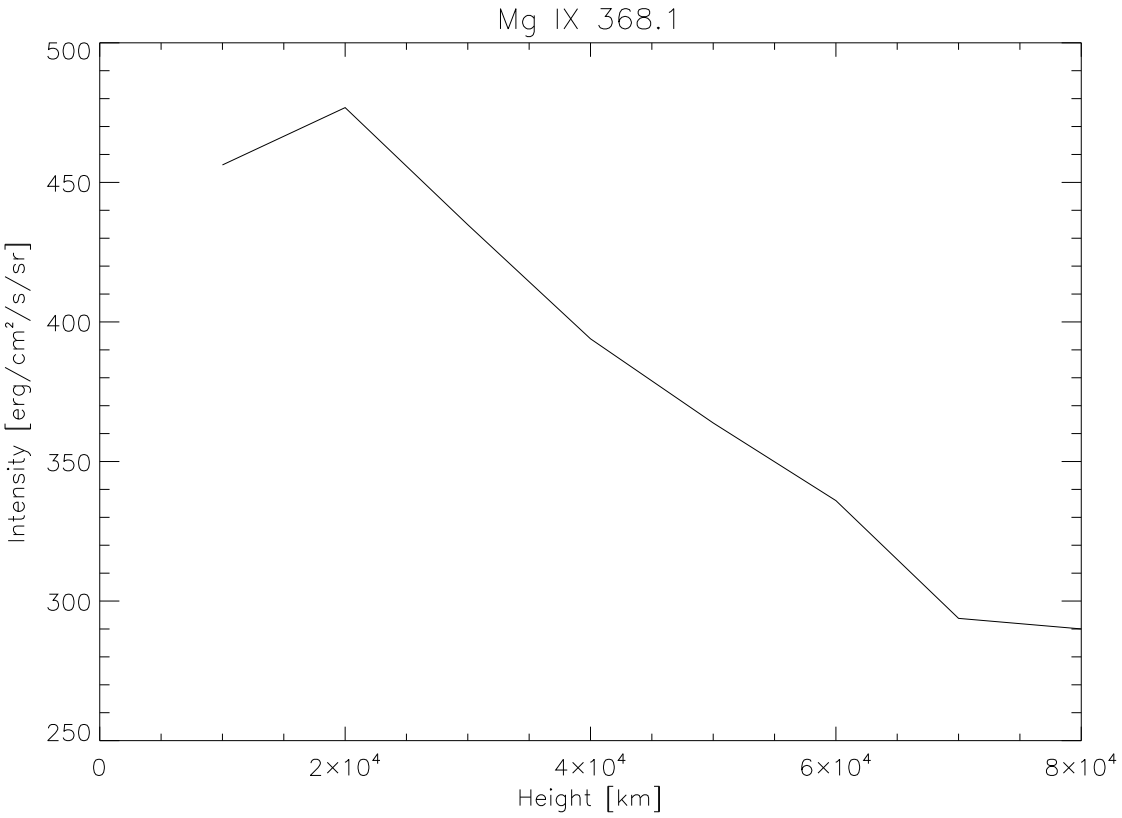

Figure 3.14: The variation of the Magnesium IX 368 Angstrom line in total intensity with height.

IX 171 line, which has a logarithmic formation temperature given by CHIANTI of $log(T) = 5.95$, and it is strongest at 10000km which at $log(T) = 5.94$ is the closest in temperature to the formation temperature, and decreases higher in the atmosphere at temperatures further from the formation temperature. The Fe X 174Å line has a formation temperature given by CHIANTI of $log(T) = 6.05$ which would correspond to between 20,000 and 30,000 km and the plot of the total intensity of this line against height, shown in figure 3.16, is at its greatest at those heights. Continuing this trend of lines with a higher formation temperature having their greatest value at higher heights is the Fe XV 284Å line shown in figure 3.17. The formation temperature given by CHIANTI of this line is $log(T) = 6.35$ which is greater than the temperature at any of the heights considered.

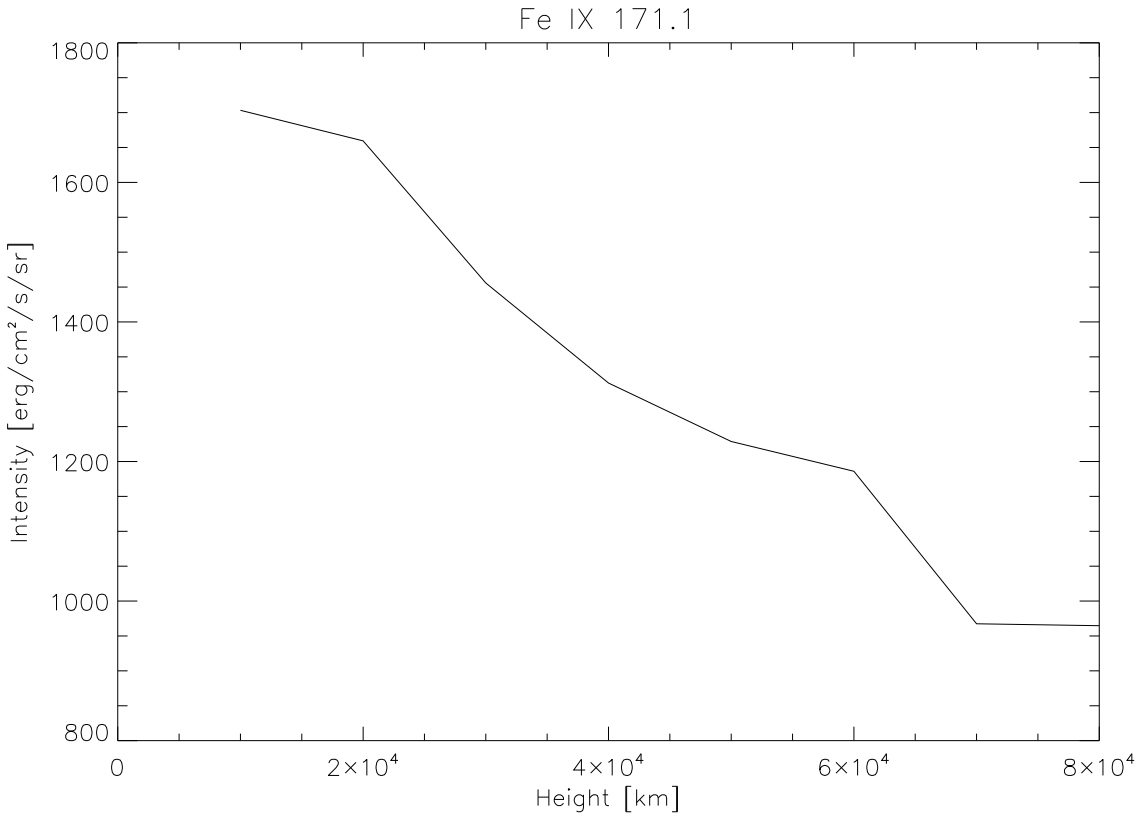

Figure 3.15: The variation of the Iron IX 171 Angstrom line in total intensity with height.

Although the intensity of the lines is being integrated over the entire corona, it is the portion of the corona nearest to where the corona is being observed, that has the greatest effect on the coronal spectrum as observed from within the corona. The intensity of each of these lines was strongest when viewed from a point in the corona closest to where they are primarily formed.

Figures 3.18 to 3.20 show how the total intensity of a wavelength range is more heavily influenced by some lines rather than others. Shown in these plots is the total intensity for all lines within the wavelength range, which is always the highest line on each plot, and the total intensity for lines within this range who each make up more than 10% of the total intensity of all lines within the range, each wavelength range features about 2 to 5 of such lines . Figure 3.20 shows a wavelength range which is

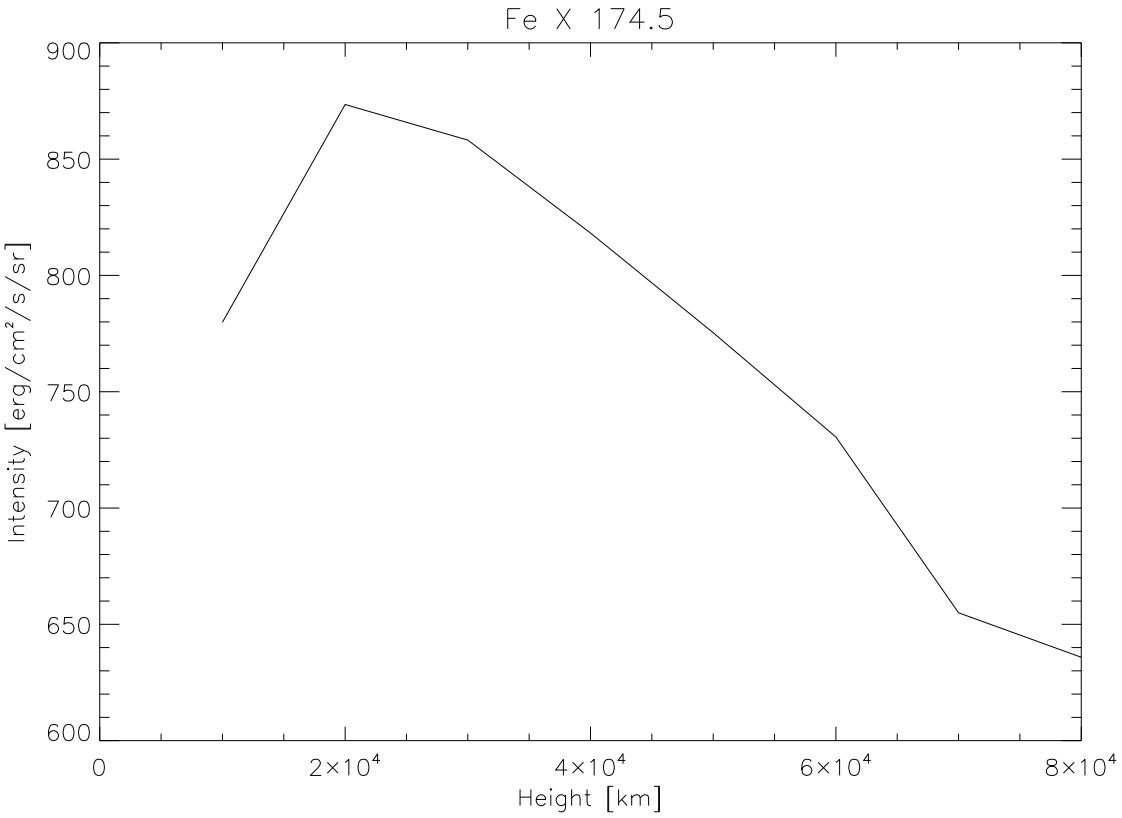

Figure 3.16: The variation of the Iron X 174 Angstrom line in total intensity with height.

dominated by one line in particular. In this plot it is clear that the O V 630Å line contributes most of the total intensity within this range, the variations of the total intensity of this range in height match the variations of the O V line. Figure 3.19 shows a wavelength range which is shaped by more than just one line. Most of the 4 lines which are the strongest in this range decrease with height, and the total intensity of this range decreases with height also. Figure 3.18 shows a range which is mostly made of weak lines, there are only two lines which are more than 10% of the total intensity so most of the light within this range will come from weaker lines.

Each line will vary with height in a different way from other lines so for different heights each line will have to be recalculated, it is not sufficient to just calculate each line once for one height and then multiply the whole spectrum by some scaling factor

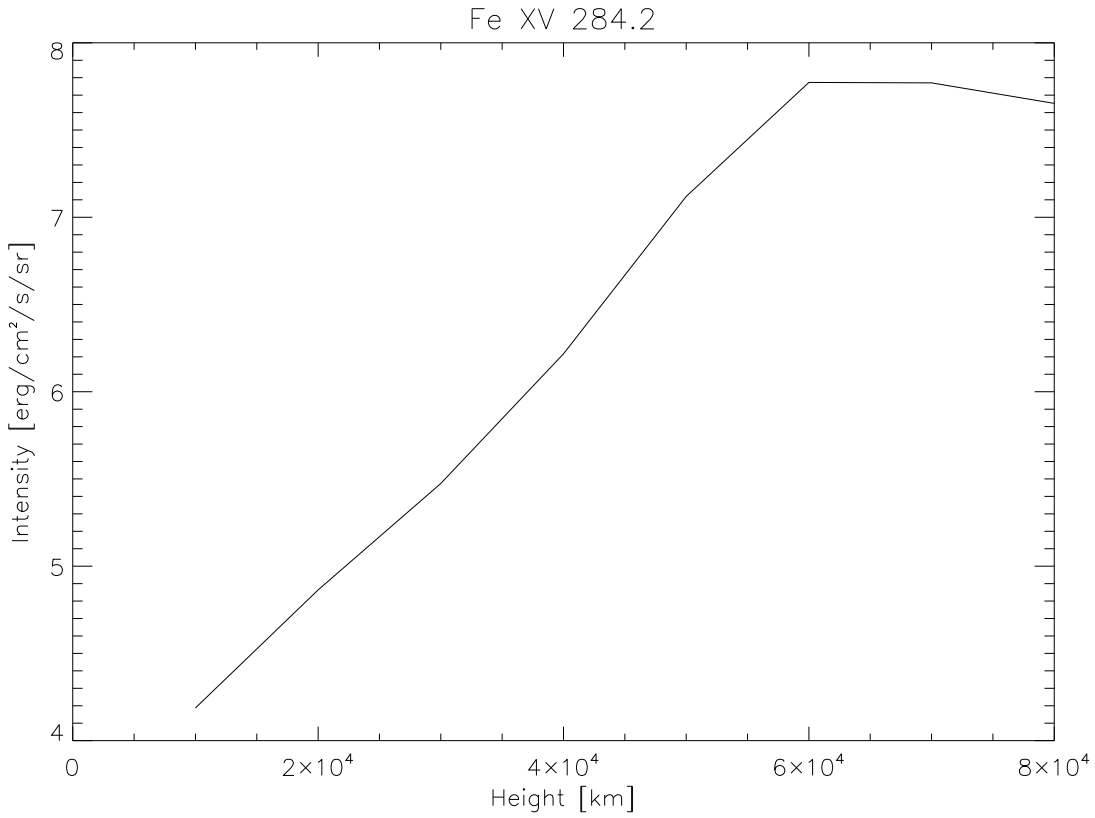

Figure 3.17: The variation of the Iron XV 284 Angstrom line in total intensity with height.

as each line scales differently with height. Summing the lines across wavelength ranges would not solve this issue, as the total intensity of different wavelength ranges will also scale differently with height.

3.5 Conclusions

This chapter has demonstrated how to obtain the radiation from the whole corona as observed from a location within the corona and why it is necessary to calculated this coronal spectrum separately for different heights within the corona. Section 3.1 explains that the results of observations of the corona cannot be used as observations of the

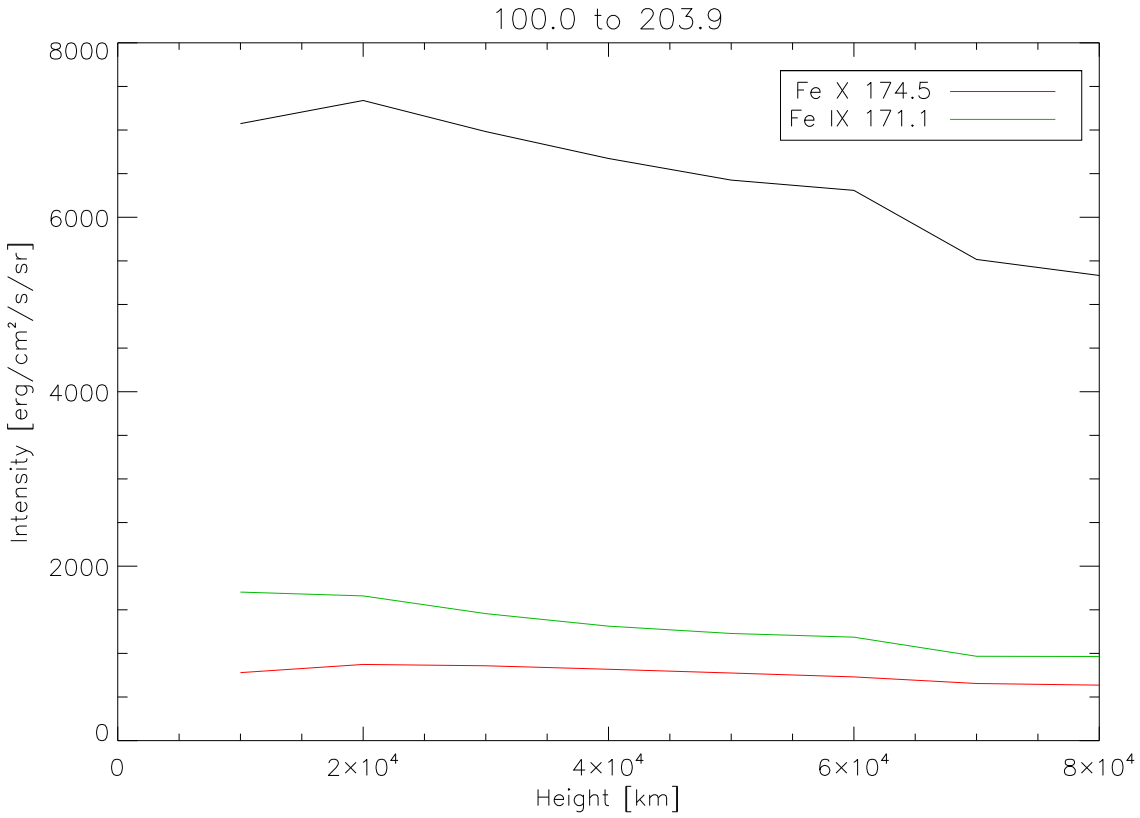

Figure 3.18: The variation of the total intensity of all lines within the range 100 to 203 Angstrom with the variation of some individual lines also plotted for comparison.

corona were made using instruments located outside the corona, either on spacecraft or on Earth, and can only tell us what the corona looks like from the outside. It is the corona as it appears from the inside that needs to be considered here and as this cannot be observed it must be calculated.

Section 3.2 details how calculations of the spectrum of the corona at different heights within the corona will be performed. Contribution functions, $G(T)$, are obtained for electron densities at various heights through the corona. These contribution functions are obtained from the CHIANTI atomic database for all lines between 100Å and 912Å, and the coronal densities and temperatures used here are the temperatures and densities from the quiet sun model corona of Fontenla et al. (2011). These contribution

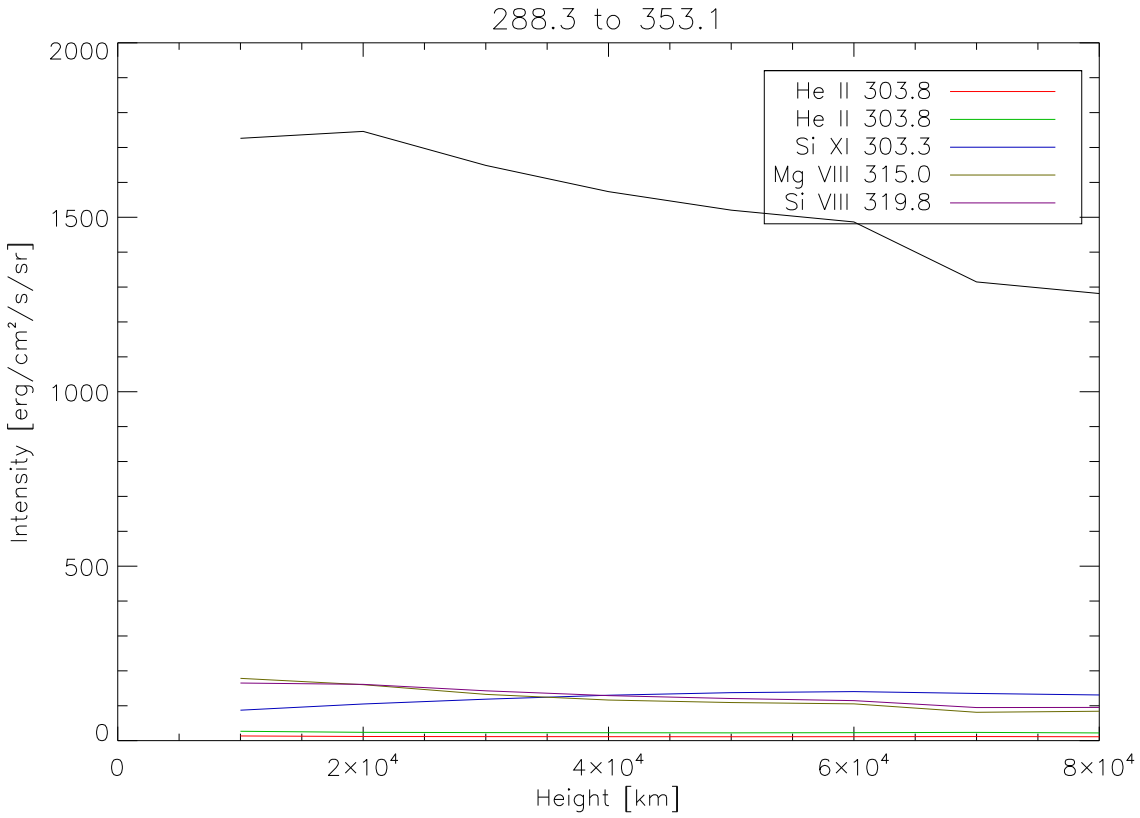

Figure 3.19: The variation of the total intensity of all lines within the range 288 to 353 Angstrom with the variation of some individual lines also plotted for comparison.

functions, densities and temperatures are used in the integration of equation 3.11 for each of the lines. The spectrum as seen from a height of 10,000km in the corona which results from this calculation is shown in figure 3.4

It is verified that the spectra obtained are actually the spectra that would be seen from within the corona in section 3.3. The intensity for the spectral lines along one path through the corona is calculated and compared to intensities provided by CHIANTI. The initial tests are with both set up to provide the intensities from an iso-thermal atmosphere and upon finding good agreement move on to a more robust test. Section 3.3.2.2 compares the intensites that the two methods provide for a realistic atmosphere and find discrepancies which can be ascribed to differences in the computational meth-

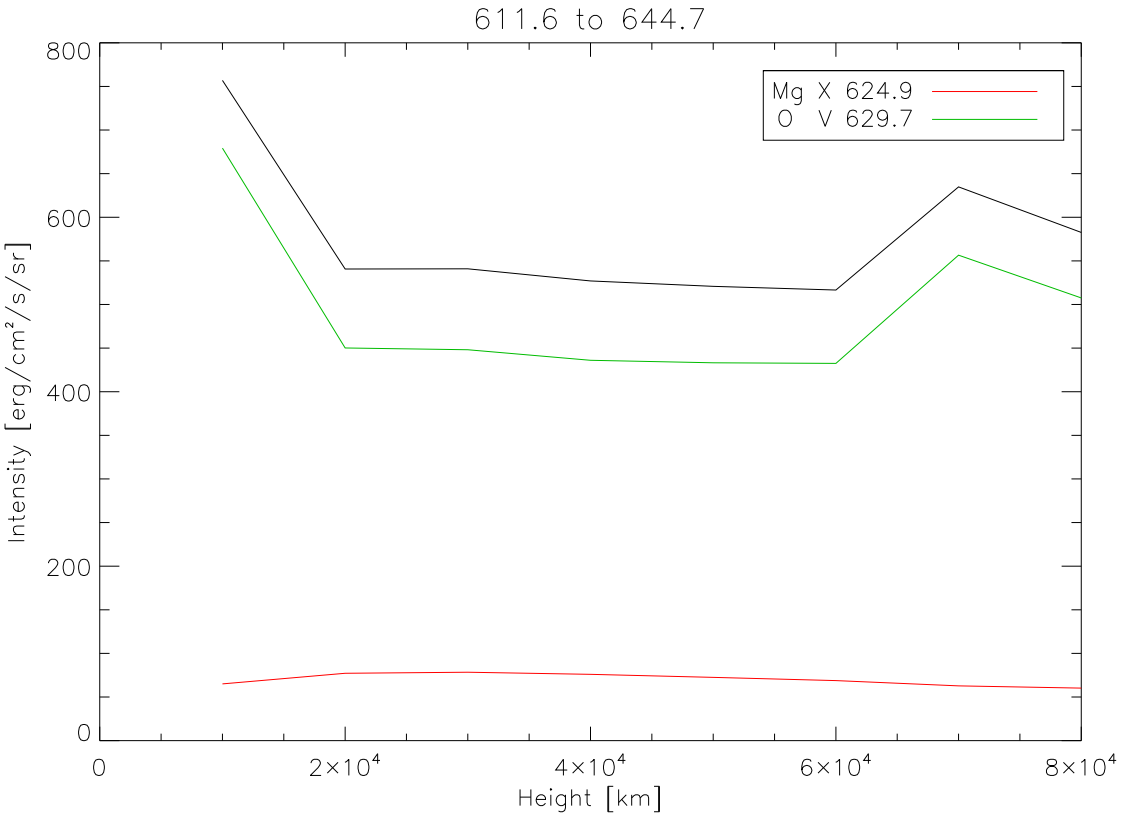

Figure 3.20: The variation of the total intensity of all lines within the range 611 to 644 Angstrom with the variation of some individual lines also plotted for comparison.

ods and after reconciliation these discrepancies disappear, which leaves confidence in the spectra obtained.

The variation in height of the intensities obtained from equation 3.11, and so the necessity of recalculating the intensities for each height, is demonstrated in section 3.4.1. The intensity of individual lines vary such that they are greatest when being observed from a height in the corona which is at a temperature closest to the formation temperature of the line. The fact that different lines have different formation temperatures means that the lines will not vary in height in the same way. This carries on to when lines are summed up within ranges of wavelength, the total intensity of the ranges of wavelength will also not vary in height in the same way. So when considering

the incident coronal radiation to a prominence at a certain height, it is necessary to calculate this coronal radiation separately for each prominence height to be considered.

Chapter 4

Hydrogen

4.1 Pre-existing code

A pre-existing radiative transfer code outlined in Gouttebroze et al. (1993) and Gouttebroze & Labrosse (2000) was used, and is the base to which modifications were made. The calculations use an equivalent two level atom method with the hydrogen atom treated as having twenty one levels; twenty bound levels and one ionised level.

Both iso-thermal prominences and prominences with a prominence to corona transition region (PCTR) can be considered, iso-thermal prominences with their temperature, pressure, thickness and altitude specified, and prominences with a PCTR with their temperature and pressure defined at each point through the prominence. The primary source of the radiative losses is hydrogen and so the code will always produce a hydrogen spectrum. Other main sources of radiative losses are helium and calcium.

The incident radiation acts as a boundary condition to the radiative transfer equations. For the bound-free transitions the incident radiation is taken to be a Planck

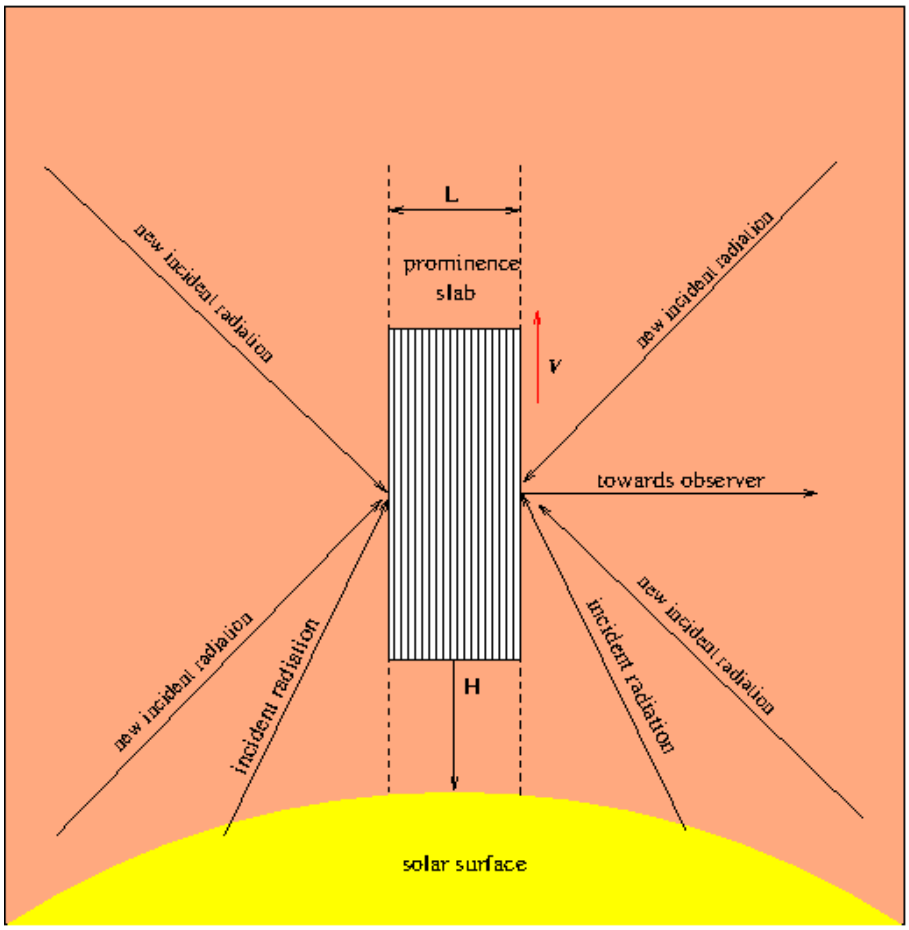

Figure 4.1: 1D parallel slab which is now considered with the coronal radiation also illuminating it.

function with ionisation edges in the continuum, such as the hydrogen Lyman edge at 912 Å, only the radiation from the solar disk was considered. The modifications which were made for this work involved changing this incident radiation to also include radiation from the solor corona and making it so the rest of the code can handle this more detailed spectrum.

4.2 Modifications to the code

Modifications are to be made which will change the incident radiation. Initially the changes are only made to the incident radiation relevant to the hydrogen continua. After this is proven to work the changes can also be applied to the helium continua.

Originally the incident radiation was considered as a Planck function with a frequency dependent effective temperature which includes the effective temperatures of the hydrogen Lyman edge and two helium edges. While this does represent the radiation incident to the prominence which has its origins in the solar surface it does not have the many lines of the corona which will also illuminate the prominence.

The data points in the original code for each continuum were spaced out logarithmically, which is necessary to properly consider the shape of the Planck function which exponentially increases in intensity. However the coronal emission lines to be considered can fall in between these points and even if one of the data points were to coincide with one of these lines then only part of the line would be described, so points have to be added to where the line is and there has to be a sufficient number of them to describe the line.

The points added are centred on the line centre so the full height of the line is considered by the program, given that the lines being added to the incident radiation are being treated as being Gaussian in shape their highest value is at their centre.

As this requires adding several points for each individual line, treating all of the very many lines within the incident radiation this way will greatly increase the computational resources required. So it is also necessary to bin the lines, to sum the intensities of the lines in a range of frequencies together and so gain a fixed amount to increase the intensity within this frequency range by. This does not require an increase in the number of data points, as the fixed height of each bin is just added to which ever data points are present.

However the placement and width of the bins themselves is worthy of consideration. The bins are arranged so that they are smaller the closer they are to the continuum edge as greater precision is more worthwhile there.

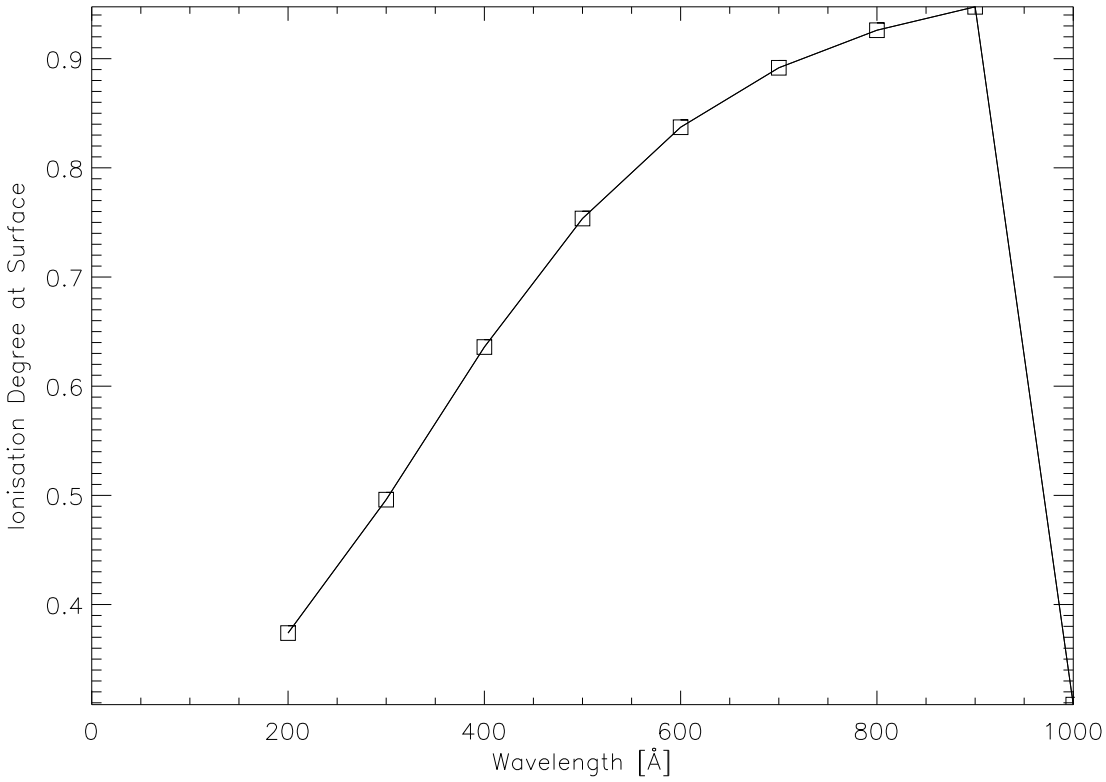

Figure 4.2: Ionisation degree $\frac{n_p}{n_H}$ at the surface plotted against the position of the single added line. The values for 1000Å are the same as those which occur if no line is added.

4.3 Checking the modifications

4.3.1 Single Test Line

A single test line was added to the incident radiation to probe how well the modifications work. It serves to investigate if there are any cases where adding a line to a certain part of the spectrum does not work as expected due to computational errors in how the line is handled. This single test line was varied in wavelength from 200Å to 1000Å. The line height was arbitrarily set to 4×10^{-7} erg s^{-1} cm^{-2} Hz^{-1} and its width 5×10^{11} Hz. The prominence under consideration in this test is an iso-thermal

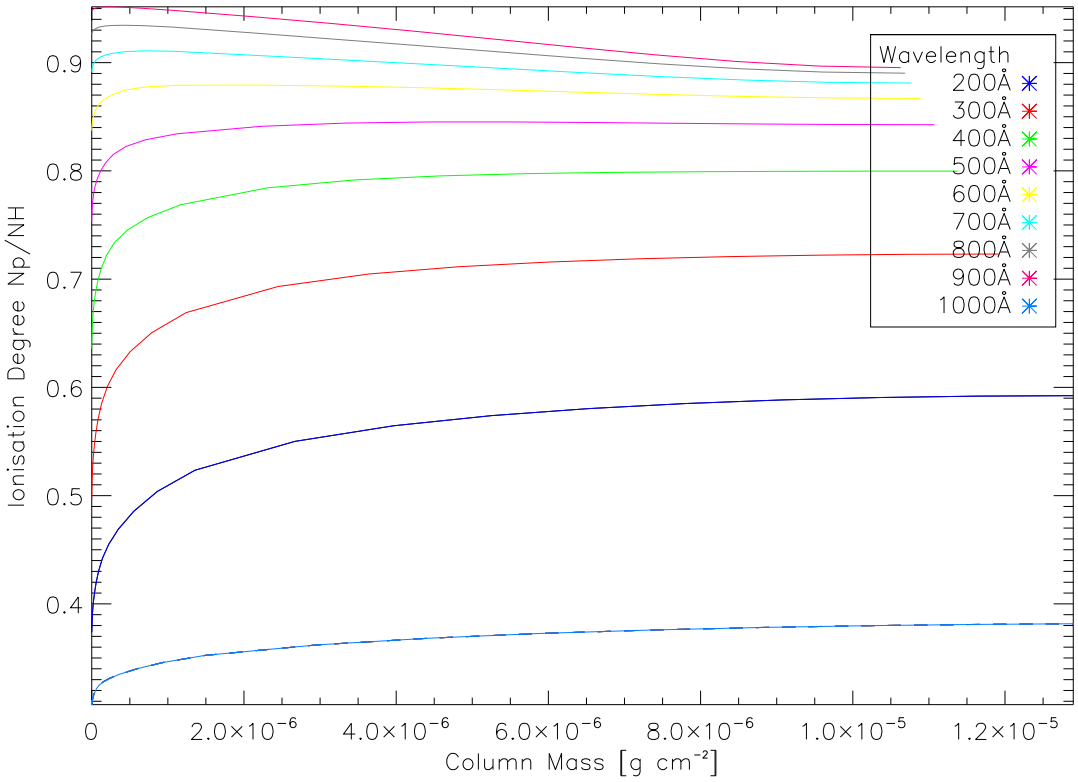

Figure 4.3: Ionisation degree at the surface versus column mass with the added emission line at varying wavelengths, indicated in the legend. The values for 1000Å are the same as those which occur if no line is added.

prominence at a height of 10,000 km above the solar surface with a temperature of 8000 K, a pressure of 0.2 dyn cm^{-2} and is 1000 km thick.

The degree of the influence a line has on the prominence plasma depends on the wavelength of the line. As the line is moved higher in wavelength the influence of the line on the prominence increases until the line is moved above 912Å the Lyman limit which corresponds to the minimum required energy necessary to ionised ground state hydrogen. Figure 4.2 shows this, as the wavelength of the added line increases the ionisation degree of the prominence increases until the line is moved above the Lyman limit because of the line contributing to the ionisation of the prominence's hydrogen. The photo-ionization cross section, and how easily the hydrogen is ionised by the line,

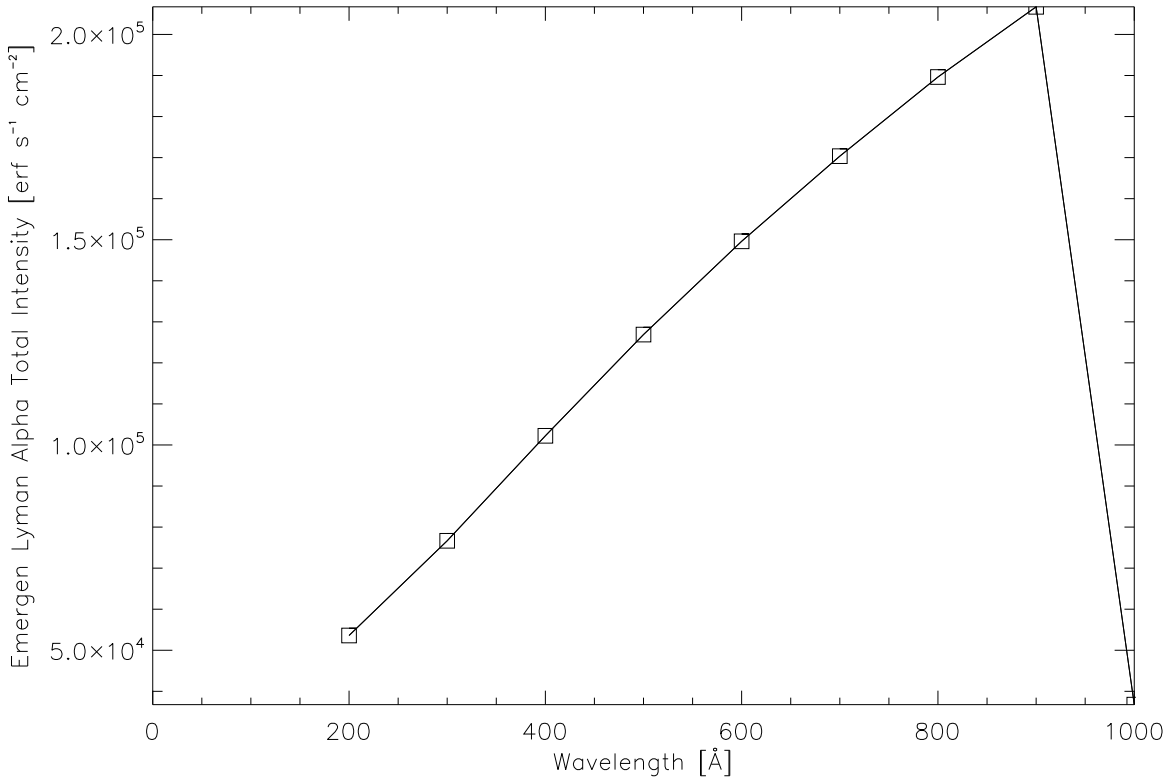

Figure 4.4: The intensity of the Lyman Alpha line emitted by the prominence against the position of the added test line. The values for 1000Å are the same as those which occur if no line is added.

depends on wavelength and increases with wavelength so an increase in radiation at higher wavelengths has more of an impact on the plasma than if the increase was at lower wavelengths.

The effects of this line are not limited to just the surface of the prominence. Figure 4.3 shows the ionisation degree of the prominence from its surface, at a column mass of zero, to its centre for the single test line at varying wavelengths. This figure shows that the effects of the line are not limited to the surface of the prominence but also extend deeper into the prominence. In the case of this prominence adding the test line results in the prominence being more ionised down to the centre of the prominence, however for different prominence conditions the effects of adding the coronal radiation

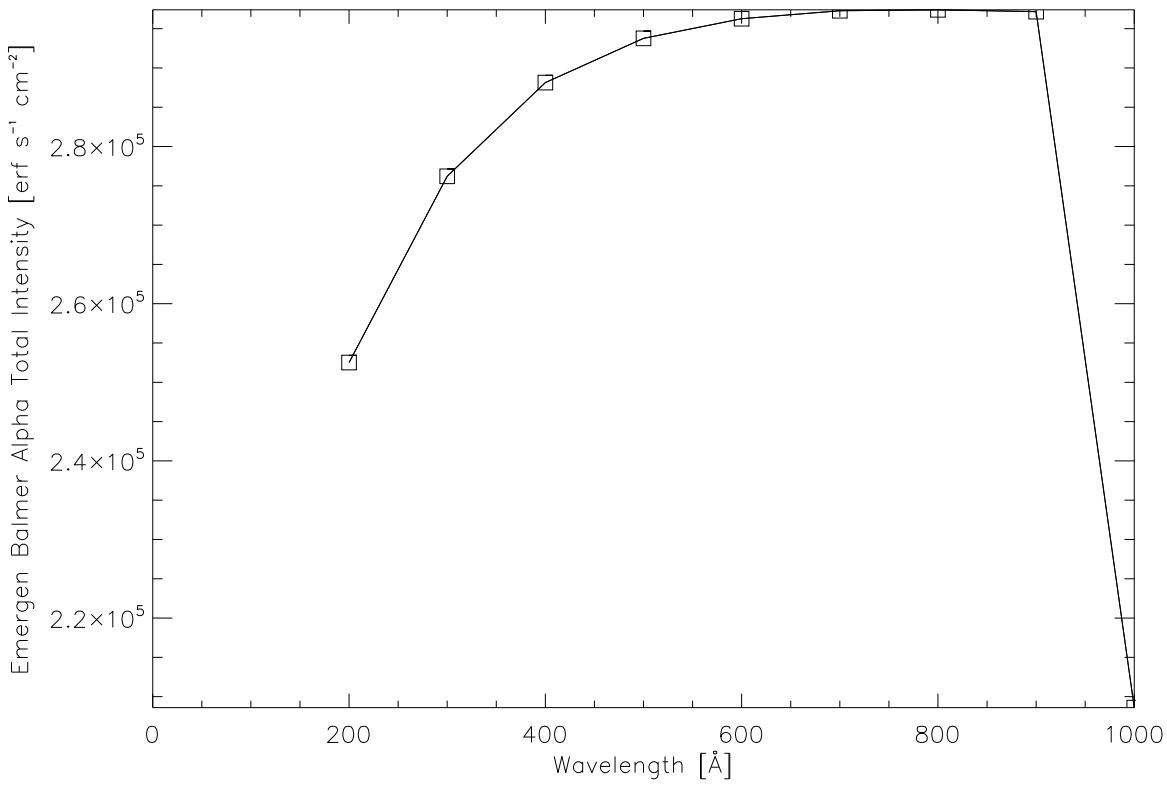

Figure 4.5: The intensity of the Balmer Alpha line emitted by the prominence against the position of the added test line. The values for 1000Å are the same as those which occur if no line is added.

may not extend down so deep. This is investigated for other prominence conditions with a realistic coronal spectrum in section 4.4.

Figures 4.4 and 4.5 show the effects of the moving test line on the emitted radiation of the prominence. These show that the emitted radiation of the prominence will be influenced by changing the incident radiation to the prominence, although this is not a direct effect.

There are two main implications from this. Firstly the wavelength of lines matter, when adding a realistic spectrum one cannot just average the intensity of all lines across the entire range of wavelengths from 100 Å to 912Å and add a fixed amount to the

incident spectrum. Secondly the increase in influence increases with wavelength up to the Lyman limit, so the position of a line matters more the closer to the Lyman limit.

The test line was then moved from 912Å to 3650Å, the Balmer limit. The effects of the line when it is above 912Å are much less than when below 912Å as then it is not capable of ionising ground state hydrogen, the energy level of most of the hydrogen. The effects of a line beyond 912Å are small enough that such lines are not going to be considered in the full spectrum.

4.3.2 Multiple Test Lines

There is a computational issue to be considered when adding individual lines to the incident radiation. Each separate line added requires additional data points to be added to describe the line and so increases the computational resources required by the radiative transfer calculations. One solution to this would be to not include all the lines, but only lines above some threshold value. The strongest lines individually will have a stronger influence on the prominence plasma, but there are many weak lines. The question there is at which point does adding more weak lines have no further benefit?

In figure 4.6 the effect of adding an increasing number of lines is shown. Although the increase in the effect is lessened with more lines, it is still a significant increase up to a few hundred lines. However this comes at the cost of the calculations taking much longer, up to 400 times longer for the amount of lines considered which was a small portion of the total number of lines within the wavelength range. The cost of computational time is too high for increased quality of calculation and so another method of adding the additional coronal radiation must be considered.

Instead of adding the lines individually their total intensities are summed across

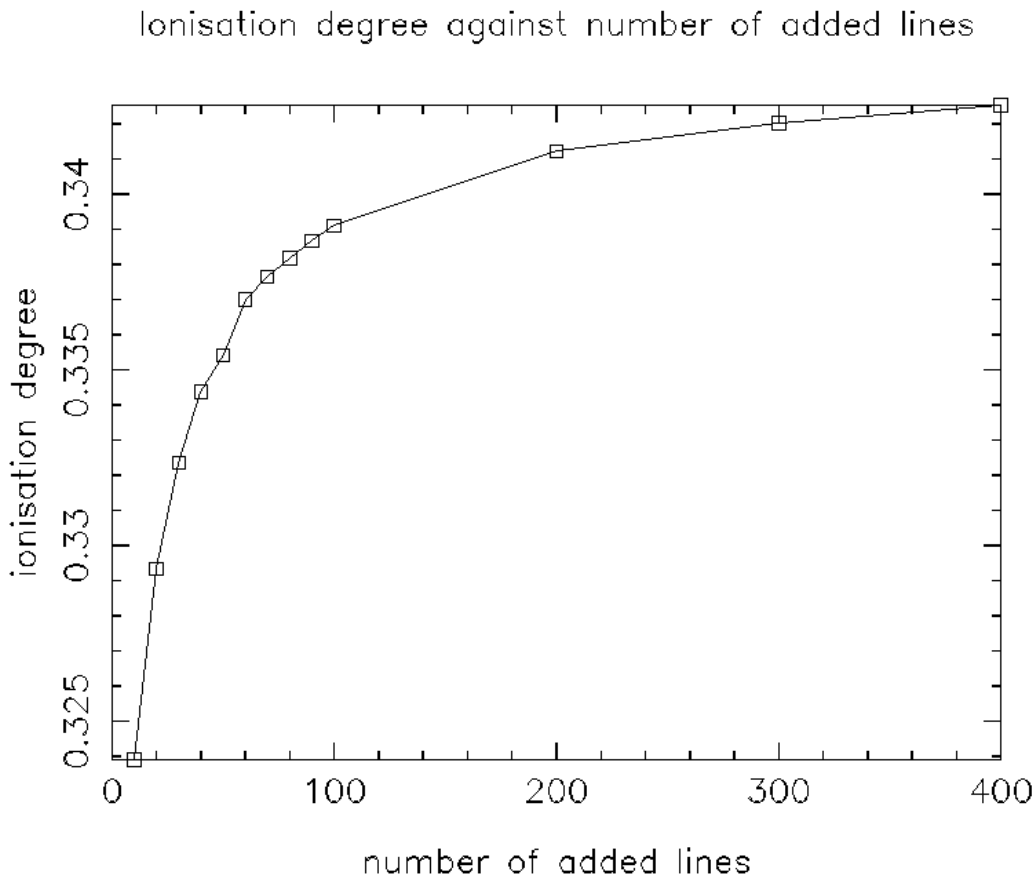

Figure 4.6: Ionisation degree against number of CHIANTI lines added, with the highest lines added first.

ranges of wavelength and the resultant sum divided by the width of the range to get flat values to add to the incident radiation. This will not result in an increase in computational time. These ranges are smaller the closer they are to the Lyman edge to retain some information about the position of the lines, given that as mentioned before the position of a line matters more the closer it is to the Lyman edge.

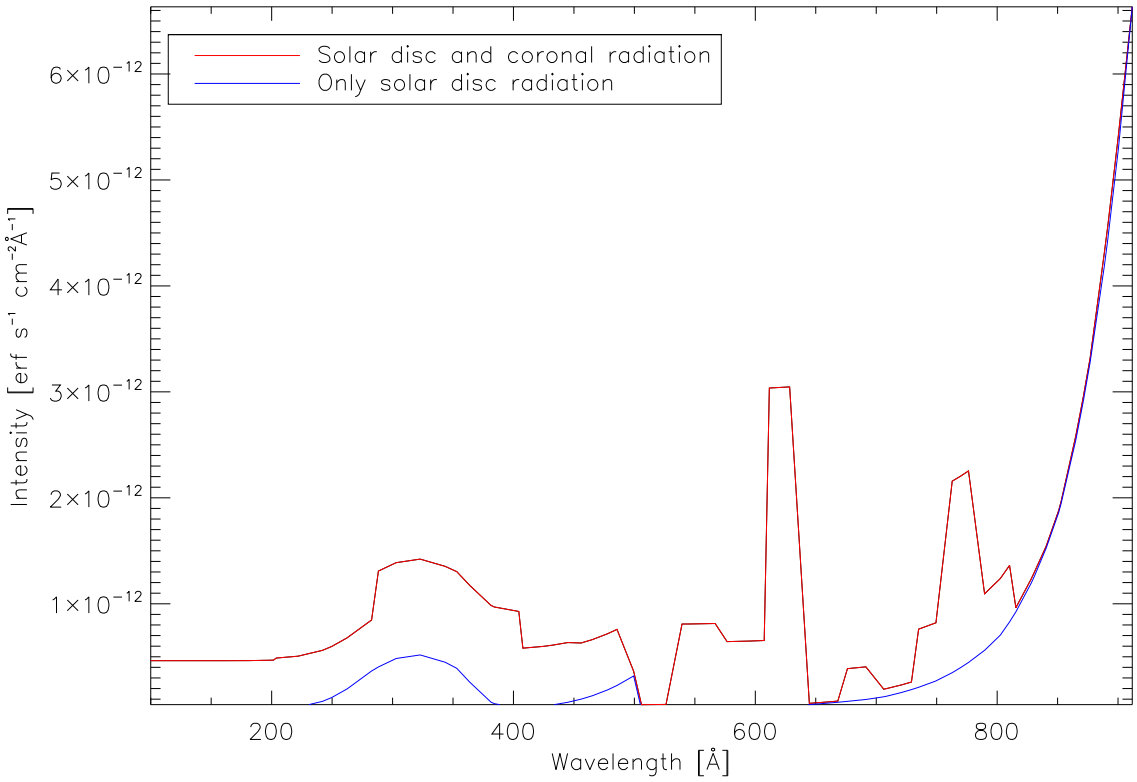

Figure 4.7: A comparison of the incident radiation with the coronal radiation and without the corona radiation below 912Å.

4.4 Adding the incident radiation

With the optimal way to add the coronal incident radiation determined, this can now be included in the radiative transfer calculations. Figure 4.7 shows the increase in incident radiation below 912 Å that results when the binned coronal radiation is added to the total incident radiation.

Table 4.1: The parameters of the iso-thermal iso-baric slabs considered.

Model	Temperature(K)	Pressure(dyn cm^{-2})	Thickness(km)	Height(km)
1	6,000	0.01	200	10,000
2	6,000	1.	200	10,000
3	6,000	0.01	5000	10,000
4	6,000	1.	5000	10,000
5	10,000	0.01	200	10,000
6	10,000	1.	200	10,000
7	10,000	0.01	5000	10,000
8	10,000	1.	5000	10,000
9	6,000	0.01	200	50,000
10	6,000	1.	200	50,000

4.4.1 Iso-Thermal Slabs

To see the difference that including the coronal radiation in the incident radiation makes a comparison of iso-thermal prominence slabs is made. The comparison is between the radiative transfer calculations using the additional radiation and the result of the radiative transfer calculations without using the additional coronal radiation.

The iso-thermal prominences are considered at a variety of temperatures, pressures, thicknesses and heights above the solar surface. Tables of the resultant prominence conditions for a selection of these iso-thermal prominences are in appendix A.1. They show prominences at high and low temperatures and pressures at heights of 10,000 and 50,000 km above the solar surface. The full list of iso-thermal prominences presented in this appendix are in table 4.1.

Reassuringly, adding the coronal radiation always results in the prominence being more ionised than it would be without the coronal radiation. Figure 4.7 shows us that

the coronal radiation makes up a very significant proportion of the incident radiation below 912 Å, incident radiation which ionises ground state hydrogen. 54% of the incident radiation in this range comes from the corona.

These prominences being further ionised results in there being more free electrons. If there were more free electrons with the same hydrogen densities then this would result in the pressure increasing. The pressure, however, is the same in each case. To have the same pressure with an increased proportion of free electrons in the prominence plasma then the total number of hydrogen atoms and ions has to be fewer. This is why for each case the total hydrogen density is shown as being lower.

In percentage terms, this reduction in hydrogen density is greater for the low pressure cases than for the high pressure cases. For the low pressure cases, the intensity of the emergent hydrogen lines is lower with the coronal radiation than it is without the coronal radiation. Given there is significantly less hydrogen to emit the emergent hydrogen lines, the intensity of these lines will be reduced.

For the high pressure cases the difference in hydrogen density is not very significant, half a percent difference, so the change in the hydrogen density will not impact the hydrogen lines emitted by the prominence in the high pressure cases. Here the emergent hydrogen lines reflect the increased number of transitions that will occur due to the increased ionisation of the prominence. There is more ionised hydrogen, and so there will be more cases of ionised hydrogen combining with an electron to form neutral hydrogen. Hydrogen formed this way will have its electrons in a very excited state. These electrons will de-excite down, until they reach the ground state and are ionised. This increase in transitions means that the intensity of the emission lines corresponding to these transitions will also increase.

This increase in line intensity is not necessarily uniform across the entire line profile. In the case of the Lyman α line the increase in intensity is greater in the wings of the

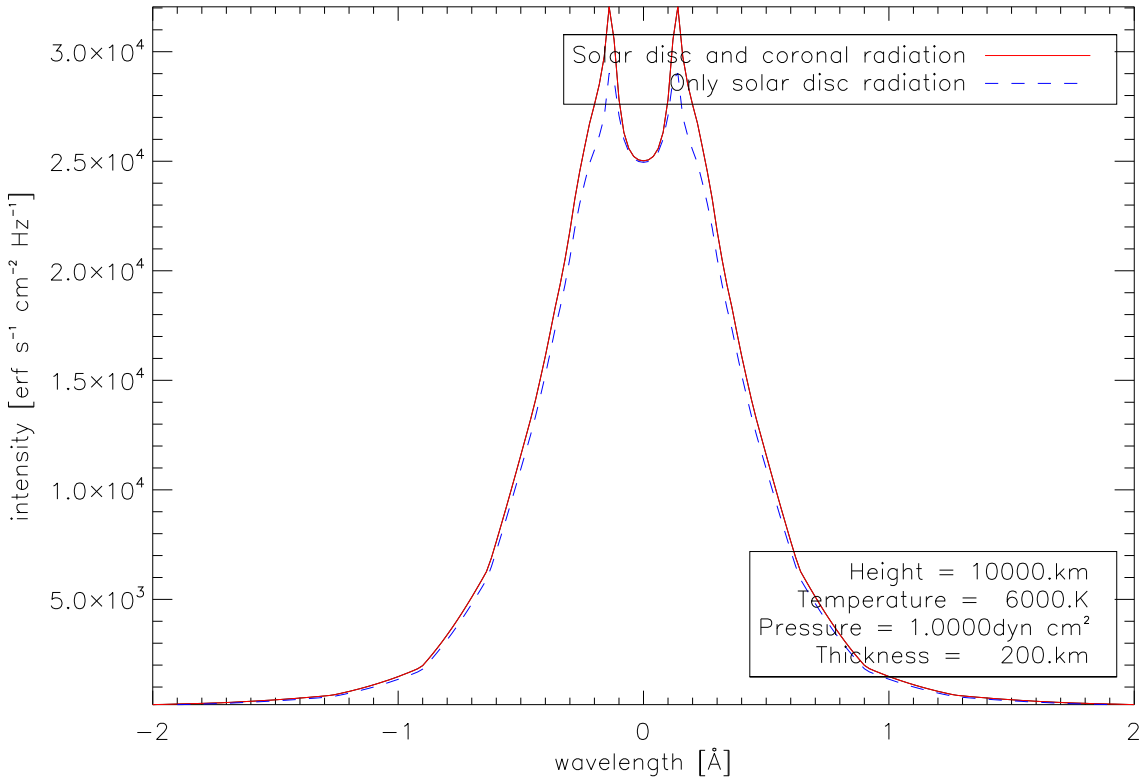

Figure 4.8: The Lyman α line profile for the low temperature high pressure thin iso-thermal case, the second case listed in table 4.1.

line than it is in the line centre, as can be seen in figure 4.8. This is due to the very high optical thickness of the centre of the line which results in the self inversion of the line being at its maximum possible depth.

The line profile of Lyman β for the second case is shown in figure 4.9. For Lyman β the change in line intensity is also more evident away from the line centre than it is in the line centre. The increase in intensity at the horns of the line is far more than the increase of intensity at the central peak.

In lines lacking a reversal, such as the Hα line any change in intensity is evident across the entire profile. 4.10.

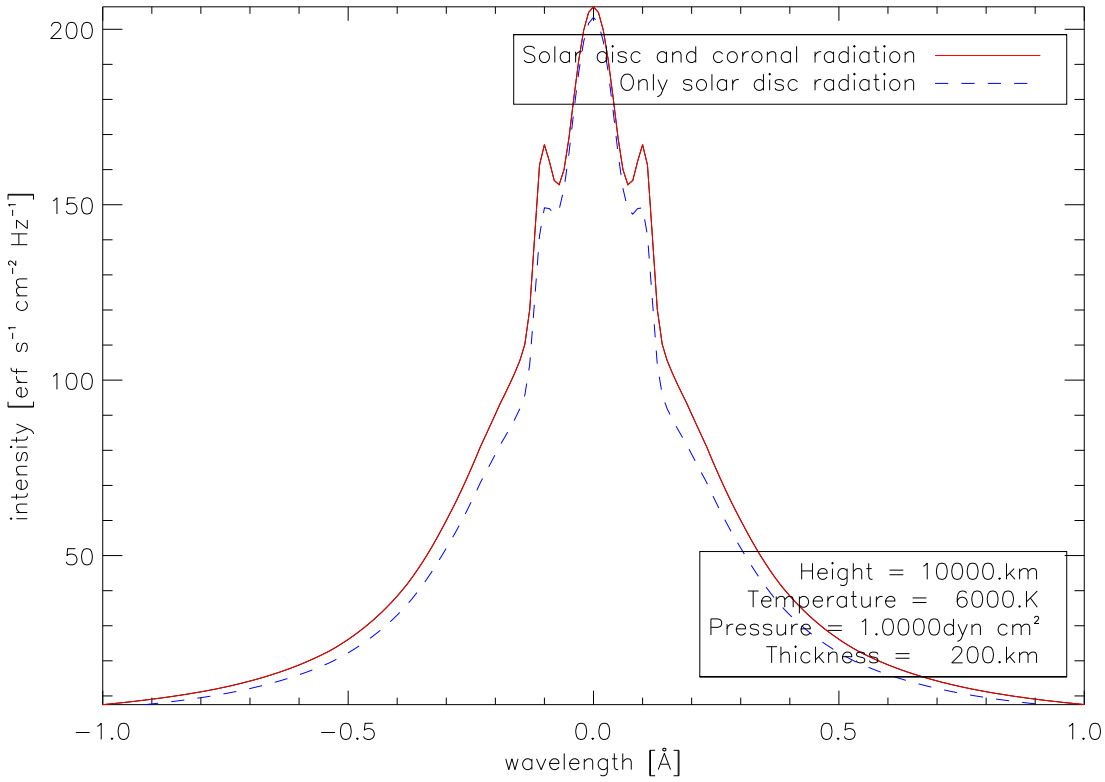

Figure 4.9: The Lyman β line profile for the low temperature high pressure thin iso-thermal case, the second case listed in table 4.1.

The continuum emissions of the prominence also show a change. Unlike the emission lines, the continuum emissions are always greater for when the incident radiation includes the coronal radiation. For most temperatures and thicknesses the Lyman Continuum emissions are stronger for the low pressure case than for the high pressure case. The optical depth of the prominence in the Lyman continuum decreases more with the inclusion of the coronal radiation in the incident radiation for the low pressure case than for the high pressure case, which allows continuum emissions from deeper in the prominence to reach the surface.

The coronal radiation has less of an effect on the high temperature cases. Here more of the ionisation is collisional due to the temperature of the plasma than in the low temperature cases and so proportionally ionisation due to radiation is a smaller

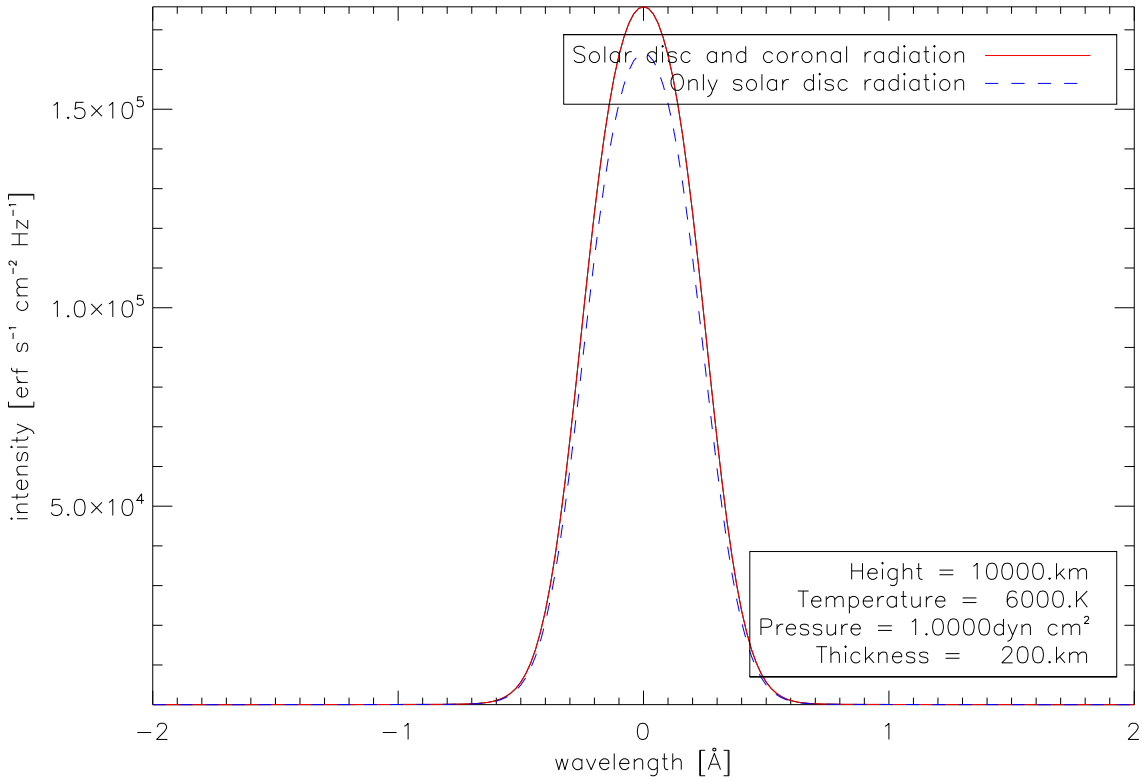

Figure 4.10: The H α line profile for the low temperature high pressure thin iso-thermal case, the second case listed in table 4.1.

part of the ionisation.

In all the low pressure cases the change due to the coronal radiation in the centre of the prominence as great as it is at the surface however for the high pressure cases this is not always true. Only in the second case, a low temperature, thin, high pressure prominence, does a high pressure prominence have its centre influenced by the coronal radiation as much as its surface. With the thick prominences high pressure prominences they have a high optical thickness because with them there is more material present than in the other cases. The radiation is absorbed before it can reach the centre.

4.4.1.1 Comparison with Previous Studies

The iso-thermal iso-baric slabs presented here were set up with temperatures, pressures and thicknesses similar to such parameters in previous studies of iso-thermal iso-baric slabs, which means the results can be compared to some others directly. Given that such modelling is how non-directly observable properties of prominences are determined, this will give us some clue as to how such non-observable estimates would have differed had coronal radiation been included in the incident radiation of previous studies.

The models presented here actually match some of the iso-thermal iso-baric models examined by Gouttebroze et al. (1993), hereafter referred to as GHV, so a direct comparison between some of the models is possible. The authors presented results for 140 model prominences. Prominences under the effects of coronal radiation differ from the GHV prominences in similar ways as the differences between prominences with and without the coronal radiationseen in section 4.4.1, though to different degrees in some cases. A table comparing some of the results with some of the GHV results can be seen in table 4.3.

The electron density of the prominences with coronal radiation is greater than the GHV prominences in the low temperature cases, the difference is more than the difference between the prominences with and without coronal radiation in the incident radiation in section 4.4.1. The hydrogen density is lower than in GHV so it is understood that the prominences with the coronal radiation are more heavily ionised than the prominences considered in GHV in the low temperature cases. In the high temperature cases, on the other hand, the difference is much smaller, so it is understood that this is because at high temperatures photo-ionisation is less of a contribution to the total ionisation of the prominence plasma as thermal sources of ionisation are more important.

The emergent hydrogen line intensities can be compared. In the low pressure cases

comparing the emergent lines of the prominences with the corona radiation to the GHV prominences' emergent lines, there is a similar reduction in intensity as was seen in section 4.4.1. For the high pressure cases, where in section 4.4.1 what was seen was a increase in the emergent line intensity by adding the coronal radiation, here it is only seen that the prominences here have a higher Lyman α intensity, while the Hα line shows a reduction in intensity. However in section 4.4.1 the prominences without the coronal radiation also show Hα as being significantly less than the GHV paper, and so the difference in Hα is not due to the addition of the coronal radiation to the incident radiation.

Heasley & Mihalas (1976) considered prominences as plane parallel slabs standing vertically on the solar surface and so unlike in Gouttebroze et al. (1993) they do not have to consider a height dependent dilution factor and can simply multiply the incident radiation by 0.5. For comparison with the results of this paper the calculations of this chapter with the coronal radiation have been applied to a few of their iso-thermal iso-baric slabs and the results of this are seen in table 4.4.

Heasley & Milkey (1976) was a follow up paper to Heasley & Mihalas (1976) to present the results for helium, but it also presented some results for hydrogen. Again the calculations of this chapter with the coronal radiation are applied to a few of their iso-thermal iso-baric slabs and the results of this are in table 4.6.

What is seen in these tables is that although the results here with the coronal radiation differ from the results of these papers, most of the difference is not due to the presence of the coronal radiation in the calculations here. The results for these slabs without the coronal radiation also differ from the results of these papers by a similar degree. So the addition of the coronal radiation to the incident radiation makes a small difference to studies of this time period compared to the difference due to all the other improvements in 1-D plane parallel radiative transfer since then.

4.4.2 PCTR Models

Table 4.2: The parameters of the slabs with a PCTR considered.

Model	Internal Temperature(K)	Internal Pressure(dyn cm^{-2})	Column Mass(g cm)	Height(km)
1	6,000	0.01	2×10^{-7}	10,000
2	6,000	1.	2×10^{-7}	10,000
3	6,000	0.01	4×10^{-6}	10,000
4	6,000	1.	4×10^{-6}	10,000
5	10,000	0.01	2×10^{-7}	10,000
6	10,000	1.	2×10^{-7}	10,000
7	10,000	0.01	4×10^{-6}	10,000
8	10,000	1.	4×10^{-6}	10,000
9	6,000	0.01	2×10^{-7}	50,000
10	6,000	1.	2×10^{-7}	50,000

Iso-thermal models can be informative about the interior of the prominence but are not as useful for outside there. To consider the effects on the whole prominence the prominence to corona transition region must be included. Prominences with a PCTR are considered whose internal conditions are similar to the iso-thermal prominences in the previous subsection. They are given column masses similar such that they have similar thicknesses to the iso-thermal prominences in the previous subsection. The prominence conditions considered are listed in table 4.2.

The tables for prominences with a PCTR are in appendix A.2. The surface of the prominence is similar to the corona and so is already mostly ionised and adding more incident radiation does not change this. The impact of the coronal radiation on the ionisation of the plasma then can only seen in the cool, dense centre of the prominence. An increase in the ionisation at the centre of the prominence is seen only for the cases

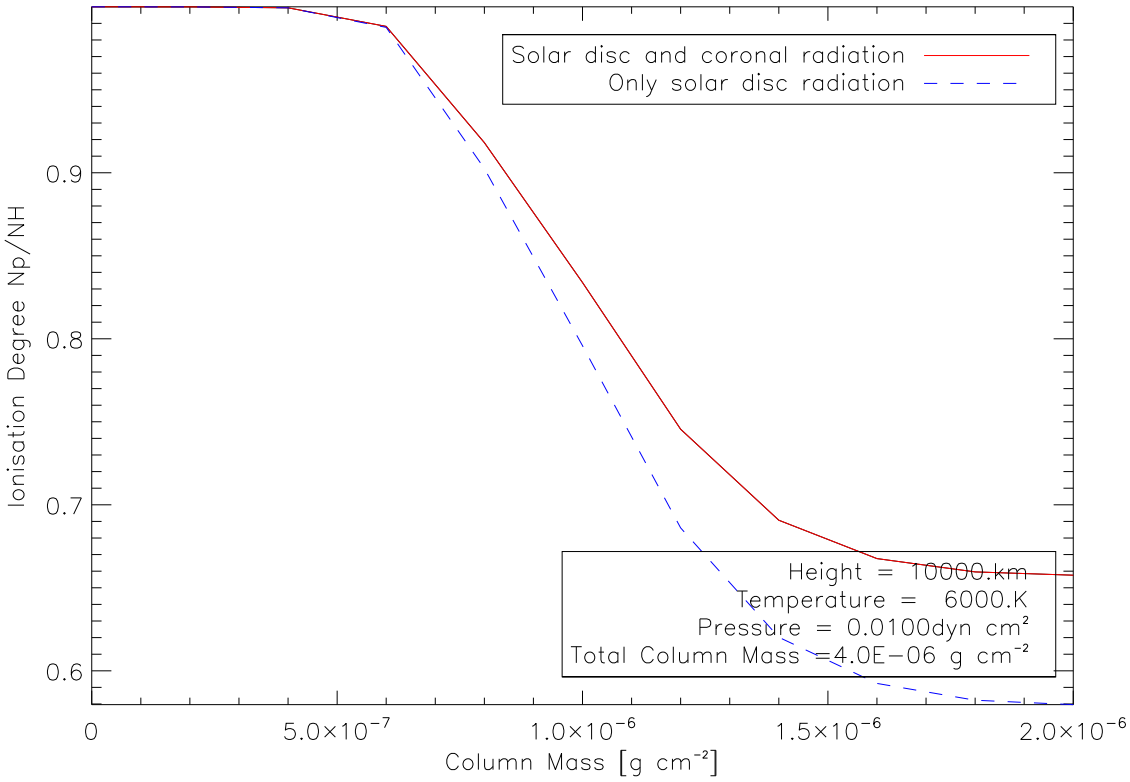

Figure 4.11: The ionisation degree $\frac{n_p}{n_H}$ against column mass for the first PCTR case listed in table 4.2. The graph shows from the surface of the prominence at column mass 0 to the centre of the prominence.

with a low central pressure. The cases with a high central pressure do not show any impact from the addition of the coronal radiation on the ionisation of the hydrogen.

This difference between the low pressure and high pressure cases can be seen in figures 4.11 and 4.12. In the low pressure case presented in figure 4.11 the gap between the ionisation degree with the additional incident radiation and the ionisation degree without it forms at the boundary of the transition region and continues on into the centre of the prominence. In the high pressure case shown in figure 4.12 there is a much smaller difference at all depths in the prominence between the ionisation degree with the coronal radiation included in the incident radiation and with it not included. Figure 4.13 shows the variations in the neutral hydrogen and the ionised hydrogen,

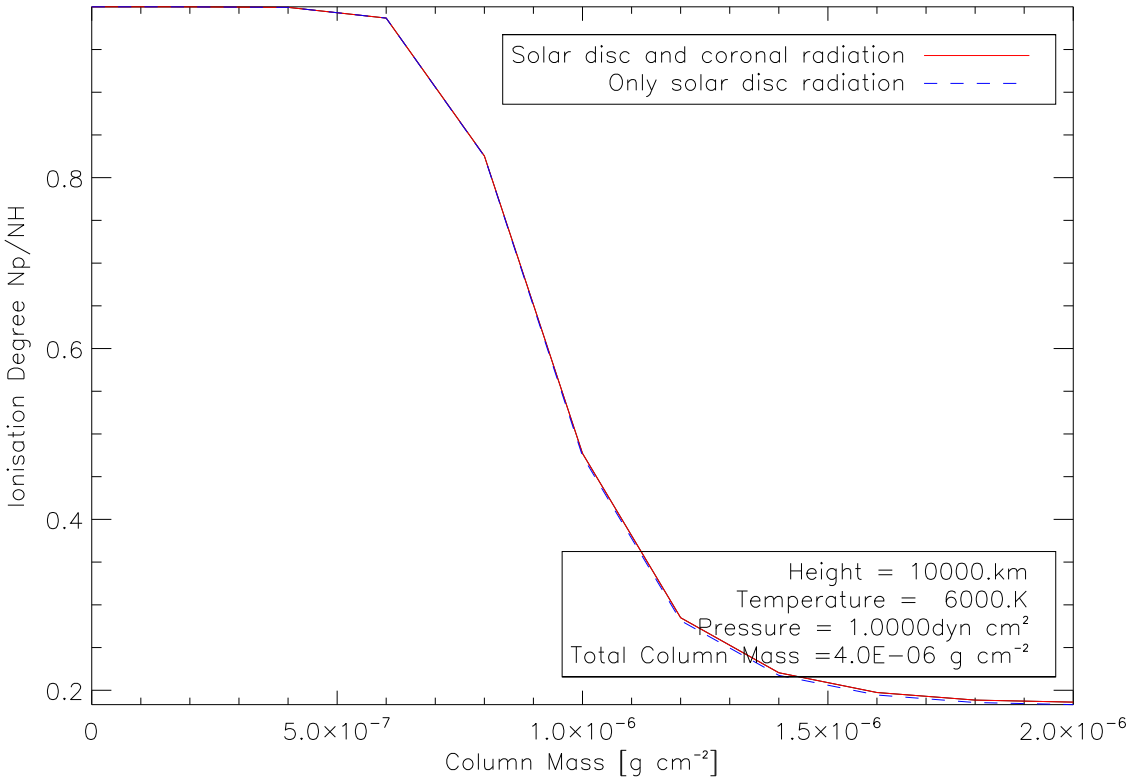

Figure 4.12: The ionisation degree $\frac{n_p}{n_H}$ against column mass for the second PCTR case listed in table 4.2. The graph shows from the surface of the prominence at column mass 0 to the centre of the prominence.

protons, through the prominence whose ionisation degree is shown in figure 4.11, it shows the increase in the ionisation degree of the prominence being due to the increase in the amount of ionised hydrogen.

The hydrogen emission lines for the case of the centre being low pressure are reduced with the introduction of the coronal radiation to a similar degree as in the iso-thermal models with low pressure. There is a significant reduction in the hydrogen density here as there is in the isothermal case. The continuum emissions also show a change which is similar to their change in the isothermal case, they are increased here as they are in the isothermal case. Although the change due to the addition of the coronal radiation is mostly in the centre of the prominence, the observable effects, the effects on the

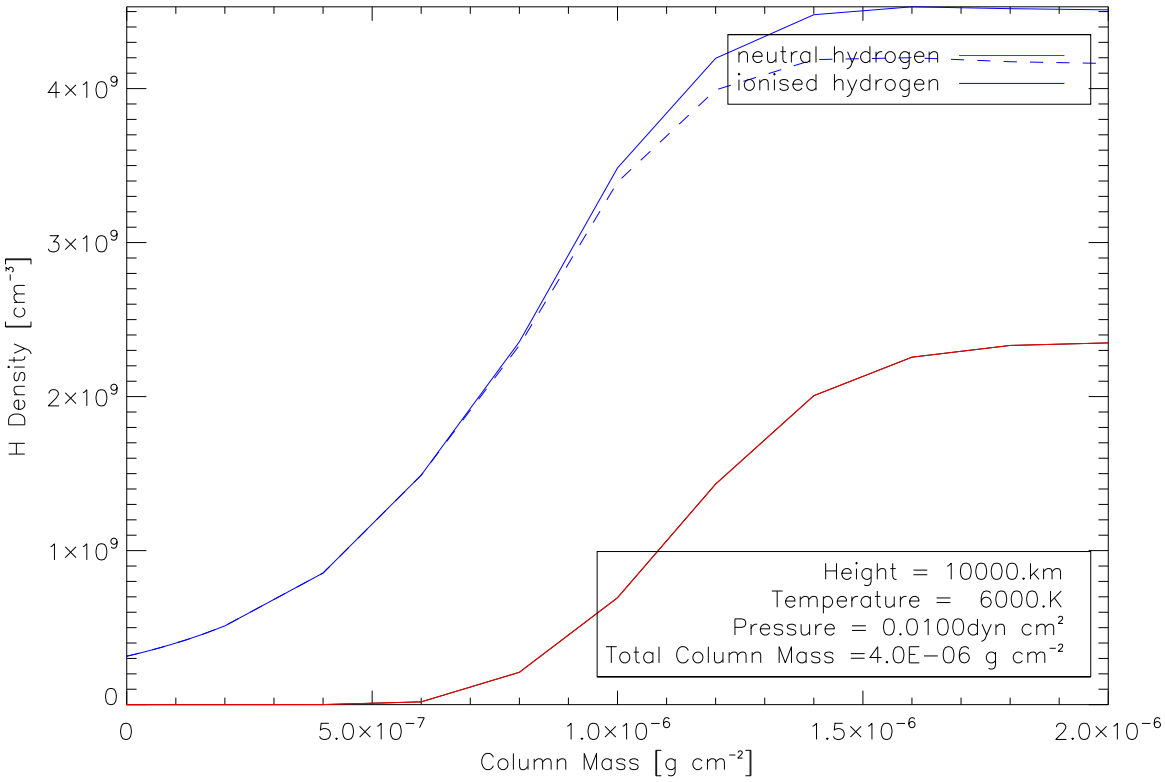

Figure 4.13: The variations in hydrogen density through the prominence, from suface to centre for the first PCTR case listed in table 4.2. Dashed lines show the hydrogen density for where the incident radiation only includes the solar disc radiation, solid lines show the hydrogen density for where the incident radiation includes the solar disc and coronal radiation.

emissions of the prominence, are still visible.

In the iso-thermal case, the intensity at the centre of the Lyman α line is not affected by the addition of the coronal radiation, because the self reversal is at its maximum depth. In the PCTR case, the self reversal of this line is not at its maximum depth, and so changes to the intensity of the Lyman α will show up at line centre. This can be seen in figure 4.14 which shows the Lyman α line profile for the third PCTR case.

There is no noticeable difference in the emission line for the high central pressure

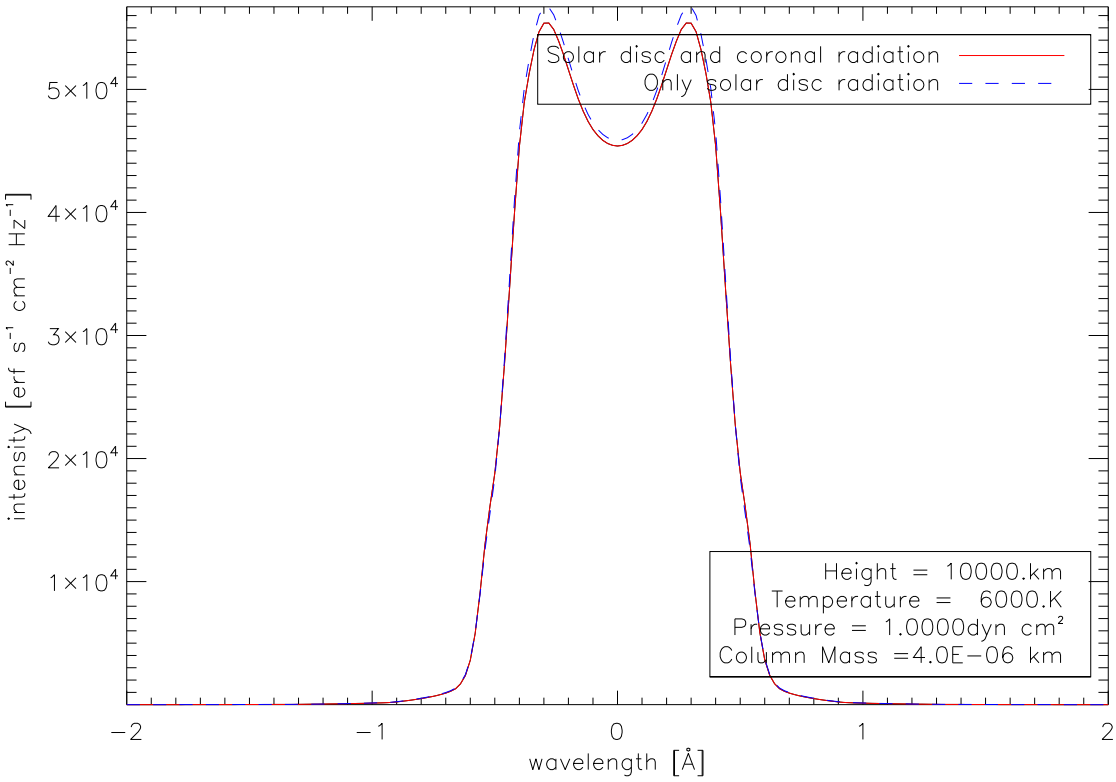

Figure 4.14: The Lyman α line profile for the third PCTR case colorredlisted in table 4.2.

cases.

4.5 Conclusions

The modifications to the radiative transfer code used are described in section 4.2. The incident radiation to the hydrogen continuum is changed so that additional radiation not from the solar surface can be added to this incident radiation. This additional incident radiation can be added either as individual lines, in which case more data points describing the incident radiation have to be added to the code to describe each individual line, or as average intensities across a wavelength range, in which case the

average intensity of the wavelength range is added to all datapoints within this range.

The functioning of these modifications to the code are examined in section 4.3. First a single test line of arbitrary height and width is added and moved in wavelength from 100Å to 1000Å and the effects of this moving line on a iso-thermal iso-baric prominence are looked at. The ionisation degree $\frac{n_p}{n_H}$, Lyman α intensity and hydrogen α intensity all show that the effects of the line on the prominence are stronger when the line is closer to 912Å, the ionisation edge. Next multiple test lines are added to test the effects of adding many separate lines at once, it was decided from this that the increased computational time is not worth the additional time the code takes to run when adding many individual lines.

As a result it was decided to sum up the intensity of all lines within a wavelength range and to add the average intensity of each range to the incident radiation, the effects of this on the incident radiation can be see in figure 4.7. The ranges get smaller the closer they are to the ionisation edge in order to take into account the fact that the position of a line matters more the closer it is to the edge.

The results of adding the actual coronal radiation are examined for iso-thermal iso-baric plane parallel slabs in section 4.4.1. The slabs considered are detailed in table 4.1 and the results are shown in appendix A.1. The coronal radiation has a significant effect on the ionisation of these models and on their emissions. It was shown that the effect on the emergent hydrogen lines is not uniform across the line profiles resulting in a slight change of shape for Lyman α and β. Comparisons were made to previous studies of is-thermal slabs and for comparisons with Gouttebroze et al. (1993) what is seen are similar differences to the differences seen in the calculations of this chapter with and without the coronal radiation.

The effects of the coronal radiation in the incident radiation were next applied to models with a PCTR in section 4.4.2. The surface is already mostly ionised and so

doesn't show any effect from the coronal radiation. The centre of the prominence only shows signs of increased ionisation in the low pressure cases. The emissions of the prominence in the PCTR case are affected, although they line intensities are reduced instead of increased as they are in the iso-thermal cases.

The coronal radiation will have an effect on the prominence plasma parameters, but it is important to include the PCTR when considering the effects of the coronal radiation.

Table 4.3: Comparison of hydrogen properties between those in Gouttebroze et al. (1993) and those from the radiative transfer code used in this work with the coronal radiation included in the incident radiation. Slab # refers to the position of the iso-thermal slab in 4.1

		n_H [cm^{-3}]		n_e [cm^{-3}]		[erg s^{-1} cm^{-2} Sr^{-1}]			
Model	Slab #	Surface	Centre	Surface	Centre	I(Lyα)	I(Hα)	$\tau(Ly\alpha)$	$\tau(H\alpha)$
GHV	1	6.7E9	6.7E9	4.7E9	4.7E9	7.32E3	5.34E2	2.75E3	5.68E-3
Solar Disc and Corona	1	6.43E9	6.42E9	4.99E9	5.01E9	7.18E3	3.53E2	1.93E3	4.17E-3
GHV	2	1.E12	1.E12	9.9E10	6.4E10	2.56E4	1.05E5	1.3E8	1.53
Solar Disc and Corona	2	9.97E11	1.04E12	1.09E11	6.33E10	2.85E4	9.46E4	1.29E6	1.62
GHV	3	6.7E9	6.6E9	4.7E9	4.8E9	1.52E4	1.44E4	6.38E4	1.62E-1
Solar Disc and Corona	3	6.53E9	6.51E9	4.88E9	4.91E9	1.53E4	1.23E4	5.4E4	1.61E-1
GHV	4	1.E12	1.1E12	1.E11	4.5E10	2.69E4	3.52E5	3.43E7	1.29E1
Solar Disc and Corona	4	9.96E11	1.08E12	1.1E11	2.22E10	2.89E4	2.12E5	3.54E7	5.77
GHV	5	3.6E9	3.6E9	3.3E9	3.3E9	7.96E3	1.67E2	6.24E2	1.31E-3
Solar Disc and Corona	5	3.54E9	3.54E9	3.35E9	3.35E9	7.7E3	1.04E2	4.25E2	8.91E-4
GHV	6	5.E11	3.8E11	1.7E11	3.E11	1.64E5	4.73E5	1.12E5	7.39
Solar Disc and Corona	6	5.02E11	3.86E11	1.71E11	2.99E11	2.02E5	4.26E5	1.14E5	7.34
GHV	7	3.6E9	3.3E9	3.3E9	3.3E9	2.3E4	4.25E3	1.33E4	3.55E-2
Solar Disc and Corona	7	3.55E9	3.53E9	3.33E9	3.35E9	1.19E4	3.2E3	1.05E4	3.04E-2
GHV	8	4.8E11	3.5E11	1.9E11	3.3E11	8.61E5	1.69E6	7.62E5	1.11E2
Solar Disc and Corona	8	4.77E11	3.54E11	1.98E11	3.34E11	1.26E6	1.63E6	7.27E5	1.11E2

Model	T [K]	p [dyn cm^{-2}]	D [km]	Ionisation Degree surface	Ionisation Degree centre	$\tau(912\AA)$	$\tau(Ly\alpha)$	$\tau(H\alpha)$	[erg s^{-1} cm^{-2} Sr^{-1}] I($Ly\alpha$)	I($H\alpha$)	I($H\beta$)
	7000	0.13	3200								
Heasley & Mihalas (1976)				1.3	1.2	36	6.5E5	1.17	5.27E4	6.52E5	1.02E5
Solar Disc and Corona				0.52	0.36	138	1.4E6	2.8	3.2E4	1.5E5	2.4E4
Only Solar Disc				0.48	0.34	143	1.5E6	2.6	3.E4	1.4E5	2.2E4
	7000	0.26	1400								
Heasley & Mihalas (1976)				0.76	0.67	47	8.4E5	1.43	5.63E4	7.5E5	1.24E5
Solar Disc and Corona				0.33	0.23	143	1.5E6	2.8	3.2E4	1.5E5	2.4E4
Only Solar Disc				0.31	0.22	146	1.5E6	2.6	3.1E4	1.4E5	2.2E4
	7000	0.26	4800								
Heasley & Mihalas (1976)				0.76	0.67	1.6E2	2.9E6	4.44	8.89E4	1.39E5	3.52E5
Solar Disc and Corona				0.34	0.21	513	5.2E6	7.6	3.7E4	2.7E6	5.9E4
Only Solar Disc				0.31	0.2	518	5.3E6	7.2	3.5E4	2.6E5	5.7E4
	8000	0.13	4100								
Heasley & Mihalas (1976)				1.7	5.	16	2.8E5	1.58	8.75E4	8.02E5	1.37E5
Solar Disc and Corona				0.64	0.92	103	9.9E5	4.4	4.1E4	2.1E5	3.9E4
Only Solar Disc				0.59	0.89	105	1.E6	4.3	4.E4	2.1E5	3.8E4

Table 4.4: Comparison of hydrogen properties between those in Heasley & Mihalas (1976) and those from the radiative transfer code used in this work both for with the coronal radiation included in the incident radiation and with the coronal radiation not included in the incident radiation.

Model	T [K]	p [dyn cm^{-2}]	D [km]	Ionisation Degree surface	Ionisation Degree centre	$\tau(912\AA)$	$\tau(Ly\alpha)$	$\tau(H\alpha)$	[erg s^{-1} cm^{-2} Sr^{-1}] I($Ly\alpha$)	I($H\alpha$)	I($H\beta$)
	8000	0.26	2000								
Heasley & Mihalas (1976)				1.	3.7	20	3.6E5	2.81	1.35E5	1.13E6	2.35E5
Solar Disc and Corona				0.414	0.735	117	1.1E6	6.5	5.2E4	2.7E5	5.7E4
Only Solar Disc				0.38	0.72	119	1.1E6	6.4	5.1E4	2.7E5	5.6E4
	8000	0.56	3000								
Heasley & Mihalas (1976)				0.63	2.5	81	1.4E6	16.6	4.03E5	2.22E6	9.45E5
Solar Disc and Corona				0.27	0.78	374	3.6E6	35	1.2E5	6.7E5	2.5E5
Only Solar Disc				0.25	0.77	375	3.6E6	35	1.2E5	6.7E5	2.5E5

Table 4.5: Table 4.4 continued.

Model	T [K]	p [dyn cm^{-2}]	D [km]	Ionisation Degree surface	Ionisation Degree centre	$\tau(912\AA)$	$\tau(Ly\alpha)$	$\tau(H\alpha)$	[erg s^{-1} cm^{-2} Sr^{-1}] I($Ly\alpha$)	I($H\alpha$)	I($H\beta$)
	7500	0.065	1500								
Heasley & Milkey (1976)				2.3	3.	8.6	9.6E4	0.25	2.54E4	2.38E4	3.16E3
Solar Disc and Corona				0.93	0.97	18	2.E5	0.62	2.4E4	4.3E4	5.1E3
Only Solar Disc				0.84	0.87	20.2	2.2E5	0.59	2.3E4	4.1E5	4.8E3
	7500	0.065	3800								
Heasley & Milkey (1976)				2.4	3.6	18.8	2.E5	0.65	4.21E4	5.79E4	8.34E3
Solar Disc and Corona				0.93	0.83	90.7	9.8E5	2.7	3.2E4	1.3E5	2.1E4
Only Solar Disc				0.84	0.77	95.7	1.E6	2.5	3.E4	1.3E5	2.E4
	7500	0.26	320								
Heasley & Milkey (1976)				0.8	1.2	15.6	1.7E5	0.56	3.92E4	5.08E4	7.17E3
Solar Disc and Corona				0.37	0.39	26.1	2.8E5	0.89	2.7E4	5.9E4	7.33E3
Only Solar Disc				0.34	0.36	27.1	2.9E5	0.82	2.6E4	5.5E4	6.7E3
	9500	0.065	2200								
Heasley & Milkey (1976)				3.9	7.3	4.8	5.2E4	0.22	2.64E4	2.12E4	2.8E3
Solar Disc and Corona				1.44	2.66	11	1.1E5	0.62	2.6E4	5.1E4	6.E3
Only Solar Disc				1.3	2.53	11.6	1.1E5	0.62	2.5E4	5.1E4	5.9E3

Table 4.6: Comparison of hydrogen properties between those in Heasley & Milkey (1976) and those from the radiative transfer code used in this work both for with the coronal radiation included in the incident radiation and with the coronal radiation not included in the incident radiation.

Model	T [K]	p [dyn cm^{-2}]	D [km]	Ionisation Degree surface	Ionisation Degree centre	$\tau(912\AA)$	$\tau(Ly\alpha)$	$\tau(H\alpha)$	[erg s^{-1} cm^{-2} Sr^{-1}] I($Ly\alpha$)	I($H\alpha$)	I($H\beta$)
	9500	0.065	7000								
Heasley & Milkey (1976)				4.3	12.8	9.2	1.E5	0.7	5.59E4	6.26E4	9.13E3
Solar Disc and Corona				1.48	3.86	26.3	2.5E5	2.2	4.1E4	1.4E5	2.E4
Only Solar Disc				1.34	3.78	27.1	2.6E5	2.2	4.E4	1.4E5	2.E4
	9500	0.26	670								
Heasley & Milkey (1976)				1.7	6.5	6.8	7.6E4	1.	8.42E4	8.63E4	1.32E4
Solar Disc and Corona				0.8	1.98	10.7	1.E5	0.95	3.3E4	7.4E4	9.1E3
Only Solar Disc				0.74	1.93	11.	1.1E5	0.95	3.2E4	7.3E4	9.E3

Table 4.7: Table 4.6 continued.

Chapter 5

Helium

5.1 Helium compared to Hydrogen

The state of helium in a prominence, its degree of ionisation and its emissions, has little effect on the hydrogen of the prominence, however the opposite is not true. The influence of the prominence's hydrogen on its helium and the lack of the converse is why the radiative transfer problem for helium has to be solved in the calculations after a solution for hydrogen has been reached, but the initial solution for hydrogen is sufficient to describe the state of hydrogen in the prominence.

Neutral hydrogen only has one electron, so there exists only one positive ion of hydrogen, when it is stripped of its sole election. Neutral helium, however, has two electrons so there exists two positive ions of helium, He II is missing one electron and He III is missing both the electrons. The energy levels of the excited electron for neutral helium are different from the energy levels of the single HeII electron, hence these two states of helium will have different transition lines.

They have different energy levels but HeII is still the ionised form of neutral helium and so they have to be treated together. This is normally done by considering an atom with both "HeI levels" and "HeII levels" as well as the final state representing fully ionised helium. This way a transition from a "HeI level" to the level representing the ground state of HeII represents ionisation, and a transition from the level representing ground state HeII to a HeI level represents recombination. Transitions from a HeI level to another of the HeII levels is not permitted, for in neutral helium there is one ground state electron and one excited electron, when the excited electron is ionised off only the ground state electron is left in the resultant HeII ion. The fully ionised level is only permitted transitions with the HeII levels, for ionisation and recombination are processes involving only one electron being stripped from or added to the ion. As far as how this is done in these radiative transfer calculations, similarly to how the calculations used treats hydrogen as having 21 energy levels, 20 actual levels and one ionised level, helium is treated as having 34 energy levels, 29 levels of neutral helium, 4 levels of HeII and 1 fully ionised level. This arrangement of 34 levels was used by Benjamin et al. (1999) to match the results of 3000 level calculations in nebulae so this arrangement of 34 levels is sufficient.

A further complication to the helium energy levels is the presence of two systems of energy levels in the neutral helium case, due to the presence of two electrons. There is the parahelium case where the two electrons have opposite spin and the orthohelium case where the excited electron's spin is parallel to the ground state electron. Also known as the singlet and triplet cases, due to the number of ways the spin of the two electrons can be combined to equal zero. Given that it is only in the singlet case that the two electrons can share the ground state, for two electrons with the same spin cannot share an energy level, it is only in the singlet case that resonant transitions occur and recombination directly to the ground state results in a helium atom in the parahelium case. However this is not to say that there is no link between the populations of the two cases. The singlet and triplet cases are coupled due to collisional transitions between the two systems, and a helium atom under one system can undergo ionisation

and then under recombination wind up in the other system. (Labrosse & Gouttebroze 2004; Haken et al. 2005)

5.2 Modifications to the Code

The modifications to the helium section of the calculations was carried out in a similar fashion to the modifications to the hydrogen section.

Again, only the incident radiation capable of ionising the ground state is considered due to the densities involved. It was shown in chapter 4 with hydrogen that lines too high in wavelength, that is too low in frequency, to ionise the ground state have a negligible effect on the ionisation of the prominence due to the comparatively lower population levels of states above the ground state, around 10^9 cm^{-2} for ground state hydrogen compared to 10^2 cm^{-2} for the first excited state in the low temperature and pressure case in the results of the radiative transfer code.

It is also the case with helium, for both HeI and HeII, that the ground state is vastly more populated than the first excited state. For the low temperature and pressure prominence the number density of ground state HeI is around 10^8 cm^{-2} compared to 10^{-1} cm^{-2} for the first excited state. Given that the densities differ by 9 orders of magnitude, compared to 7 order of magnitude for hydrogen, it can again be expected that incident radiation which cannot ionise the ground state of HeI to have as little effect as radiation not capable of ionising ground state hydrogen.

The same is true of HeII. Here for the low pressure, low temperature prominence the ground state number density is around 10^8 cm^{-2} compared to 10^{-1} cm^{-2} for the first excited state, so with HeII it again can be expected that only radiation capable of ionising the ground state to have a significant impact on the population levels.

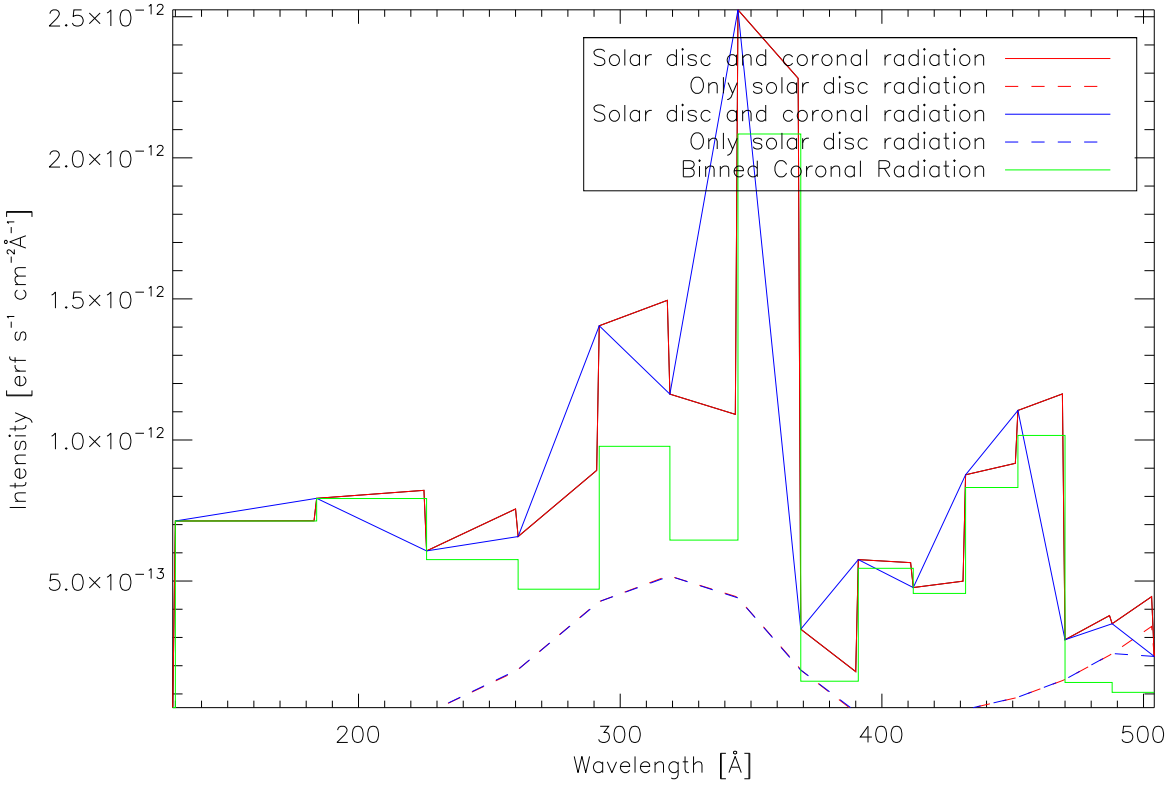

Figure 5.1: A comparison of the incident radiation to the HeI ground state continuum, the 504 Å continuum, with and without the additional coronal radiation. The dashed lines show the incident radiation without the coronal radiation. The green line shows only the binned coronal radiation. The blue line shows the result of adding the coronal radiation without modifying the data points which describe the continuum. The red line shows the full incident radiation adjusted so the binned coronal radiation is properly described.

Only the ionisation of the ground state being relevant means that it is only necessary to add to the incident radiation coronal lines below 504 Å for HeI and below 228 Å for HeII. It is necessary to include the coronal radiation for the two different ranges separately due to computational issues. Just as with hydrogen, the coronal incident radiation will have to be summed into bins in order to add them to the incident radiation and avoid the massive increase in computational time that would result from adding each line individually. However, it is also known from the test with a single test

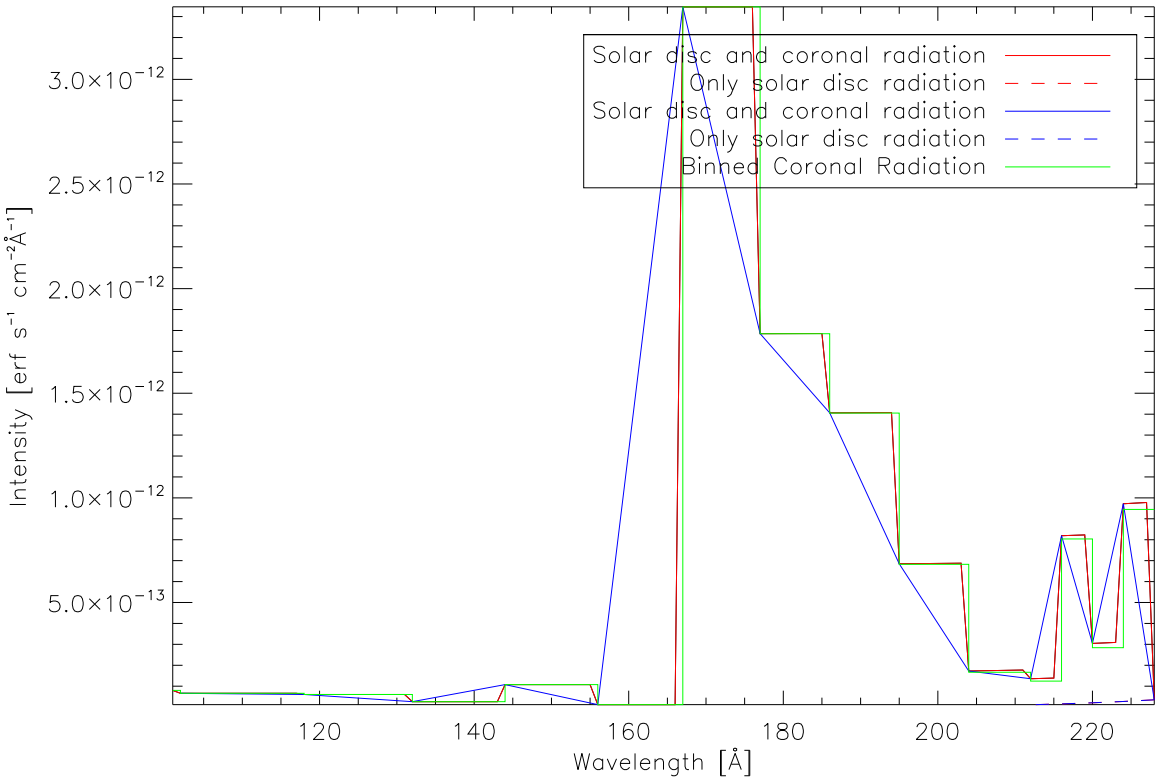

Figure 5.2: A comparison of the incident radiation to the HeII ground state continuum, the 228 Å continuum, with and without the additional coronal radiation. The lines represent the same quantities as they do in figure 5.1.

line added to the incident radiation to hydrogen that the position of a line is correlated with the degree of its influence on the ionisation of the prominence plasma. So it is again preferable to use bin ranges which decrease in size the closer they are to the ionisation edge. So the bin ranges for hydrogen cannot be re-used, as with the bin ranges used for hydrogen, only 1/3 of the bins would be applicable to HeI which would mean a significant loss in positional precision as instead of saying that a line is within one of 20 ranges, it is only within one of 7. This situation is worse for HeII as line below 228 Å are only found in two of the hydrogen wavelength bins.

So coronal lines relevant to HeI and HeII are summed into bins whose ranges are chosen so based off the data points already used by the calculations to describe the

continuum from the surface. These values for the wavelength ranges are chosen because to ensure that the added coronal radiation is treated properly there needs to be a data point at the start and end of every wavelength range, or else each bin of coronal radiation is not added to the incident radiation fully described, only partially.

The consequences of not adding additional points to describe the incident radiation can be seen in figures 5.1 and 5.2. Here the blue solid line shows the result of adding the coronal radiation to the incident radiation without adding points to describe it. Compared to the red solid line, which shows the result of adding the corona radiation with points to describe it, it is seen that not making this adjustment results in some wavelength ranges having their intensity either over or under estimated.

Using boundaries for the wavelength ranges which already have datapoints in the calculations reduces the number of datapoints which have to be added.

The total range of wavelengths for the two helium continua falls within the range of wavelengths for which lines were calculated for the hydrogen continuum. Given that the individual line intensities are already calculated all that is necessary is to sum them within the relevant wavelength ranges.

5.3 Adding the incident radiation

For the two helium continua, the coronal radiation makes up a greater proportion of the total incident radiation than was the case with hydrogen. For hydrogen, it was the case that with the coronal radiation added, the coronal radiation made up 54% of the total incident radiation below 912 Å. Comparing figure 4.7 with figures 5.1 and 5.2 the greater share in the helium continua can be see. Below 504Å, in the HeI resonant continuum, the coronal radiation makes up 80.9% of the total incident radiation. This situation is even more exaggerated below 228Å, in the HeII resonant continuum, where

the coronal radiation makes up 99.4% of the incident radiation. To put it another way, the incident radiation to the hydrogen ground state continuum is 2.2 times greater with the coronal radiation than without, while it is 5.2 times greater for the HeI ground state continuum and 174 times greater for the HeII ground state continuum.

While this is a very significant increase in the proportion of the incident radiation made up of the coronal radiation compared to hydrogen, it should not be expected that the effects on the prominence will increase by the same degree. Photoionisation is not the only source of ionisation in the prominence, although it is the only one directly increased by an increase in the incident radiation being considered. There is also thermal collisional ionisation, which will be under no direct influence of the coronal radiation. So when the photoionisation is increased the total ionisation will not be increased by the same degree.

5.3.1 Iso-Thermal models

Again to see the effect of the additional incident radiation a comparison of iso-thermal slabs is made. The same isothermal slabs considered in the hydrogen case are again considered only this time when the coronal radiation is included in the incident radiation, it is also present in the incident radiation to the helium continua. The tables of the resultant prominence conditions are in appendix B.1. It is always the case that increasing the amount of incident radiation to the helium continua results in the helium being more heavily ionised.

Just looking at the changes to the helium densities, the difference between having the coronal radiation and not having the coronal radiation may make the changes to ionised helium seem rather extreme in some cases, with the density of ionised helium increasing by several order of magnitude but this just shows the vast order of magnitude differences in density between the density of neutral helium and the density of ionised

helium, where the ratio of HeII to neutral helium, HeI, can be as low as 0.00001. This is different from hydrogen where the densities of ionised and neutral hydrogen were within an order of magnitude, $n_p/n_{neutralH}$ had values which were around 1.

This order of magnitude difference in density between neutral and ionised helium means that a small change in the density of neutral helium, due to it being ionised, will have a large change in the density of ionised helium. This is unlike hydrogen where due to the densities being of the same order of magnitude a small change in the neutral hydrogen density, due to it being more ionised, only results in a small change to the ionised hydrogen.

However this is less pronounced for the high temperature prominences. The higher temperature prominences have more collisional ionisation occurring, due to the higher temperatures, and so even without the coronal radiation the ionised helium has densities closer to that of neutral helium, albeit still a few orders of magnitude off. So a change of 3% in the density of neutral helium may simply result in the HeII density being 3 times greater than it was before, a 300% increase, rather than being 300 times greater than before, a 30,000% increase, as in the low temperature case.

For the high pressure prominences, the HeII density at the centre is much less than the HeII density at the surface, whilst the neutral helium density at the centre is comparatively closer to the surface density. In contrast the low pressure prominences have similar HeI densities at the surface and centre. So for the high pressure prominences a change in the density of neutral helium, due to it being ionised into HeII, will have a larger impact on the density of HeII at the centre than a similar change would have at the surface.

This is clear for the low pressure, thin prominences where the surface and central densities for each of the forms of helium being very close to each other. This results in the changes at the surface and centre being very close to each other. While in the

other cases the changes at the surface and centre are different from each other.

These prominences are represented by slabs of constant temperature and pressure so it is worth noting that, just as with hydrogen, in the low pressure thin cases the increase in ionisation results in a drop in the overall helium density. The increase in ionisation results in more free electrons and in order to maintain the same pressure the density of helium has to decrease.

The emergent ground state continua of helium, both the neutral helium and HeII ionised helium, are greater with the coronal radiation present than without it present. The continua are formed when free electrons re-combine with ionised helium and the ground state continua are where the electron finds itself in the ground state directly after recombination. An increase in the amount of ionised helium results in more recombination and the increase in recombination results in an increase in the intensity of the continua. This is true with both continua, there is more HeII to turn into HeI and so the HeI continuum increases and likewise with HeIII turning into HeII.

The 228Å emergent continuum experiences a greater increase with the addition of the coronal incident radiation than the 504Å continuum does. The increase in the 504Å continuum is normally within an order of magnitude, while the 228Å continuum increases by two orders of magnitude. This is similar to the changes to the incident radiation within the ranges of these continua. The incident radiation below 504Å increases by a factor of 5.2, which is a change within an order of magnitude. While the incident radiation below 228Å increases by a factor of 174, a change of just over two orders of magnitude. The increase in incident radiation results in a proportionate increase in photo-ionisation, and so more ionised helium. This increase in ionisation is not evident in the densities of ionised helium, so this excess of ionised helium has undergone recombination back to its original condition and in doing so emitted continuum radiation.

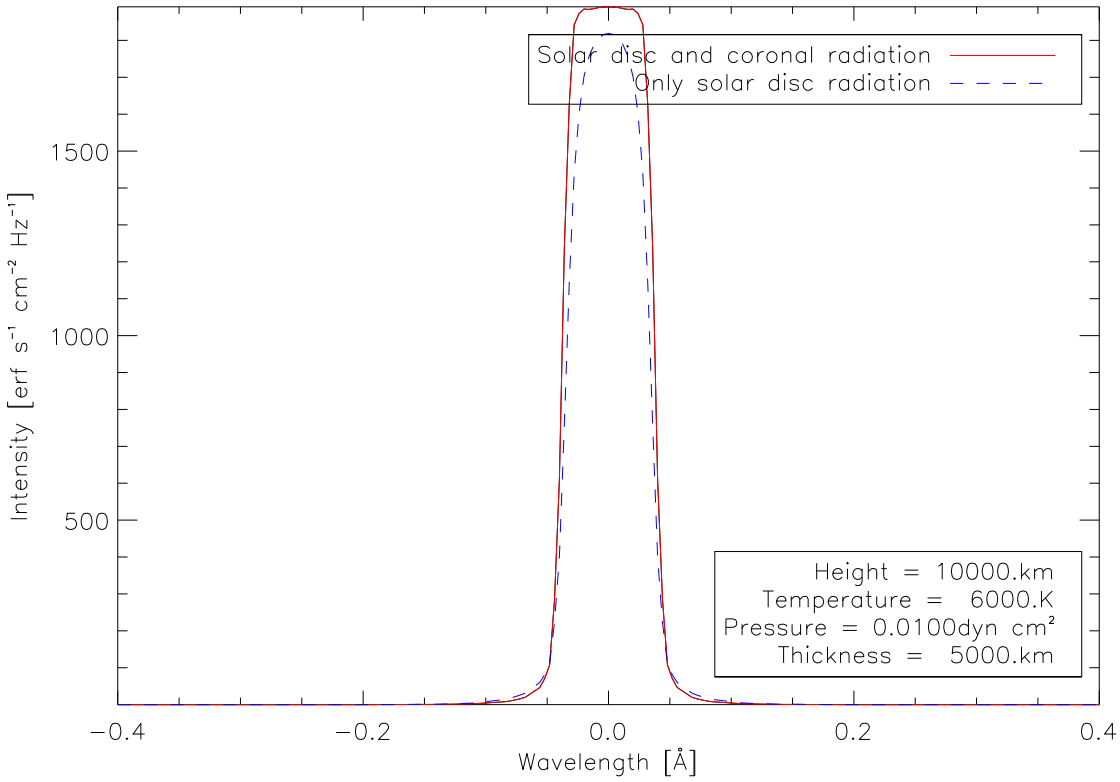

Figure 5.3: A profile of the HeI 584Å line for the third iso-thermal iso-baric prominence, showing the line profile for the case with and without the additional coronal radiation.

Provided in the tables are the intensities for one resonant line for both HeI and HeII, the 584Å line of HeI and the 304Å line of HeII. The intensities of these lines is greater in all cases. When recombination occurs, the freshly absorbed electron will not find itself in the ground state all the time, but will find itself in a excited state. It will then undergo de-excitation until it reaches the ground state and in doing so emit emission lines. The fact that there is more ionised helium means that there will be more helium ions undergoing recombination, and so more excited electrons being de-excited and thus more emission in the emission lines, such as the 584Å and 304Å lines.

These resonant lines are optically thick for all the considered iso-thermal iso-baric

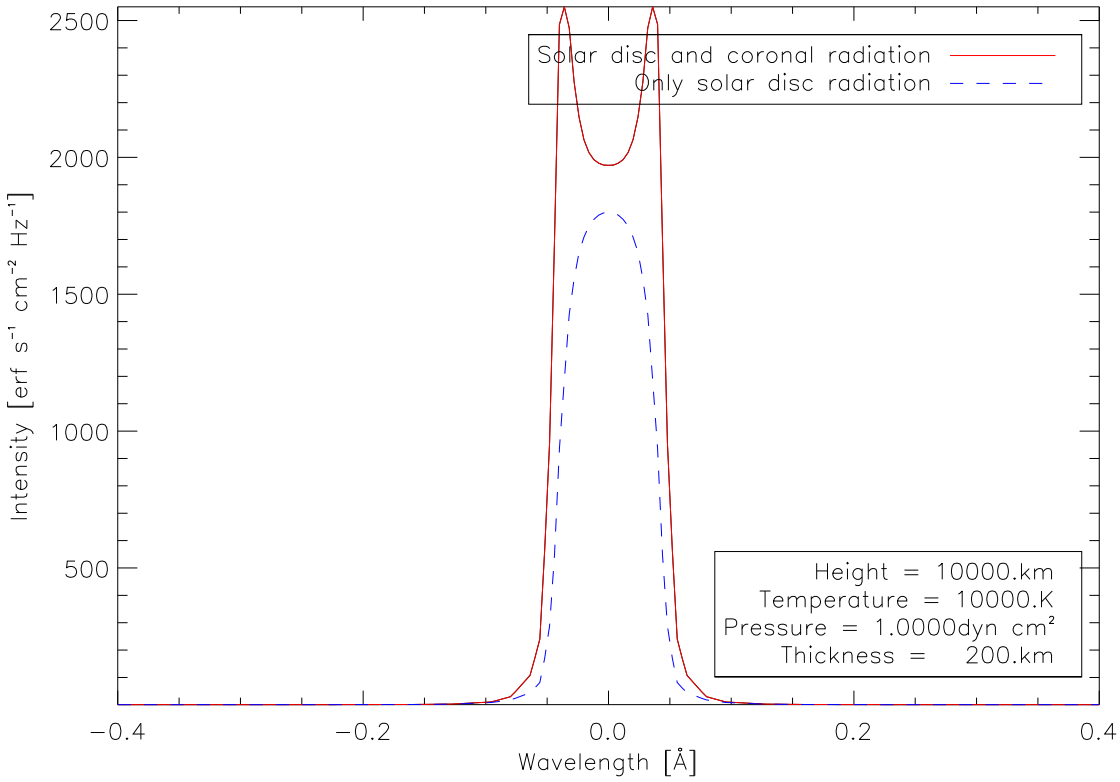

Figure 5.4: A profile of the HeI 584Å line for the sixth iso-thermal iso-baric prominence, showing the line profile for the case with and without the additional coronal radiation.

slabs for both when the incident radiation to the continua includes the coronal radiation and for when it does not. Yet the resonant lines do not display a central inversion or any flattening when the coronal radiation is not included, they appeared as simple Gaussians for the resonant lines under these conditions are not bright enough to have the effects of optical depth displayed. In the cases where the addition of the coronal radiation results in an increase in the intensity of the resonant lines, this increase in intensity brings these lines to the point where they have sufficient intensity to be affected by the central optical thickness of these lines.

This is just apparent for the HeI 584Å line in the third iso-thermal iso-baric case, as seen in figure 5.3, which shows the line profile of the 584Å line for the third case,

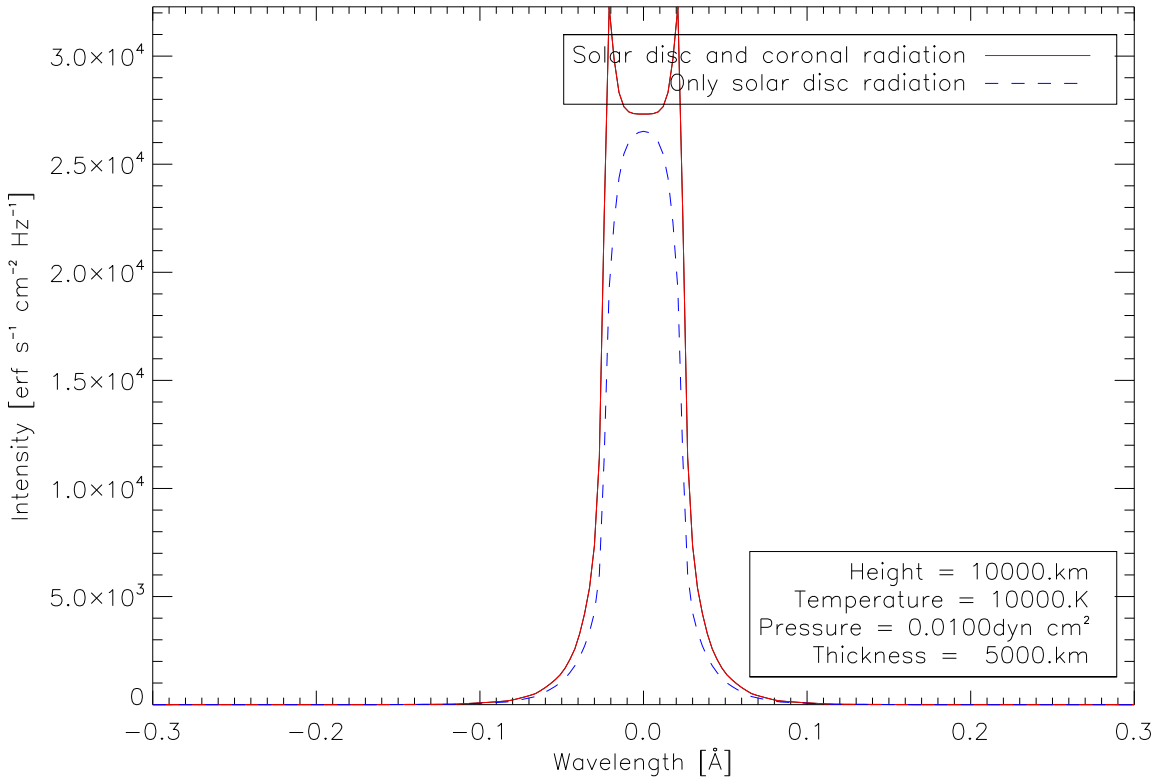

Figure 5.5: A profile of the HeII 304Å line for the seventh iso-thermal iso-baric prominence, showing the line profile for the case with and without the additional coronal radiation.

where the peak of the emergent 584Å line is flattened for when the incident radiation includes the coronal radiation, but is rounded without. This emergent line is 1.15 times more intense with the additional incident radiation than without it. For lines where the increase in intensity is greater, this goes from a flattening of the emergent line to the emergent line displaying full out central inversion. Figure 5.4 displays line profiles for the 584Å line for the sixth case, where the increase in total line intensity is by a factor of 1.51.

This can also occur with the HeII 304Å line seen in figure 5.5, however of the cases considered the full reversal is only evident in the seventh case. It is not necessarily the case that the case which shows the most pronounced inversion also has the greatest

increase in total intensity of the line, for the HeII 304Å line the prominence which gave the line shown in figure 5.5 does not have the greatest increase in total intensity of the 304Å line for the iso-thermal prominence slabs considered here.

The ratio of one triplet line to another is the same in all cases where they are optically thin, so to investigate the changes adding the coronal radiation to the incident radiation makes, it is sufficient to only look at one triplet line for the changes to the others shall be of the same proportion (Labrosse & Gouttebroze 2001). The triplet line provided here is the 5877Å line. It is greatly increased in the high pressure cases, this increase is far more than the increase in intensity of the singlet lines. A similar increase in the low pressure cases is only seen in the thick cases. The triplet lines will be more useful in confirming the coronal effects on the prominence helium than the singlet lines in observations, as the effects on total intensity are far more noticeable.

5.3.1.1 Comparison with Previous Studies

Heasley et al. (1974) calculated the helium emissions for iso-thermal prominences for a ranges of temperatures and densities with a width of 6000km. They use a dilution factor of 1/2 for the radiation from the solar disk, which corresponds to a location directly on the solar surface. Labrosse & Gouttebroze (2001) investigated the helium emissions of prominences. The authors compared iso-thermal models with Heasley et al. (1974)'s results so it is possible to compare to both at the same time.

So for this comparison four iso-thermal prominences are considered, each of a width of 6000km. Two have a temperature of 6000K, and two have 8000K. One slab at each temperature has its pressure set such that it has a hydrogen density near 10^{10} cm^{-2} and the others have pressure set for a density near 10^{12} cm^{-2}.

Comparisons between these results and these two papers are shown in tables 5.1

and 5.2. It is seen that the results with the coronal radiation show significantly more ionisation of the prominence than the previous studies do. The ratios n_{HeII}/n_{HeI} and n_{HeIII}/n_{HeII} show greater degrees of ionisation for the results with coronal radiation, but the differences are not by several order of magnitude. The line intensities for the helium lines considered in table 5.2 all show the results with the modified incident radiation to produce greater emergent helium intensities than these previous studies. The optical thickness at 584Å is reduced, this is most noticeable in the first case where the prominence with the incident coronal radiation is optically thin at 584Å where in all other cases it is optically thick. There is also a reduction in optical depth at 504Å any change is less clear at the other wavelengths.

It was mentioned in section 4.4.1.1 that Heasley & Milkey (1976) examined the hydrogen and helium in plane parallel slab and comparisons with their hydrogen results were made in that section. Here comparisons are made with their helium results, these comparisons are shown in table 5.3. It is seen that the results with the modified incident radiation show there to be more helium ionisation, it can be seen that this is due to the coronal radiation as calculations without the coronal radiation show degrees of ionisation comparable with Heasley & Milkey (1976). Also seen are reductions in the optical depth at 584Å and 504ÅṪhe intensities of the triplet lines shown here, 5876Å and 10830Å show increases in intensity.

Comparisons with previous radiative transfer studies of helium show results consistent with the differences seen with and without the coronal radiation in section 5.3.1.

5.3.2 PCTR models

The same PCTR models considered for hydrogen are again considered for helium. The tables for the effects on helium in these prominences are given in appendix B.2.

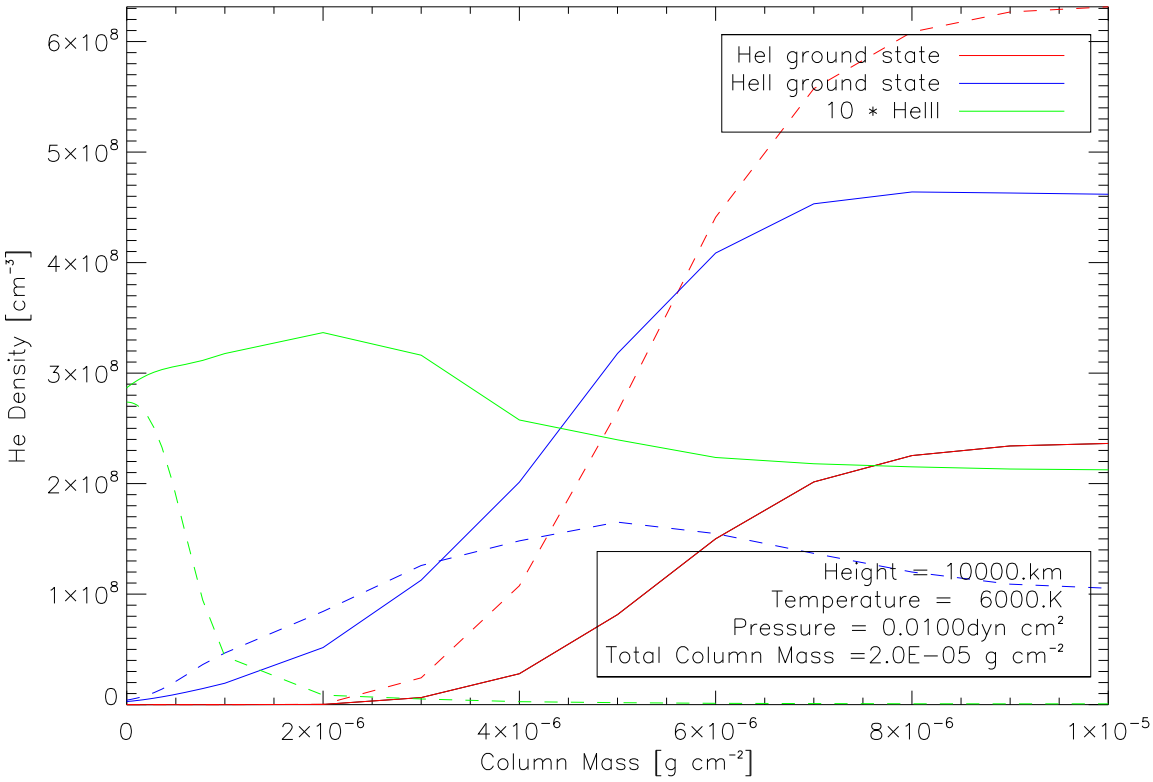

Figure 5.6: Profiles of the density of ground state HeI, ground state HeII and HeIII from the surface to centre for the third PCTR case. Solid lines are where the coronal radiation is included in the incident radiation and dotted lines are where it is not.

Unlike with hydrogen, where there was no change to the surface ionisation of hydrogen as a result of the addition of the coronal radiation, the additional incident radiation results in changes to the ionisation of helium at the surface of the prominence. In the majority of the cases considered the density of neutral helium drops by almost a third, this only fails to happen for the two cases where the column mass is the lower column mass considered with a high pressure core.

However the density of HeII is also reduced by the same proportion so the ratio of HeII to neutral helium at the surface has no change at all. However, the density of fully ionised helium at the surface is affected by the addition of the coronal radiation

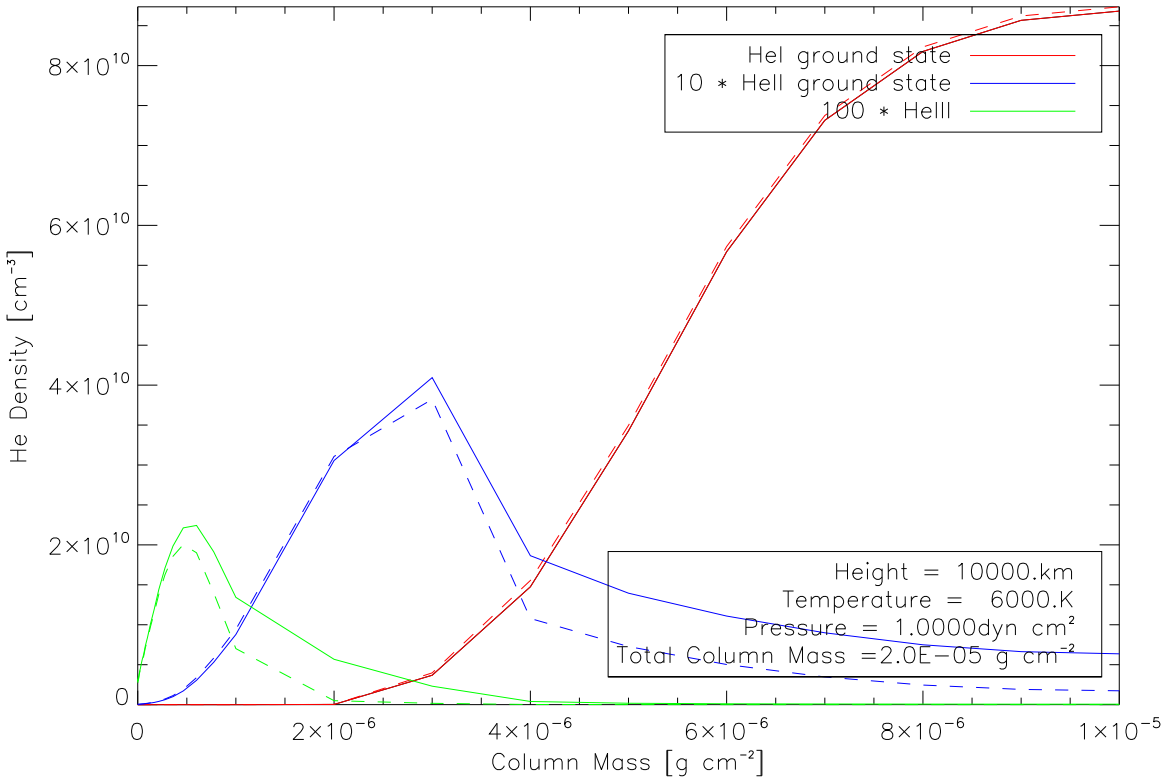

Figure 5.7: Profiles of the density of ground state HeI, ground state HeII and HeIII from the surface to centre for the fourth PCTR case. Solid lines are where the coronal radiation is included in the incident radiation and dotted lines are where it is not.

to the incident radiation by a lesser degree and so the ratio of HeIII to HeII increases. It is in this respect that the surface helium can be said to be more heavily ionised by the inclusion of the coronal radiation in the incident radiation.

The helium densities do not vary through the transition region as smoothly as the hydrogen densities did in figure 4.13 where both the ionised and neutral hydrogen increase smoothly towards the centre. Neutral and ionised helium vary in different ways through the prominence. Neutral helium increases in all cases towards the centre of the prominence, due to the overall greater densities of everything at the centre of the prominence, but ionised helium does not necessarily do the same. Normally without

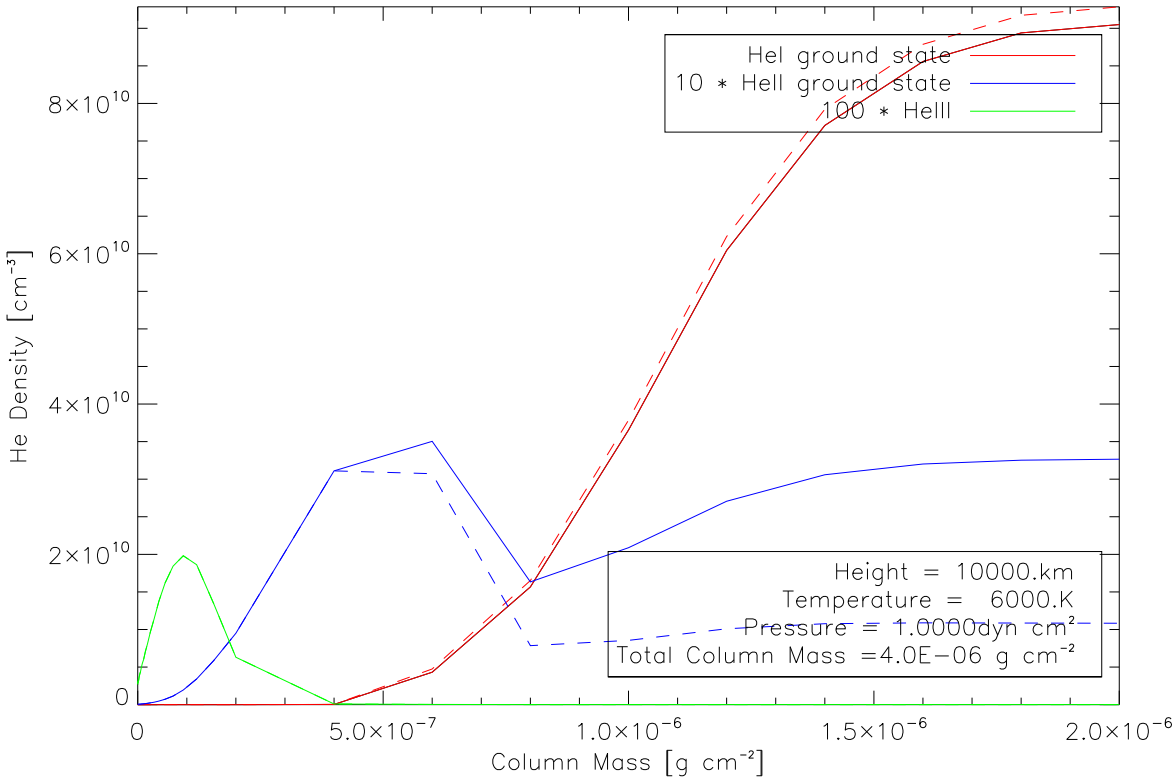

Figure 5.8: Profiles of the density of ground state HeI, ground state HeII and HeIII from the surface to centre for the second PCTR case. Solid lines are where the coronal radiation is included in the incident radiation and dotted lines are where it is not.

the coronal radiation the density of ionised helium will increase from the surface to a peak before decreasing towards slab centre due to an increased number of collisions depopulating the ionised state through recombination, but the addition of the coronal radiation changes this.

Shown in figure 5.6 is the density variations through the prominence for the third PCTR model, with a low pressure centre. The neutral helium varies as expected, it increases towards slab centre, although it increases less when the coronal radiation is added due to the increased ionisation. The singularly ionised helium, HeII, is not just affected in its numbers alone by the addition of the coronal radiation, the HeII density

changes through the prominence in a different way. The density of the HeII increases more gradually near the surface than it does without the coronal radiation. Given that the HeII 304Å line is mostly formed near the surface of the prominence this explains the reduced intensity of the prominence's 304Å emissions seen in appendix B.2 for as the density of HeII is less near the surface, there is less HeII to emit the line and so its intensity is reduced.

The fully ionised helium, HeIII, in the low central pressure case varies quite differently with the addition of the coronal radiation. Without the coronal radiation the HeIII decreases sharply from an initial peak, adding the coronal radiation results in the density of HeIII not decreasing as much, staying within an order of magnitude of the surface value through the prominence. The HeIII reaches an initial peak at around 2×10^{-6} g cm^{-2} before decreasing slightly towards the centre. The 228Å continuum is formed by the recombination of HeIII to form HeII. Without the coronal radiation this mostly happens near the surface of the prominence given that this is where almost all of the HeIII can be found, however the increased density of HeIII through the entire prominence means that the 228Å continuum will come from the entire prominence. This is why in appendix B.2 the intensity of this continuum is greatly increased.

The density variations in the high central pressure cases follow a different pattern. Shown in figure 5.7 are the density variations for the fourth case, which has a high pressure centre. The higher pressure in the centre results in more collisions, this increase in collisions and the resultant recombination causes the densities of the ionised forms of helium to fall off more than they do in the low pressure case. This is noticeable in the intensity of the 228Å continuum. Unlike in the low pressure case, where the increased density of HeIII was much higher throughout the prominence causing a large increase in the intensity of the 228Å continuum, here the increase in HeIII caused by the addition of the coronal radiation does not cause as large an increase in the intensity of the 228Å continuum as the overall increase in the HeIII density is less due to it being more localised.

The variation of the density of HeII is also affected by the increased central pressure. Instead of increasing towards the centre under the influence of coronal radiation as it did in the low pressure case, the HeII reaches a peak before decreasing towards the centre, although the density of HeII is still greater with the coronal radiation than it is without the coronal radiation so the centre of the prominence is still affected by the coronal radiation. This was with a prominence with the higher of the two column masses considered here. Figure 5.8 shows the density variations for the second case, which only differs from the fourth case in the column mass as the second case has the smaller of the two column masses considered. This prominence is lower mass and so smaller than the second case prominence, and so it is easier for the incident radiation to reach the centre of the prominence. This shows in the density of HeII which does not decrease all the way from the peak value to the centre of the slab, here after the peak HeII density the density decreases before increasing again, although the density never reaches its peak value.

In the iso-thermal case lines were seen to gain a reversal due to their total intensity increasing due to an increase in non-scattering sources of these lines. With the PCTR there is one case where a change in the shape of the line is seen. Shown in figure 5.9 is the line profile of the HeII 304Å line for the fifth PCTR case. Although the total intensity of this line is reduced with the addition of the coronal radiation to the incident radiation, there is a small increase in intensity at 0.04Å from the line centre. This deviation from a line profile dominated by scattering processes, such as the profile shown without the influence of coronal radiation, can be understood as arising from there being more collisions due to the overall greater population of HeII in the prominence and so more collisional effects.

Although the singlet line 584Å shows a reduction in intensity, the triplet line 5877Å shows an increase in intensity which is noticeable in all PCTR cases considered here. These increases are not always as great as the increases in the iso-thermal cases.

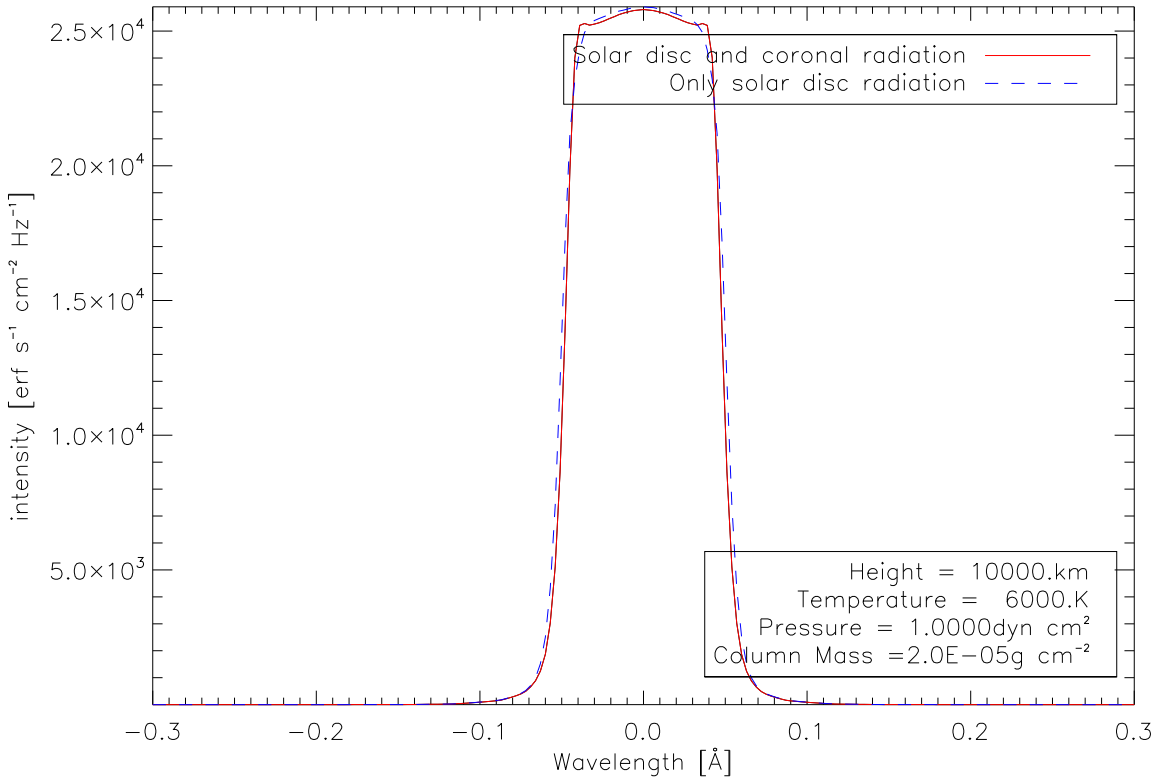

Figure 5.9: A profile of the HeII 304Å line for the fifth prominence with a PCTR, showing the line profile for the case with and without the additional coronal radiation.

5.4 Conclusions

The modifications to the helium part of the code, described in section 5.2, have one advantage over the modifications made to the hydrogen part of the code. Given that it has been chosen to focus on adding binned intensities rather than individual lines, it is only necessary to modify the helium section of the code to deal with these binned intensities, but this needs to be done in a way that does not miss represent the binned intensities.

The effects on helium of adding the coronal radiation are considered in section

5.3. First examined are the effects on helium in iso-thermal slabs, using the same iso-thermal slabs examined for hydrogen, which are detailed in table 4.1. It is seen that with the coronal radiation the helium is greatly more ionised than it is without the coronal radiation, though this is largely due to the differences in neutral and ionised helium densities. A small change in neutral helium density due to ionisation results in a large change in the ionised helium density, for example in the second iso-thermal slab considered, a 5% reduction in the neutral helium density results in a threefold increase in the HeII density.

The intensities of the emergent continua of helium shows large increases in intensity. This increase in intensity is far greater for the 228Å continuum than the 504Å continuum, but the changes to the emergent continua are proportional to the size of the change to the incident continua due to the addition of the coronal radiation. The emergent line intensities are also increased by the addition of the coronal radiation, and this is most notable with the HeI 584Å line, for the addition of the coronal radiation changes the shape of this line. For the prominence models considered here, there is no central reversal of the HeI 584Å line without the coronal radiation, but adding the coronal radiation results in a reversal at line centre forming due to a increase in non-scattering sources of this line's formation. This is evident to a lesser degree in HeII 304Å as for this line the full reversal is only evident for the seventh case. The effects on intensity are more noticeable in the triplet lines than in the resonant lines where the intensities increase by 2 to 5 times instead of only by a third.

Comparisons to previous helium modelling of prominences are made in section 5.3.1.1. Seen are changes which are very similar to the changes seen from examining the iso-thermal slabs.

Comparisons are then made using the PCTR models previously considered for hydrogen, which are detailed in table 4.2. Changes are seen in the helium densities across the entire prominence. In hydrogen changes were not seen at the surface but

with helium changes are seen at the surface as well as at the centre. Increases in the HeIII density are especially noteworthy in the low central pressure cases, where large increases in absolute terms are seen across the entire prominence. Such absolute increases are smaller in the high central pressure cases, although the tables show that the proportional increases are still high at the centre. The larger absolute increase in HeIII density for the low pressure cases than the high pressure cases shows in the increase of the 228Å continuum where changes such as were seen in the iso-thermal cases are only seen with the low central pressure cases, the changes to 228Å in the high central pressure case are far more modest.

The intensities of the resonant lines show decreases in total intensity, rather than increases as they did in the iso-thermal cases, and the shapes of the lines do not change as much. The triplet lines still show increases in total intensity, but to a far lesser degree than the iso-thermal cases.

Model	T [K]	n_H [cm $^{-2}$]	Optical Depths (Whole Slab) $\tau(912)$	$\tau(504)$	$\tau(584)$	$\tau(228)$	$\frac{n_{HeII}}{n_{HeI}}$ surface	centre	$\frac{n_{HeIII}}{n_{HeII}}$ surface	centre
Heasley et al. (1974)	6000	10^{10}	2.6	3.8	2.2E4	0.8	0.4	0.3	1.E-4	8.E-8
Labrosse & Gouttebroze (2001)			11	4.2	2.8E4	0.1	3.E-1	7.E-2	1.E-2	9.E-3
Solar Disc and Corona			11.3	3.4	1.5.E-4	0.39	1.35	0.347	2.37E-2	2.12E-2
Only Solar Disc			14.6	4.9	2.3E4	0.12	0.409	5.01E-2	3.44E-4	2.81E-4
Heasley et al. (1974)	6000	10^{12}	3.6E3	1140	3.E6	152	1.E-2	1.E-10	4.E-6	1.E-10
Labrosse & Gouttebroze (2001)			3.5E3	4.8E2	3.1E6	6.E-3	2.E-2	1.E-11	4.E-4	3.E-6
Solar Disc and Corona			3.66E4	4.5E2	2.1E8	2.6E-2	5.99E-2	3.21E-11	7.91E-3	2.09E-7
Only Solar Disc			3.66E4	4.5E2	2.1E8	5.5E-3	2.08E-2	3.68E-11	1.67E-5	1.89E-10
Heasley et al. (1974)	8000	10^{10}	2.3	3.4	1.7E4	0.8	0.53	0.46	2.E-4	1.E-4
Labrosse & Gouttebroze (2001)			7.8	3.8	2.2E4	0.1	0.42	0.11	1.E-2	1.E-2
Solar Disc and Corona			7.8	2.7	1.2E4	0.44	1.6	0.534	2.81E-2	2.51E-2
Only Solar Disc			10.4	4.4	1.9E4	0.14	0.472	7.66E-2	4.12E-4	3.45E-4
Heasley et al. (1974)	6000	10^{12}	2.18E3	870	2.4E6	126	0.01	3.E-7	4.E-6	3.E-16
Labrosse & Gouttebroze (2001)			1900	400	2.2E6	3.E-3	0.02	5.E-8	4.E-4	4.E-6
Solar Disc and Corona			2.021E3	410	2.8E6	9.6E-3	4.64E-2	1.09E-7	1.19E-5	2.92E-12
Only Solar Disc			2.02E3	4.1E2	1.8E6	2.4E-3	1.55E-2	1.09E-7	1.32E-5	2.93E-12

Table 5.1: Comparison optical depths and ionisation degrees of helium between those in Heasley et al. (1974) and Labrosse & Gouttebroze (2001) and those from the modfied radiative transfer code both for with the coronal radiation included in the incident radiation and with it not included.

Table 5.2: Comparison optical depths and ionisation degrees of helium between here and in Heasley et al. (1974) and Labrosse & Gouttebroze (2001).

			Line Intensities [erg s^{-1} cm^{-2} Sr^{-1}]				
Model	T [K]	n_H [cm^{-2}]	304Å	537 Å	584Å	5877Å	10833Å
Heasley et al. (1974)	6000	10^{10}	341.	7.56	356.	1844.	8438
Labrosse & Gouttebroze (2001)			906	5	134	1300	6190
Solar Disc and Corona			1500	14	190	6300	29000
Only Solar Disc			1100	10	150	1800	8600
Heasley et al. (1974)	6000	10^{12}	132	3.74	54.2	567.	2624.
Labrosse & Gouttebroze (2001)			414	5	117	661	3140
Solar Disc and Corona			720	13	170	2600	12000
Only Solar Disc			570	9.6	130	640	2800
Heasley et al. (1974)	8000	10^{10}	424	8.86	370.4	2032	9300
Labrosse & Gouttebroze (2001)			1100	6	154	1500	7160
Solar Disc and Corona			1700	16	210	5800	27000
Only Solar Disc			1200	11	160	4800	8500
Heasley et al. (1974)	6000	10^{12}	150	4.28	65.4	784.	3615.
Labrosse & Gouttebroze (2001)			431	6	134	449	2110
Solar Disc and Corona			700	14	180	1800	5600
Only Solar Disc			520	10	140	920	1700

Model	T [K]	p [dyn cm^{-2}]	D [km]	$\frac{n_{HeII}}{n_{HeI}}$ surface	$\frac{n_{HeII}}{n_{HeI}}$ centre	$\tau(504\AA)$	$\tau(584\AA)$	[erg s^{-1} cm^{-2} Sr^{-1}] I(5876Å)	[erg s^{-1} cm^{-2} Sr^{-1}] I(10830Å)
Heasley & Milkey (1976)	7500	0.065	1500	0.17	0.1	5.	2.E4	1.63E3	7.52E3
Solar Disc and Corona				0.576	0.124	3.6	2.1E4	4.4E4	2.4E5
Only Solar Disc				0.153	0.0183	4.3	2.5E4	1.E3	5.9E3
Heasley & Milkey (1976)	7500	0.065	3800	0.16	0.03	12.5	5.4E4	2.2E3	1.01E4
Solar Disc and Corona				0.552	0.0123	19	1.1E5	6.1E3	3.2E4
Only Solar Disc				0.151	1.12E-4	20	1.2E5	1.1E3	6.1E3
Heasley & Milkey (1976)	7500	0.26	320	0.05	0.02	6.68	2.2E4	1.32E3	5.66E3
Solar Disc and Corona				0.192	0.0314	4.1	2.4E4	2.7E3	1.5E4
Only Solar Disc				0.0523	4.83E-3	4.3	2.5E4	6.1E2	3.4E3
Heasley & Milkey (1976)	9500	0.065	2200	0.3	0.23	4.16	2.E4	2.43E3	1.12E4
Solar Disc and Corona				0.734	0.174	3.5	1.8E4	4.6E3	2.5E4
Only Solar Disc				0.192	2.65E-2	4.3	2.2E4	1.1E3	6.2E3
Heasley & Milkey (1976)	9500	0.065	7000	0.29	0.07	12.84	6.8E4	4.33E3	1.97E4
Solar Disc and Corona				0.693	0.026	13	6.5E4	5.7E3	3.E4
Only Solar Disc				0.186	2.5E-3	14	7.E4	1.2E3	6.7E3
Heasley & Milkey (1976)	9500	0.26	670	0.08	0.04	6.08	3.E4	2.7E3	1.28E4
Solar Disc and Corona				0.33	0.0734	3.1	1.6E4	2.9E3	1.6E4
Only Solar Disc				0.0871	0.0135	3.4	1.8E4	690	3.9E3

Table 5.3: Comparison optical depths and ionisation degrees of helium between here those in Heasley & Milkey (1976) and those from the modfied radiative transfer code both for with the coronal radiation included in the incident radiation and with the coronal radiation not included in the incident radiation.

Chapter 6

Conclusions and Future Work

6.1 Conclusions

The aim of this work was to study the effects of radiation from the corona on prominences through the use of 1-D NLTE radiative transfer. The coronal radiation was calculated and applied to the incident radiation to the continuum in the radiative transfer calculations, which acts as a boundary condition to the bound-free transitions. The effects of this change on the hydrogen and helium of the prominence were then examined.

Chapter 3 examines how the coronal radiation is to be obtained. Measurements of the corona from outside it are not useful as the prominence is inside the corona, so it is necessary to know how the coronal radiation looks from its view point. To do this the intensity is integrated over all lines of sight visible from a location within the corona using equation 3.11. The contribution function G(T) is obtained from the CHIANTI atomic database and the list of coronal temperatures and electron densities with height are obtained from Fontenla et al. (2011). It is first verified that the correct values of

intensity are obtained by comparing the intensity obtained from one path with the intensity that CHIANTI provides for an identical path to see if they give the same values, and see that any discrepancies that are merely computational in nature and can be ignored. It is shown that it is necessary to consider the radiation of the corona at different heights by calculating the intensity of the corona as seen within the corona at different heights. The intensity of different lines are seen to vary with observed height in different ways, they peak at the observed height closest to the height in the corona with a temperature that corresponds to their formation temperature. Even if you sum the lines across wavelength ranges the different wavelength ranges will also not vary uniformly with observed height.

In chapter 4 the coronal radiation is added to the incident radiation to the hydrogen continuum. The modifications to the code were made so that separate lines could be added to the incident radiation. A single test line was added to the incident radiation and moved from 100Å to 1000Å, the effects of this line on the ionisation of the prominence increased as the line moved towards 912Å, the ionisation edge of ground state hydrogen. The position of lines matter when determining their effect on the prominence, and so any method of adding them to the incident radiation needs to preserve some information about the position of the lines. Next many lines are added to the incident radiation to see how well the code handles many lines. There is a very significant increase in computational time before the point is reached where adding more lines does not significantly change the ionisation of the prominence, so it is decided to add the coronal radiation averaged over wavelength ranges. These ranges get smaller the closer they are to 912Å to take into account the increased importance of the position of the lines there. With a suitable way to add the coronal radiation which was calculated in chapter 3 determined the effect of it on various prominence models is investigated. Section 4.4.1 examines the effects of the coronal radiation on a series of iso-thermal iso-baric slabs which are detailed in table 4.1. It is seen that the prominence material is significantly more ionised with the corona radiation for all cases, though the difference is less for the high pressure cases as photionisation makes

up less of the ionisation processes in the high temperature cases due to collisions. The emissions of the prominence for these iso-thermal models are changed. The emissions in the continuum are increased while the emissions in the hydrogen lines are decreased for the low pressure cases and increased in the high pressure cases, for lines with a reversal this increase is more noticeable in the wings than the centre of the line. The results of this are compared with the results of previous 1-D NLTE modelling of the hydrogen in a prominence and find the same difference with previous results that was found with section 4.4.1's results with and without the coronal radiation. Models which feature a PCTR are investigated next, which are detailed in table 4.2. The surface of the prominence is at coronal conditions and so is mostly ionised and so the addition of more incident radiation does not result in any additional ionisation. The effects of increased ionisation in the centre for the low pressure case are larger than the effects in the high central pressure cases. Effects on the emissions of the prominence are only seen in the low central pressure cases, where the differences are much the same as they were in the iso-thermal cases.

In chapter 5 the coronal radiation is applied to the incident radiation to the helium continua. The modifications here only need to be made to add intensities summed over wavelength ranges given that this method of adding to the incident radiation is being used rather than adding the lines indivdually due to the computational resources that many individual lines proved to have. First considered are the same iso-thermal slabs that were considered for hydrogen. The ionisation degrees n_{HeII}/n_{HeI} and n_{HeIII}/n_{HeII} are greatly increased, though this is mostly due to the differences between the densities of neutral and ionised helium, a small change in the density of neutral helium due to ionisation will result in a large change to the density of ionised helium. The emergent continua of helium are seen to increase, this increase is far greater for the 228Å HeII continuum than for the 504Å HeI continua, the increases in each continuum are proportional to the increases in the incident radiation in these ranges. Increases are seen in the resonant lines of HeI and HeII, with some changing of the shape of these lines. The HeI triplet lines increase in intensity by a greater amount than the resonant lines

and so it will be more useful to look at the triplet lines in observations when looking for signs of the influence of the coronal radiation in actual prominences. Comparisons with previous studies show differences much the same as seen in section 5.3.1 with and without the coronal radiation. Examined are the effects in helium for prominence slabs with a PCTR present, looking at the same slabs with a PCTR that were looked at for hydrogen. Unlike in hydrogen when there was no difference seen at the surface, in helium a difference is seen in ionisation from the surface of the slab to the centre. This difference in the centre is large in absolute terms for the low central pressure cases than in the high central pressure cases and this shows in the intensity of the 228Å continuum, where the increase in intensity is greater for the low central pressure cases than the high central pressure cases. With these PCTR slabs is seen a decrease in the intensity of the resonant lines, but the triplet lines still show an increase in intensity.

6.2 Future Work

The radiative transfer modelling in this work has been performed on vertical slabs, which correspond to the case of a prominence observed above the solar limb. The modified incident radiation has not been applied to horizontal slabs, which represent a filament observed against the solar disc. A horizontal slab will differ from a vertical slab in that both sides of a vertical slab receive light from all directions, which is part of why they can be treated as being symmetric, but with a horizontal slab the bottom side of the slab will only receive light coming from below and the top side of the slab will only receive light coming from above, which is why when only the radiation from the solar disc is considered only the bottom of the slab is illuminated (Gouttebroze 1989). To investigate the effects of the coronal radiation on a horizontal slab it will be necessary to calculate the coronal radiation for directions from $\theta = 0$ to π in figure 3.1 for the coronal radiation illuminating the bottom of the slab and directions π to 2π for the coronal radiation illuminating the top of the slab.

The coronal radiation has only been applied to the radiative processes of hydrogen and helium, but the radiative transfer code which was modified is also capable of examining calcium. To make the modifications to the calcium section of the code will involve much the same modifications as were made to the helium section, for only the binned radiation has been used rather than individual lines when looking at the effects of the coronal radiation. Calcium plays an important role in the radiative processes of the prominence so it will be good to investigate the effects of the coronal radiation on the calcium in the prominence (Heasley & Milkey 1978) (Gouttebroze & Heinzel 2002) (Labrosse et al. 2002).

The calculations of the coronal radiation have assumed uniform coronal conditions across the entire Sun, when in reality this is not the case, even for the Sun during it more quiet conditions (Fontenla et al. 2009) (Fontenla et al. 2011). Further work in refining the coronal incident radiation would be to take into account different solar conditions, which would allow this work in investigating the effects of coronal radiation on the prominences to be extended to active prominences as this work has only looked at quiet Sun conditions, which means these results are only applicable to quiescent prominences.

Bibliography

Anzer, U. & Heinzel, P. 1999, Astronomy and Astrophysics, 349, 974

Auer, L. H. & Mihalas, D. 1969, Astrophysical Journal, 156, 681

Auer, L. H. & Paletou, F. 1994, Astronomy and Astrophysics, 285, 675

Avrett, E. H. & Loeser, R. 1987, Iterative Solution of Multilevel Transfer Problems, ed. Kalkofen, W., 135–+

Babcock, H. W. & Babcock, H. D. 1955, Astrophysical Journal, 121, 349

Benjamin, R. A., Skillman, E. D., & Smits, D. P. 1999, Astrophysical Journal, 514, 307

Berger, T. E., Liu, W., & Low, B. C. 2012, Astrophysical Journal, Letters, 758, L37

Böhm-Vitense, E. 1989, Introduction to stellar astrophysics. Vol. 2. Stellar atmospheres.

Curdt, W., Brekke, P., Feldman, U., et al. 2001, Astronomy and Astrophysics, 375, 591

Dere, K. P., Landi, E., Mason, H. E., Monsignori Fossi, B. C., & Young, P. R. 1997, A&A Supplimental Series, 125, 149

Engvold, O. 2015, in Astrophysics and Space Science Library, Vol. 415, Astrophysics and Space Science Library, ed. J.-C. Vial & O. Engvold, 31

Fontenla, J. M., Curdt, W., Haberreiter, M., Harder, J., & Tian, H. 2009, Astrophysical Journal, 707, 482

Fontenla, J. M., Harder, J., Livingston, W., Snow, M., & Woods, T. 2011, Journal of Geophysical Research (Atmospheres), 116, 20108

Fontenla, J. M., Rovira, M., Vial, J.-C., & Gouttebroze, P. 1996, Astrophysical Journal, 466, 496

Gontikakis, C., Vial, J.-C., & Gouttebroze, P. 1997, Astronomy and Astrophysics, 325, 803

Gouttebroze, P. 1989, Hvar Observatory Bulletin, 13, 305

Gouttebroze, P. & Heinzel, P. 2002, Astronomy and Astrophysics, 385, 273

Gouttebroze, P., Heinzel, P., & Vial, J. C. 1993, Astronomy and Astrophysics, Supplement, 99, 513

Gouttebroze, P. & Labrosse, N. 2000, Solar Physics, 196, 349

Gouttebroze, P. & Labrosse, N. 2009, Astronomy and Astrophysics, 503, 663

Gunár, S., Heinzel, P., & Anzer, U. 2007, Astronomy and Astrophysics, 463, 737

Haken, H., Wolf, H. C., & Brewer, W. D. 2005, The Physics of Atoms and Quanta

Harrison, R. A., Sawyer, E. C., Carter, M. K., et al. 1995, Solar Physics, 162, 233

Heasley, J. N. & Mihalas, D. 1976, Astrophysical Journal, 205, 273

Heasley, J. N., Mihalas, D., & Poland, A. I. 1974, Astrophysical Journal, 192, 181

Heasley, J. N. & Milkey, R. W. 1976, Astrophysical Journal, 210, 827

Heasley, J. N. & Milkey, R. W. 1978, Astrophysical Journal, 221, 677

Heinzel, P. 2015, in Astrophysics and Space Science Library, Vol. 415, Astrophysics and Space Science Library, ed. J.-C. Vial & O. Engvold, 103

Heinzel, P., Bommier, V., & Vial, J. C. 1996, Solar Physics, 164, 211

Heinzel, P., Gouttebroze, P., & Vial, J.-C. 1994, Astronomy and Astrophysics, 292, 656

Heinzel, P., Schmieder, B., Fárník, F., et al. 2008, Astrophysical Journal, 686, 1383

Heinzel, P., Schmieder, B., & Tziotziou, K. 2001, Astrophysical Journal, Letters, 561, L223

Hirayama, T. 1963, Publications of the ASJ, 15, 122

Hirayama, T. 1985, Solar Physics, 100, 415

Hubeny, I. & Mihalas, D. 2014, Theory of Stellar Atmospheres

Hyder, C. L. & Lites, B. W. 1970, Solar Physics, 14, 147

Kunasz, P. & Auer, L. H. 1988, Journal of Quantitiative Spectroscopy and Radiative Transfer, 39, 67

Labrosse, N. & Gouttebroze, P. 1999, in ESA Special Publication, Vol. 446, 8th SOHO Workshop: Plasma Dynamics and Diagnostics in the Solar Transition Region and Corona, ed. J.-C. Vial & B. Kaldeich-Schü, 399–+

Labrosse, N. & Gouttebroze, P. 2001, Astronomy and Astrophysics, 380, 323

Labrosse, N. & Gouttebroze, P. 2004, Astrophysical Journal, 617, 614

Labrosse, N., Gouttebroze, P., Heinzel, P., & Vial, J.-C. 2002, in ESA Special Publication, Vol. 506, Solar Variability: From Core to Outer Frontiers, ed. A. Wilson, 451–454

Labrosse, N., Gouttebroze, P., & Vial, J.-C. 2007, Astronomy and Astrophysics, 463, 1171

Labrosse, N., Heinzel, P., Vial, J.-C., et al. 2010, Space Science Reviews, 151, 243

Labrosse, N., Vial, J.-C., & Gouttebroze, P. 2008, Annales Geophysicae, 26, 2961

Landi, E., Del Zanna, G., Young, P. R., Dere, K. P., & Mason, H. E. 2012, Astrophysical Journal, 744, 99

Levens, P., Labrosse, N., Fletcher, L., & Schmieder, B. 2015, ArXiv e-prints

Lin, Y., Martin, S. F., & Engvold, O. 2008, in Astronomical Society of the Pacific Conference Series, Vol. 383, Subsurface and Atmospheric Influences on Solar Activity, ed. R. Howe, R. W. Komm, K. S. Balasubramaniam, & G. J. D. Petrie, 235

Mackay, D. H., Karpen, J. T., Ballester, J. L., Schmieder, B., & Aulanier, G. 2010, Space Science Reviews, 151, 333

Martin, S. F., Marquette, W. H., & Bilimoria, R. 1992, in Astronomical Society of the Pacific Conference Series, Vol. 27, The Solar Cycle, ed. K. L. Harvey, 53

Patsourakos, S. & Vial, J.-C. 2002, Solar Physics, 208, 253

Rust, D. M. & Kumar, A. 1994, Solar Physics, 155, 69

Rutten, R. J. 2003, Radiative Transfer in Stellar Atmospheres

Vial, J. C. 1982, Astrophysical Journal, 254, 780

Vial, J.-C. 2015, in Astrophysics and Space Science Library, Vol. 415, Astrophysics and Space Science Library, ed. J.-C. Vial & O. Engvold, 1

W. Curdt, E. Landi, & U. Feldman. 2004, A&A, 427, 1045

Wedemeyer, S., Scullion, E., Rouppe van der Voort, L., Bosnjak, A., & Antolin, P. 2013, Astrophysical Journal, 774, 123

-

Appendix A

Hydrogen Tables

A.1 Isothermal Models

The following tables show the conditions of iso-thermal prominences with and without the additional coronal radiation.

Densities are number densities given in units of cm^{-2}. Line intensites are the total intensity of the line and given in erg s^{-1} cm^{-2} Sr^{-1} while continua intensites are the intenity at the head of the continua and given in erg s^{-1} cm^{-2} Hz^{-1} Sr^{-1}.

Altitude=10000.km Temperature= 6000.K, Thickness= 200.km						
	Pressure= 0.01dyn cm^{-2}			Pressure= 1.00dyn cm^{-2}		
	With	Without	Ratio	With	Without	Ratio
Surface n_e	4.99E+09	4.83E+09	1.03	1.09E+11	1.04E+11	1.05
Central n_e	5.01E+09	4.83E+09	1.04	6.33E+10	5.91E+10	1.07
Surface n_H	6.43E+09	6.57E+09	0.98	9.97E+11	1.00E+12	0.99
Central n_H	6.42E+09	6.57E+09	0.98	1.04E+12	1.04E+12	1.00
Surface (np/nneut)	3.46E+00	2.76E+00	1.25	1.23E-01	1.15E-01	1.07
Central (np/nneut)	3.54E+00	2.76E+00	1.28	6.42E-02	5.95E-02	1.08
Surface (np/nhyd)	7.76E-01	7.34E-01	1.06	1.09E-01	1.03E-01	1.06
Central (np/nhyd)	7.80E-01	7.34E-01	1.06	6.03E-02	5.62E-02	1.07
I(Ly Continum)	4.82E+00	4.40E+00	1.09	2.12E+01	1.79E+01	1.19
τ(Ly Continuum)	1.78E-01	2.20E-01	0.81	1.19E+02	1.21E+02	0.99
τ(H)	1.03E-07	1.24E-07	0.83	4.01E-05	3.56E-05	1.12
Emergent Lyα	7.18E+03	7.29E+03	0.98	2.85E+04	2.70E+04	1.06
$\tau(Ly\alpha)$	1.93E+03	2.38E+03	0.81	1.29E+06	1.30E+06	0.99
Emergent Hα	3.53E+02	4.17E+02	0.85	9.46E+04	8.65E+04	1.09
$\tau(H\alpha)$	4.17E-03	5.03E-03	0.83	1.62E+00	1.44E+00	1.12

Altitude=10000.km Temperature= 6000.K, Thickness= 5000.km						
	Pressure= 0.01dyn cm^{-2}			Pressure= 1.00dyn cm^{-2}		
	With	Without	Ratio	With	Without	Ratio
Surface n_e	4.88E+09	4.77E+09	1.02	1.10E+11	1.04E+11	1.05
Central n_e	4.91E+09	4.75E+09	1.03	2.22E+10	2.20E+10	1.01
Surface n_H	6.53E+09	6.63E+09	0.98	9.96E+11	1.00E+12	0.99
Central n_H	6.51E+09	6.65E+09	0.98	1.08E+12	1.08E+12	1.00
Surface (np/nneut)	2.95E+00	2.54E+00	1.16	1.23E-01	1.16E-01	1.07
Central (np/nneut)	3.06E+00	2.50E+00	1.22	2.04E-02	2.02E-02	1.01
Surface (np/nhyd)	7.47E-01	7.18E-01	1.04	1.10E-01	1.04E-01	1.06
Central (np/nhyd)	7.54E-01	7.14E-01	1.06	2.00E-02	1.98E-02	1.01
I(Ly Continum)	2.53E+01	2.03E+01	1.24	2.15E+01	1.81E+01	1.19
τ(Ly Continuum)	4.99E+00	5.89E+00	0.85	3.27E+03	3.28E+03	1.00
τ(H)	3.99E-06	4.09E-06	0.97	1.43E-04	1.32E-04	1.08
Emergent Lyα	1.53E+04	1.55E+04	0.99	2.89E+04	2.72E+04	1.06
$\tau(Ly\alpha)$	5.40E+04	6.38E+04	0.85	3.54E+07	3.55E+07	1.00
Emergent Hα	1.23E+04	1.26E+04	0.98	2.12E+05	2.02E+05	1.05
$\tau(H\alpha)$	1.61E-01	1.66E-01	0.97	5.77E+00	5.34E+00	1.08

Altitude=10000.km Temperature=10000.K, Thickness= 200.km						
	Pressure= 0.01dyn cm^{-2}			Pressure= 1.00dyn cm^{-2}		
	With	Without	Ratio	With	Without	Ratio
Surface n_e	3.35E+09	3.31E+09	1.01	1.71E+11	1.69E+11	1.01
Central n_e	3.35E+09	3.31E+09	1.01	2.99E+11	2.99E+11	1.00
Surface n_H	3.54E+09	3.57E+09	0.99	5.02E+11	5.04E+11	1.00
Central n_H	3.54E+09	3.57E+09	0.99	3.86E+11	3.86E+11	1.00
Surface (np/nneut)	8.10E+00	6.64E+00	1.22	5.08E-01	4.97E-01	1.02
Central (np/nneut)	8.14E+00	6.67E+00	1.22	3.41E+00	3.40E+00	1.00
Surface (np/nhyd)	8.90E-01	8.69E-01	1.02	3.37E-01	3.32E-01	1.01
Central (np/nhyd)	8.91E-01	8.70E-01	1.02	7.73E-01	7.73E-01	1.00
I(Ly Continum)	1.01E+00	9.77E-01	1.03	3.92E+02	3.89E+02	1.01
τ(Ly Continuum)	4.86E-02	5.85E-02	0.83	1.31E+01	1.31E+01	1.00
τ(H)	2.73E-08	3.29E-08	0.83	2.25E-04	2.25E-04	1.00
Emergent Lyα	7.70E+03	7.82E+03	0.98	2.02E+05	2.01E+05	1.00
$\tau(Ly\alpha)$	4.25E+02	5.12E+02	0.83	1.14E+05	1.14E+05	1.00
Emergent Hα	1.04E+02	1.22E+02	0.85	4.26E+05	4.26E+05	1.00
$\tau(H\alpha)$	8.91E-04	1.08E-03	0.83	7.34E+00	7.34E+00	1.00

Altitude=10000.km Temperature=10000.K, Thickness= 5000.km						
	Pressure= 0.01dyn cm^{-2}			Pressure= 1.00dyn cm^{-2}		
	With	Without	Ratio	With	Without	Ratio
Surface n_e	3.33E+09	3.29E+09	1.01	1.98E+11	1.97E+11	1.01
Central n_e	3.35E+09	3.31E+09	1.01	3.34E+11	3.34E+11	1.00
Surface n_H	3.55E+09	3.59E+09	0.99	4.77E+11	4.79E+11	1.00
Central n_H	3.53E+09	3.57E+09	0.99	3.54E+11	3.54E+11	1.00
Surface (np/nneut)	7.43E+00	6.18E+00	1.20	7.03E-01	6.93E-01	1.01
Central (np/nneut)	8.31E+00	6.84E+00	1.21	1.61E+01	1.61E+01	1.00
Surface (np/nhyd)	8.81E-01	8.61E-01	1.02	4.13E-01	4.09E-01	1.01
Central (np/nhyd)	8.93E-01	8.72E-01	1.02	9.41E-01	9.41E-01	1.00
I(Ly Continum)	1.50E+01	1.33E+01	1.12	7.32E+02	7.28E+02	1.01
τ(Ly Continuum)	1.21E+00	1.44E+00	0.84	8.32E+01	8.32E+01	1.00
τ(H)	9.29E-07	1.06E-06	0.88	3.44E-03	3.44E-03	1.00
Emergent Lyα	1.19E+04	1.20E+04	0.99	1.26E+06	1.26E+06	1.00
$\tau(Ly\alpha)$	1.05E+04	1.26E+04	0.84	7.27E+05	7.27E+05	1.00
Emergent Hα	3.20E+03	3.61E+03	0.89	1.63E+06	1.63E+06	1.00
$\tau(H\alpha)$	3.04E-02	3.45E-02	0.88	1.11E+02	1.11E+02	1.00

Altitude=50000.km Temperature= 6000.K, Thickness= 200.km						
	Pressure= 0.01dyn cm^{-2}			Pressure= 1.00dyn cm^{-2}		
	With	Without	Ratio	With	Without	Ratio
Surface n_e	4.73E+09	4.53E+09	1.04	9.11E+10	8.50E+10	1.07
Central n_e	4.74E+09	4.52E+09	1.05	5.17E+10	4.80E+10	1.08
Surface n_H	6.67E+09	6.85E+09	0.97	1.01E+12	1.02E+12	0.99
Central n_H	6.66E+09	6.85E+09	0.97	1.05E+12	1.05E+12	1.00
Surface (np/nneut)	2.43E+00	1.95E+00	1.25	9.82E-02	9.04E-02	1.09
Central (np/nneut)	2.45E+00	1.93E+00	1.27	5.11E-02	4.74E-02	1.08
Surface (np/nhyd)	7.09E-01	6.61E-01	1.07	8.94E-02	8.29E-02	1.08
Central (np/nhyd)	7.10E-01	6.59E-01	1.08	4.86E-02	4.53E-02	1.07
I(Ly Continum)	4.19E+00	3.73E+00	1.12	1.34E+01	1.10E+01	1.22
τ(Ly Continuum)	1.78E-01	2.20E-01	0.81	1.19E+02	1.21E+02	0.99
τ(H)	1.03E-07	1.24E-07	0.83	4.01E-05	3.56E-05	1.12
Emergent Lyα	5.77E+03	5.85E+03	0.99	2.26E+04	2.12E+04	1.06
$\tau(Ly\alpha)$	2.62E+03	3.17E+03	0.83	1.33E+06	1.34E+06	0.99
Emergent Hα	3.05E+02	3.53E+02	0.86	6.87E+04	6.22E+04	1.11
$\tau(H\alpha)$	4.51E-03	5.32E-03	0.85	1.42E+00	1.25E+00	1.14

A.2 PCTR Models

The following tables show the conditions of prominencies with a PCTR with and without the additional coronal radiation.

Densities are number densities given in units of cm^{-2}. Line intensites are the total intensity of the line and given in erg s^{-1} cm^{-2} Sr^{-1} while continua intensites are the intenity at the head of the continua and given in erg s^{-1} cm^{-2} Hz^{-1} Sr^{-1}.

Altitude=10000.km Temperature= 6000.K, Column Mass= 4.00E-06g cm^{-2}						
	Pressure= 0.01dyn cm^{-2}			Pressure= 1.00dyn cm^{-2}		
	With	Without	Ratio	With	Without	Ratio
Surface n_e	3.78E+08	3.78E+08	1.00	3.78E+08	3.78E+08	1.00
Central n_e	4.52E+09	4.16E+09	1.09	1.75E+11	1.73E+11	1.01
Surface n_H	3.15E+08	3.15E+08	1.00	3.15E+08	3.15E+08	1.00
Central n_H	6.86E+09	7.18E+09	0.96	9.38E+11	9.39E+11	1.00
Surface (np/nneut)	5.04E+04	5.04E+04	1.00	5.50E+04	5.50E+04	1.00
Central (np/nneut)	1.92E+00	1.38E+00	1.39	2.29E-01	2.24E-01	1.02
Surface (np/nhyd)	1.00E+00	1.00E+00	1.00	1.00E+00	1.00E+00	1.00
Central (np/nhyd)	6.58E-01	5.80E-01	1.13	1.86E-01	1.83E-01	1.02
I(Ly Continum)	1.39E+01	1.07E+01	1.29	2.22E+02	2.20E+02	1.01
τ(Ly Continuum)	1.81E+00	2.22E+00	0.82	4.74E+00	4.76E+00	1.00
τ(H)	4.87E-07	5.32E-07	0.92	1.20E-05	1.20E-05	1.00
Emergent Lyα	2.97E+04	3.01E+04	0.99	5.52E+05	5.53E+05	1.00
$\tau(Ly\alpha)$	5.11E+03	6.27E+03	0.82	1.34E+04	1.35E+04	1.00
Emergent Hα	3.28E+03	3.55E+03	0.93	8.15E+04	8.12E+04	1.00
$\tau(H\alpha)$	5.14E-03	5.61E-03	0.92	1.27E-01	1.27E-01	1.00

Altitude=10000.km Temperature= 6000.K, Column Mass= 2.00E-05g cm^{-2}						
	Pressure= 0.01dyn cm^{-2}			Pressure= 1.00dyn cm^{-2}		
	With	Without	Ratio	With	Without	Ratio
Surface n_e	3.78E+08	3.78E+08	1.00	3.78E+08	3.78E+08	1.00
Central n_e	4.15E+09	3.96E+09	1.05	2.44E+11	2.43E+11	1.00
Surface n_H	3.15E+08	3.15E+08	1.00	3.15E+08	3.15E+08	1.00
Central n_H	7.19E+09	7.37E+09	0.98	8.75E+11	8.75E+11	1.00
Surface (np/nneut)	5.06E+04	5.05E+04	1.00	6.36E+04	6.35E+04	1.00
Central (np/nneut)	1.35E+00	1.16E+00	1.16	3.85E-01	3.85E-01	1.00
Surface (np/nhyd)	1.00E+00	1.00E+00	1.00	1.00E+00	1.00E+00	1.00
Central (np/nhyd)	5.75E-01	5.37E-01	1.07	2.78E-01	2.78E-01	1.00
I(Ly Continum)	1.73E+01	1.55E+01	1.12	7.52E+02	7.51E+02	1.00
τ(Ly Continuum)	1.09E+01	1.22E+01	0.90	1.97E+01	1.97E+01	1.00
τ(H)	3.20E-06	3.27E-06	0.98	1.15E-04	1.15E-04	1.00
Emergent Lyα	4.92E+04	5.00E+04	0.98	1.42E+06	1.42E+06	1.00
$\tau(Ly\alpha)$	3.09E+04	3.44E+04	0.90	5.56E+04	5.57E+04	1.00
Emergent Hα	2.09E+04	2.13E+04	0.98	6.37E+05	6.36E+05	1.00
$\tau(H\alpha)$	3.38E-02	3.45E-02	0.98	1.21E+00	1.21E+00	1.00

Altitude=10000.km Temperature=10000.K, Column Mass= 4.00E-06g cm^{-2}						
	Pressure= 0.01dyn cm^{-2}			Pressure= 1.00dyn cm^{-2}		
	With	Without	Ratio	With	Without	Ratio
Surface n_e	3.78E+08	3.78E+08	1.00	3.78E+08	3.78E+08	1.00
Central n_e	3.30E+09	3.24E+09	1.02	2.50E+11	2.49E+11	1.00
Surface n_H	3.15E+08	3.15E+08	1.00	3.15E+08	3.15E+08	1.00
Central n_H	3.58E+09	3.64E+09	0.98	4.30E+11	4.31E+11	1.00
Surface (np/nneut)	5.04E+04	5.04E+04	1.00	5.49E+04	5.49E+04	1.00
Central (np/nneut)	6.56E+00	5.05E+00	1.30	1.37E+00	1.36E+00	1.01
Surface (np/nhyd)	1.00E+00	1.00E+00	1.00	1.00E+00	1.00E+00	1.00
Central (np/nhyd)	8.68E-01	8.35E-01	1.04	5.78E-01	5.76E-01	1.00
I(Ly Continum)	9.80E+00	8.83E+00	1.11	3.43E+02	3.41E+02	1.01
τ(Ly Continuum)	7.41E-01	9.13E-01	0.81	2.18E+00	2.19E+00	0.99
τ(H)	3.11E-07	3.65E-07	0.85	1.81E-05	1.81E-05	1.00
Emergent Lyα	2.98E+04	3.02E+04	0.99	5.33E+05	5.33E+05	1.00
$\tau(Ly\alpha)$	2.10E+03	2.58E+03	0.81	6.16E+03	6.19E+03	0.99
Emergent Hα	2.10E+03	2.44E+03	0.86	1.19E+05	1.19E+05	1.00
$\tau(H\alpha)$	3.28E-03	3.85E-03	0.85	1.91E-01	1.91E-01	1.00

Altitude=10000.km Temperature=10000.K, Column Mass= 2.00E-05g cm^{-2}						
	Pressure= 0.01dyn cm^{-2}			Pressure= 1.00dyn cm^{-2}		
	With	Without	Ratio	With	Without	Ratio
Surface n_e	3.78E+08	3.78E+08	1.00	3.78E+08	3.78E+08	1.00
Central n_e	3.21E+09	3.08E+09	1.04	2.61E+11	2.61E+11	1.00
Surface n_H	3.15E+08	3.15E+08	1.00	3.15E+08	3.15E+08	1.00
Central n_H	3.66E+09	3.78E+09	0.97	4.21E+11	4.21E+11	1.00
Surface (np/nneut)	5.05E+04	5.05E+04	1.00	6.27E+04	6.26E+04	1.00
Central (np/nneut)	4.61E+00	3.14E+00	1.47	1.61E+00	1.60E+00	1.01
Surface (np/nhyd)	1.00E+00	1.00E+00	1.00	1.00E+00	1.00E+00	1.00
Central (np/nhyd)	8.22E-01	7.59E-01	1.08	6.17E-01	6.16E-01	1.00
I(Ly Continum)	1.84E+01	1.58E+01	1.16	9.18E+02	9.16E+02	1.00
τ(Ly Continuum)	4.20E+00	5.28E+00	0.80	7.98E+00	8.01E+00	1.00
τ(H)	1.99E-06	2.13E-06	0.93	1.05E-04	1.05E-04	1.00
Emergent Lyα	4.71E+04	4.77E+04	0.99	1.31E+06	1.32E+06	1.00
$\tau(Ly\alpha)$	1.19E+04	1.49E+04	0.80	2.26E+04	2.26E+04	1.00
Emergent Hα	1.31E+04	1.39E+04	0.94	6.15E+05	6.15E+05	1.00
$\tau(H\alpha)$	2.10E-02	2.25E-02	0.93	1.11E+00	1.11E+00	1.00

Altitude=50000.km Temperature= 6000.K, Column Mass= 4.00E-06g cm^{-2}						
	Pressure= 0.01dyn cm^{-2}			Pressure= 1.00dyn cm^{-2}		
	With	Without	Ratio	With	Without	Ratio
Surface n_e	3.78E+08	3.78E+08	1.00	3.78E+08	3.78E+08	1.00
Central n_e	4.13E+09	3.67E+09	1.12	1.60E+11	1.59E+11	1.01
Surface n_H	3.15E+08	3.15E+08	1.00	3.15E+08	3.15E+08	1.00
Central n_H	7.21E+09	7.63E+09	0.95	9.51E+11	9.52E+11	1.00
Surface (np/nneut)	5.00E+04	5.00E+04	1.00	5.41E+04	5.41E+04	1.00
Central (np/nneut)	1.33E+00	9.25E-01	1.44	2.03E-01	1.99E-01	1.02
Surface (np/nhyd)	1.00E+00	1.00E+00	1.00	1.00E+00	1.00E+00	1.00
Central (np/nhyd)	5.71E-01	4.81E-01	1.19	1.68E-01	1.66E-01	1.01
I(Ly Continum)	1.02E+01	7.64E+00	1.34	2.08E+02	2.07E+02	1.01
τ(Ly Continuum)	2.30E+00	2.80E+00	0.82	4.91E+00	4.93E+00	1.00
τ(H)	4.91E-07	5.35E-07	0.92	1.36E-05	1.36E-05	1.00
Emergent Lyα	2.56E+04	2.61E+04	0.98	5.95E+05	5.96E+05	1.00
$\tau(Ly\alpha)$	6.50E+03	7.91E+03	0.82	1.39E+04	1.39E+04	1.00
Emergent Hα	2.68E+03	2.88E+03	0.93	7.48E+04	7.47E+04	1.00
$\tau(H\alpha)$	5.19E-03	5.65E-03	0.92	1.44E-01	1.44E-01	1.00

Appendix B

Helium Tables

B.1 Isothermal Models

The following tables show the conditions of iso-thermal prominences with and without the additional coronal radiation.

Densities are number densities given in units of cm^{-2}. Line intensites are the total intensity of the line and given in erg s^{-1} cm^{-2} Sr^{-1} while continua intensites are the intenity at the head of the continua and given in erg s^{-1} cm^{-2} Hz^{-1} Sr^{-1}.

Altitude=10000.km Temperature= 6000.K, Thickness= 200.km						
	Pressure= 0.01dyn cm^{-2}			Pressure= 1.00dyn cm^{-2}		
	With	Without	Ratio	With	Without	Ratio
Surface HeI density	3.07E+08	3.08E+08	1.00	9.34E+10	9.83E+10	0.95
Central HeI density	3.07E+08	3.09E+08	0.99	1.04E+11	1.04E+11	0.99
Surface HeII density	3.36E+08	3.49E+08	0.96	6.24E+09	1.84E+09	3.39
Central HeII density	3.34E+08	3.48E+08	0.96	2.18E+08	4.16E+06	52.39
Surface HeIII density	2.17E+05	2.34E+05	0.93	9.55E+04	2.97E+04	3.22
Central HeIII density	2.16E+05	2.33E+05	0.93	1.69E+03	3.40E+01	49.61
Surface HeII/HeI	1.09E+00	1.13E+00	0.97	6.68E-02	1.87E-02	3.57
Central HeII/HeI	1.09E+00	1.13E+00	0.96	2.10E-03	3.99E-05	52.69
Surface HeIII/HeII	6.48E-04	6.70E-04	0.97	1.53E-05	1.61E-05	0.95
Central HeIII/HeII	6.46E-04	6.69E-04	0.97	7.74E-06	8.17E-06	0.95
I(504Å Continuum)	2.06E-20	1.96E-20	1.05	1.86E-20	1.20E-20	1.55
τ(504Å Continuum)	4.59E-02	4.61E-02	1.00	1.52E+01	1.54E+01	0.99
I(228Å Continuum)	1.04E-13	1.08E-15	96.96	1.20E-13	2.47E-16	486.32
τ(228Å Continuum)	1.06E-02	1.11E-02	0.95	2.61E-02	4.96E-03	5.26
Helium I 584Å intensity	1.24E+02	1.21E+02	1.02	1.44E+02	1.10E+02	1.30
$\tau(HeI584\mathring{A}\ )$	2.10E+02	2.11E+02	1.00	6.98E+04	7.06E+04	0.99
Helium II 304Å intensity	9.32E+02	9.33E+02	1.00	6.07E+02	4.61E+02	1.32

Altitude=10000.km Temperature= 6000.K, Thickness= 200.km						
	Pressure= 0.01dyn cm^{-2}			Pressure= 1.00dyn cm^{-2}		
	With	Without	Ratio	With	Without	Ratio
$\tau(HeII304\mathring{A}$)	1.79E+02	1.86E+02	0.96	4.39E+02	8.34E+01	5.27
Helium I 5877Å intensity	1.07E+02	1.08E+02	0.99	2.31E+03	4.43E+02	5.21
Helium I 10833Å intensity	6.21E+02	6.26E+02	0.99	1.29E+04	2.52E+03	5.11

Altitude=10000.km Temperature= 6000.K, Thickness= 5000.km						
	Pressure= 0.01dyn cm^{-2}			Pressure= 1.00dyn cm^{-2}		
	With	Without	Ratio	With	Without	Ratio
Surface HeI density	1.67E+08	4.04E+08	0.41	9.34E+10	9.83E+10	0.95
Central HeI density	2.18E+08	5.17E+08	0.42	1.08E+11	1.08E+11	1.00
Surface HeII density	4.60E+08	2.60E+08	1.77	6.20E+09	1.83E+09	3.39
Central HeII density	4.11E+08	1.47E+08	2.79	3.36E+00	3.20E+00	1.05
Surface HeIII density	2.59E+07	1.42E+05	182.46	7.39E+06	2.83E+04	261.06
Central HeIII density	2.18E+07	7.41E+04	293.94	1.49E-06	3.43E-10	4352.05
Surface HeII/HeI	2.76E+00	6.43E-01	4.29	6.64E-02	1.86E-02	3.57
Central HeII/HeI	1.88E+00	2.85E-01	6.62	3.12E-11	2.97E-11	1.05
Surface HeIII/HeII	5.64E-02	5.48E-04	102.95	1.19E-03	1.55E-05	77.03
Central HeIII/HeII	5.30E-02	5.03E-04	105.43	4.44E-07	1.07E-10	4148.28

Altitude=10000.km Temperature= 6000.K, Thickness= 5000.km						
	Pressure= 0.01dyn cm^{-2}			Pressure= 1.00dyn cm^{-2}		
	With	Without	Ratio	With	Without	Ratio
I(504Å Continuum)	2.96E-19	3.85E-20	7.69	5.16E-16	1.21E-20	42664.68
τ(504Å Continuum)	7.54E-01	1.81E+00	0.42	4.00E+02	4.01E+02	1.00
I(228Å Continuum)	2.18E-12	1.22E-14	178.03	1.09E-13	2.24E-16	484.61
τ(228Å Continuum)	3.38E-01	1.42E-01	2.38	3.14E-02	5.01E-03	6.27
Helium I 584Å intensity	1.46E+02	1.27E+02	1.15	1.44E+02	1.10E+02	1.30
$\tau(HeI584\mathring{A}$)	3.45E+03	8.30E+03	0.42	1.83E+06	1.84E+06	1.00
Helium II 304Å intensity	1.51E+03	1.05E+03	1.44	6.10E+02	4.61E+02	1.32
$\tau(HeII304\mathring{A}$)	5.68E+03	2.39E+03	2.38	5.28E+02	8.43E+01	6.27
Helium I 5877Å intensity	3.34E+03	1.37E+03	2.44	2.63E+03	4.91E+02	5.37
Helium I 10833Å intensity	1.86E+04	7.79E+03	2.39	1.45E+04	2.57E+03	5.66

Altitude=10000.km Temperature=10000.K, Thickness= 200.km						
	Pressure= 0.01dyn cm^{-2}			Pressure= 1.00dyn cm^{-2}		
	With	Without	Ratio	With	Without	Ratio
Surface HeI density	1.11E+08	1.11E+08	1.00	4.76E+10	4.97E+10	0.96
Central HeI density	1.11E+08	1.11E+08	1.00	3.84E+10	3.86E+10	1.00
Surface HeII density	2.43E+08	2.46E+08	0.99	2.63E+09	7.22E+08	3.64

Altitude=10000.km Temperature=10000.K, Thickness= 200.km						
	Pressure= 0.01dyn cm^{-2}			Pressure= 1.00dyn cm^{-2}		
	With	Without	Ratio	With	Without	Ratio
Central HeII density	2.43E+08	2.46E+08	0.99	1.83E+08	2.97E+07	6.17
Surface HeIII density	3.12E+05	3.20E+05	0.97	5.37E+04	1.49E+04	3.61
Central HeIII density	3.12E+05	3.20E+05	0.97	1.99E+03	3.23E+02	6.18
Surface HeII/HeI	2.19E+00	2.22E+00	0.99	5.53E-02	1.45E-02	3.80
Central HeII/HeI	2.19E+00	2.22E+00	0.99	4.78E-03	7.70E-04	6.20
Surface HeIII/HeII	1.29E-03	1.30E-03	0.99	2.04E-05	2.06E-05	0.99
Central HeIII/HeII	1.28E-03	1.30E-03	0.99	1.09E-05	1.09E-05	1.00
I(504Å Continuum)	9.69E-19	9.44E-19	1.03	7.70E-16	7.60E-16	1.01
τ(504Å Continuum)	1.66E-02	1.66E-02	1.00	5.83E+00	5.87E+00	0.99
I(228Å Continuum)	4.69E-14	4.70E-16	99.61	6.59E-14	1.42E-16	463.68
τ(228Å Continuum)	7.72E-03	7.83E-03	0.99	1.23E-02	2.65E-03	4.64
Helium I 584Å intensity	1.25E+02	1.25E+02	1.01	2.17E+02	1.43E+02	1.51
$\tau(HeI584\mathring{A}$)	6.57E+01	6.58E+01	1.00	2.31E+04	2.33E+04	0.99
Helium II 304Å intensity	1.02E+03	1.02E+03	1.00	7.20E+02	5.43E+02	1.33
$\tau(HeII304\mathring{A}$)	1.12E+02	1.14E+02	0.99	1.78E+02	3.85E+01	4.63
Helium I 5877Å intensity	3.69E+01	3.70E+01	1.00	9.53E+02	2.16E+02	4.41
Helium I 10833Å intensity	2.14E+02	2.14E+02	1.00	5.24E+03	1.15E+03	4.54

Altitude=10000.km Temperature=10000.K, Thickness= 5000.km						
	Pressure= 0.01dyn cm^{-2}			Pressure= 1.00dyn cm^{-2}		
	With	Without	Ratio	With	Without	Ratio
Surface HeI density	4.49E+07	1.40E+08	0.32	4.57E+10	4.73E+10	0.97
Central HeI density	4.73E+07	1.59E+08	0.30	3.54E+10	3.54E+10	1.00
Surface HeII density	2.78E+08	2.19E+08	1.27	2.09E+09	5.77E+08	3.62
Central HeII density	2.74E+08	1.98E+08	1.39	3.20E+05	3.04E+05	1.05
Surface HeIII density	3.29E+07	2.86E+05	115.05	2.46E+04	6.82E+03	3.60
Central HeIII density	3.18E+07	2.57E+05	123.76	9.80E-01	9.31E-01	1.05
Surface HeII/HeI	6.18E+00	1.56E+00	3.95	4.58E-02	1.22E-02	3.75
Central HeII/HeI	5.80E+00	1.25E+00	4.66	9.03E-06	8.58E-06	1.05
Surface HeIII/HeII	1.18E-01	1.31E-03	90.65	1.18E-05	1.18E-05	0.99
Central HeIII/HeII	1.16E-01	1.30E-03	89.26	3.07E-06	3.06E-06	1.00
I(504Å Continuum)	2.02E-17	1.60E-17	1.26	1.04E-15	1.03E-15	1.01
τ(504Å Continuum)	1.74E-01	5.71E-01	0.30	1.33E+02	1.33E+02	1.00
I(228Å Continuum)	1.06E-12	8.92E-15	118.40	4.92E-14	1.06E-16	462.41
τ(228Å Continuum)	2.19E-01	1.62E-01	1.35	1.39E-02	2.93E-03	4.74
Helium I 584Å intensity	1.58E+02	1.54E+02	1.03	2.40E+02	1.53E+02	1.57
$\tau(HeI584\mathring{A}\ )$	6.89E+02	2.27E+03	0.30	5.29E+05	5.29E+05	1.00
Helium II 304Å intensity	1.70E+03	1.34E+03	1.26	6.97E+02	5.11E+02	1.36

Altitude=10000.km Temperature=10000.K, Thickness= 5000.km						
	Pressure= 0.01dyn cm^{-2}			Pressure= 1.00dyn cm^{-2}		
	With	Without	Ratio	With	Without	Ratio
$\tau(HeII304\mathring{A}$)	3.18E+03	2.36E+03	1.35	2.03E+02	4.27E+01	4.75
Helium I 5877Å intensity	1.05E+03	7.68E+02	1.36	1.55E+03	6.17E+02	2.52
Helium I 10833Å intensity	5.99E+03	4.41E+03	1.36	6.80E+03	1.70E+03	4.01

Altitude=50000.km Temperature= 6000.K, Thickness= 200.km						
	Pressure= 0.01dyn cm^{-2}			Pressure= 1.00dyn cm^{-2}		
	With	Without	Ratio	With	Without	Ratio
Surface HeI density	3.57E+08	3.59E+08	0.99	9.55E+10	1.00E+11	0.95
Central HeI density	3.58E+08	3.60E+08	0.99	1.05E+11	1.05E+11	0.99
Surface HeII density	3.09E+08	3.25E+08	0.95	5.87E+09	1.69E+09	3.47
Central HeII density	3.08E+08	3.26E+08	0.95	2.23E+08	3.49E+06	63.87
Surface HeIII density	1.62E+05	1.79E+05	0.91	8.27E+04	2.55E+04	3.24
Central HeIII density	1.62E+05	1.79E+05	0.90	1.56E+03	2.59E+01	60.03
Surface HeII/HeI	8.64E-01	9.05E-01	0.96	6.14E-02	1.69E-02	3.64
Central HeII/HeI	8.61E-01	9.05E-01	0.95	2.13E-03	3.32E-05	64.21
Surface HeIII/HeII	5.26E-04	5.49E-04	0.96	1.41E-05	1.51E-05	0.93
Central HeIII/HeII	5.25E-04	5.50E-04	0.95	6.99E-06	7.43E-06	0.94

Altitude=50000.km Temperature= 6000.K, Thickness= 200.km						
	Pressure= 0.01dyn cm^{-2}			Pressure= 1.00dyn cm^{-2}		
	With	Without	Ratio	With	Without	Ratio
I(504Å Continuum)	1.51E-20	1.41E-20	1.07	1.17E-20	7.33E-21	1.59
τ(504Å Continuum)	5.34E-02	5.37E-02	0.99	1.54E+01	1.56E+01	0.99
I(228Å Continuum)	9.10E-14	7.72E-16	117.81	1.14E-13	1.75E-16	651.61
τ(228Å Continuum)	9.81E-03	1.04E-02	0.94	2.66E-02	4.59E-03	5.80
Helium I 584Å intensity	9.53E+01	9.34E+01	1.02	1.13E+02	8.50E+01	1.33
$\tau(HeI584\mathring{A}$)	2.45E+02	2.46E+02	0.99	7.07E+04	7.15E+04	0.99
Helium II 304Å intensity	7.07E+02	7.08E+02	1.00	4.63E+02	3.46E+02	1.34
$\tau(HeII304\mathring{A}$)	1.65E+02	1.74E+02	0.95	4.47E+02	7.71E+01	5.80
Helium I 5877Å intensity	9.78E+01	9.91E+01	0.99	1.75E+03	3.03E+02	5.75
Helium I 10833Å intensity	7.33E+02	7.42E+02	0.99	1.25E+04	2.23E+03	5.60

B.2 PCTR Models

The following tables show the conditions of prominencies with a PCTR with and without the additional coronal radiation.

Densities are number densities given in units of cm^{-2}. Line intensites are the total intensity of the line and given in erg s^{-1} cm^{-2} Sr^{-1} while continua intensites are the intenity at the head of the continua and given in erg s^{-1} cm^{-2} Hz^{-1} Sr^{-1}.

Altitude=10000.km Temperature= 6000.K, Column Mass= 4.00E-06g cm^{-2}						
	Pressure= 0.01dyn cm^{-2}			Pressure= 1.00dyn cm^{-2}		
	With	Without	Ratio	With	Without	Ratio
Surface HeI density	4.19E+01	6.14E+01	0.68	6.12E+01	6.13E+01	1.00
Central HeI density	1.61E+08	4.07E+08	0.40	9.05E+10	9.29E+10	0.97
Surface HeII density	2.80E+06	4.09E+06	0.68	4.09E+06	4.09E+06	1.00
Central HeII density	4.99E+08	3.11E+08	1.61	3.27E+09	1.08E+09	3.02
Surface HeIII density	2.87E+07	2.74E+07	1.05	2.74E+07	2.74E+07	1.00
Central HeIII density	2.56E+07	2.41E+05	106.05	6.05E+04	2.03E+04	2.98
Surface HeII/HeI	6.68E+04	6.66E+04	1.00	6.69E+04	6.68E+04	1.00
Central HeII/HeI	3.10E+00	7.62E-01	4.07	3.61E-02	1.17E-02	3.09
Surface HeIII/HeII	1.02E+01	6.69E+00	1.53	6.69E+00	6.69E+00	1.00
Central HeIII/HeII	5.12E-02	7.77E-04	65.96	1.85E-05	1.87E-05	0.99
I(504Å Continuum)	1.92E-14	2.05E-14	0.93	1.08E-12	1.14E-12	0.95
τ(504Å Continuum)	1.67E-01	4.37E-01	0.38	9.29E-01	9.65E-01	0.96
I(228Å Continuum)	1.08E-12	1.12E-14	97.19	2.31E-13	4.10E-14	5.64
τ(228Å Continuum)	1.86E-01	1.69E-01	1.10	8.39E-02	7.64E-02	1.10
Helium I 584Å intensity	2.16E+02	2.54E+02	0.85	1.27E+04	1.36E+04	0.94
$\tau(HeI584\mathring{A}$)	3.84E+02	1.00E+03	0.38	2.11E+03	2.19E+03	0.96
Helium II 304Å intensity	2.42E+03	2.51E+03	0.96	7.79E+03	7.75E+03	1.01

Altitude=10000.km Temperature= 6000.K, Column Mass= 4.00E-06g cm^{-2}						
	Pressure= 0.01dyn cm^{-2}			Pressure= 1.00dyn cm^{-2}		
	With	Without	Ratio	With	Without	Ratio
$\tau(HeII304\mathring{A}$)	1.48E+03	1.28E+03	1.16	5.60E+02	5.00E+02	1.12
Helium I 5877Å intensity	1.04E+03	6.86E+02	1.51	2.69E+03	2.25E+03	1.20
Helium I 10833Å intensity	6.04E+03	4.01E+03	1.51	1.55E+04	1.30E+04	1.19

Altitude=10000.km Temperature= 6000.K, Column Mass= 2.00E-05g cm^{-2}						
	Pressure= 0.01dyn cm^{-2}			Pressure= 1.00dyn cm^{-2}		
	With	Without	Ratio	With	Without	Ratio
Surface HeI density	4.17E+01	6.13E+01	0.68	3.98E+01	5.81E+01	0.69
Central HeI density	2.36E+08	6.31E+08	0.37	8.68E+10	8.74E+10	0.99
Surface HeII density	2.78E+06	4.08E+06	0.68	2.68E+06	3.91E+06	0.69
Central HeII density	4.62E+08	1.05E+08	4.39	6.36E+08	1.73E+08	3.67
Surface HeIII density	2.87E+07	2.74E+07	1.05	2.88E+07	2.75E+07	1.04
Central HeIII density	2.12E+07	6.93E+04	306.41	5.38E+05	9.65E+03	55.71
Surface HeII/HeI	6.68E+04	6.66E+04	1.00	6.74E+04	6.73E+04	1.00
Central HeII/HeI	1.95E+00	1.67E-01	11.72	7.33E-03	1.99E-03	3.69
Surface HeIII/HeII	1.03E+01	6.71E+00	1.54	1.07E+01	7.04E+00	1.52
Central HeIII/HeII	4.60E-02	6.58E-04	69.87	8.45E-04	5.56E-05	15.19

Altitude=10000.km Temperature= 6000.K, Column Mass= 2.00E-05g cm^{-2}						
	Pressure= 0.01dyn cm^{-2}			Pressure= 1.00dyn cm^{-2}		
	With	Without	Ratio	With	Without	Ratio
I(504Å Continuum)	1.38E-12	7.84E-14	17.65	5.78E-12	4.58E-12	1.26
τ(504Å Continuum)	1.11E+00	3.17E+00	0.35	4.64E+00	4.74E+00	0.98
I(228Å Continuum)	2.07E-12	2.89E-14	71.56	6.02E-13	1.88E-13	3.21
τ(228Å Continuum)	8.79E-01	6.36E-01	1.38	4.02E-01	3.94E-01	1.02
Helium I 584Å intensity	3.39E+02	5.93E+02	0.57	5.95E+04	6.30E+04	0.94
$\tau(HeI584\mathring{A}$)	2.56E+03	7.29E+03	0.35	1.06E+04	1.08E+04	0.98
Helium II 304Å intensity	3.51E+03	4.16E+03	0.84	2.37E+04	2.47E+04	0.96
$\tau(HeII304\mathring{A}$)	6.99E+03	4.62E+03	1.51	2.67E+03	2.58E+03	1.03
Helium I 5877Å intensity	4.53E+03	1.88E+03	2.41	1.15E+04	1.07E+04	1.08
Helium I 10833Å intensity	2.58E+04	1.10E+04	2.36	6.37E+04	5.96E+04	1.07

Altitude=10000.km Temperature=10000.K, Column Mass= 4.00E-06g cm^{-2}						
	Pressure= 0.01dyn cm^{-2}			Pressure= 1.00dyn cm^{-2}		
	With	Without	Ratio	With	Without	Ratio
Surface HeI density	4.17E+01	6.14E+01	0.68	6.12E+01	6.13E+01	1.00
Central HeI density	4.39E+07	1.39E+08	0.32	4.14E+10	4.26E+10	0.97
Surface HeII density	2.78E+06	4.09E+06	0.68	4.09E+06	4.09E+06	1.00

Altitude=10000.km Temperature=10000.K, Column Mass= 4.00E-06g cm^{-2}						
	Pressure= 0.01dyn cm^{-2}			Pressure= 1.00dyn cm^{-2}		
	With	Without	Ratio	With	Without	Ratio
Central HeII density	2.86E+08	2.24E+08	1.28	1.64E+09	5.59E+08	2.94
Surface HeIII density	2.87E+07	2.74E+07	1.05	2.74E+07	2.74E+07	1.00
Central HeIII density	2.74E+07	2.82E+05	97.29	2.82E+04	9.63E+03	2.93
Surface HeII/HeI	6.68E+04	6.66E+04	1.00	6.69E+04	6.67E+04	1.00
Central HeII/HeI	6.52E+00	1.61E+00	4.04	3.96E-02	1.31E-02	3.02
Surface HeIII/HeII	1.03E+01	6.69E+00	1.54	6.69E+00	6.69E+00	1.00
Central HeIII/HeII	9.57E-02	1.26E-03	76.19	1.72E-05	1.72E-05	1.00
I(504Å Continuum)	1.78E-14	1.88E-14	0.95	9.35E-13	9.64E-13	0.97
τ(504Å Continuum)	8.97E-02	2.88E-01	0.31	8.41E-01	8.76E-01	0.96
I(228Å Continuum)	7.76E-13	1.05E-14	74.11	2.39E-13	4.65E-14	5.14
τ(228Å Continuum)	1.89E-01	1.97E-01	0.96	9.49E-02	8.75E-02	1.08
Helium I 584Å intensity	2.23E+02	2.59E+02	0.86	1.07E+04	1.11E+04	0.96
$\tau(HeI584\mathring{A}$)	1.98E+02	6.37E+02	0.31	1.85E+03	1.92E+03	0.96
Helium II 304Å intensity	2.56E+03	2.63E+03	0.97	8.34E+03	8.30E+03	1.01
$\tau(HeII304\mathring{A}$)	1.46E+03	1.46E+03	1.00	6.32E+02	5.73E+02	1.10
Helium I 5877Å intensity	6.09E+02	5.37E+02	1.13	2.92E+03	2.64E+03	1.11
Helium I 10833Å intensity	3.57E+03	3.15E+03	1.13	1.68E+04	1.53E+04	1.10

Altitude=10000.km Temperature=10000.K, Column Mass= 2.00E-05g cm^{-2}						
	Pressure= 0.01dyn cm^{-2}			Pressure= 1.00dyn cm^{-2}		
	With	Without	Ratio	With	Without	Ratio
Surface HeI density	4.13E+01	6.12E+01	0.67	3.89E+01	5.78E+01	0.67
Central HeI density	6.41E+07	2.50E+08	0.26	4.14E+10	4.19E+10	0.99
Surface HeII density	2.76E+06	4.08E+06	0.68	2.61E+06	3.88E+06	0.67
Central HeII density	2.78E+08	1.28E+08	2.17	6.74E+08	2.30E+08	2.93
Surface HeIII density	2.87E+07	2.74E+07	1.05	2.88E+07	2.76E+07	1.05
Central HeIII density	2.37E+07	1.54E+05	153.62	8.44E+05	2.34E+04	36.16
Surface HeII/HeI	6.68E+04	6.66E+04	1.00	6.73E+04	6.72E+04	1.00
Central HeII/HeI	4.34E+00	5.13E-01	8.46	1.63E-02	5.49E-03	2.97
Surface HeIII/HeII	1.04E+01	6.71E+00	1.55	1.10E+01	7.11E+00	1.55
Central HeIII/HeII	8.52E-02	1.20E-03	70.72	1.25E-03	1.02E-04	12.32
I(504Å Continuum)	6.43E-14	6.34E-14	1.01	4.58E-12	3.68E-12	1.25
τ(504Å Continuum)	6.02E-01	2.31E+00	0.26	4.22E+00	4.32E+00	0.98
I(228Å Continuum)	1.70E-12	3.16E-14	54.00	7.43E-13	2.31E-13	3.22
τ(228Å Continuum)	9.23E-01	7.98E-01	1.16	4.53E-01	4.45E-01	1.02
Helium I 584Å intensity	3.30E+02	5.20E+02	0.63	4.85E+04	5.04E+04	0.96
$\tau(HeI584\mathring{A}$)	1.33E+03	5.11E+03	0.26	9.28E+03	9.52E+03	0.98
Helium II 304Å intensity	3.76E+03	4.43E+03	0.85	2.78E+04	2.90E+04	0.96

Altitude=10000.km Temperature=10000.K, Column Mass= 2.00E-05g cm^{-2}						
	Pressure= 0.01dyn cm^{-2}			Pressure= 1.00dyn cm^{-2}		
	With	Without	Ratio	With	Without	Ratio
$\tau(HeII304\mathring{A}$)	7.14E+03	5.81E+03	1.23	3.02E+03	2.92E+03	1.03
Helium I 5877Å intensity	2.92E+03	1.92E+03	1.52	1.35E+04	1.28E+04	1.05
Helium I 10833Å intensity	1.69E+04	1.12E+04	1.51	7.40E+04	7.06E+04	1.05

Altitude=50000.km Temperature= 6000.K, Column Mass= 4.00E-06g cm^{-2}						
	Pressure= 0.01dyn cm^{-2}			Pressure= 1.00dyn cm^{-2}		
	With	Without	Ratio	With	Without	Ratio
Surface HeI density	4.44E+01	6.38E+01	0.70	6.36E+01	6.37E+01	1.00
Central HeI density	1.86E+08	4.74E+08	0.39	9.22E+10	9.43E+10	0.98
Surface HeII density	2.86E+06	4.10E+06	0.70	4.10E+06	4.10E+06	1.00
Central HeII density	5.09E+08	2.88E+08	1.77	2.88E+09	9.30E+08	3.10
Surface HeIII density	2.86E+07	2.74E+07	1.05	2.74E+07	2.74E+07	1.00
Central HeIII density	2.67E+07	1.95E+05	136.81	4.47E+04	1.46E+04	3.07
Surface HeII/HeI	6.44E+04	6.42E+04	1.00	6.45E+04	6.44E+04	1.00
Central HeII/HeI	2.74E+00	6.07E-01	4.50	3.13E-02	9.86E-03	3.17
Surface HeIII/HeII	1.00E+01	6.68E+00	1.50	6.68E+00	6.68E+00	1.00
Central HeIII/HeII	5.25E-02	6.77E-04	77.47	1.55E-05	1.57E-05	0.99

Altitude=50000.km Temperature= 6000.K, Column Mass= 4.00E-06g cm^{-2}						
	Pressure= 0.01dyn cm^{-2}			Pressure= 1.00dyn cm^{-2}		
	With	Without	Ratio	With	Without	Ratio
I(504Å Continuum)	1.92E-14	2.13E-14	0.90	1.03E-12	1.08E-12	0.96
τ(504Å Continuum)	1.87E-01	4.94E-01	0.38	9.45E-01	9.76E-01	0.97
I(228Å Continuum)	9.99E-13	8.76E-15	113.95	2.09E-13	4.06E-14	5.14
τ(228Å Continuum)	1.83E-01	1.58E-01	1.16	8.08E-02	7.42E-02	1.09
Helium I 584Å intensity	1.77E+02	2.23E+02	0.79	1.47E+04	1.55E+04	0.95
$\tau(HeI584\mathring{A}$)	4.31E+02	1.13E+03	0.38	2.14E+03	2.21E+03	0.97
Helium II 304Å intensity	1.91E+03	2.01E+03	0.95	7.29E+03	7.25E+03	1.01
$\tau(HeII304\mathring{A}$)	1.46E+03	1.18E+03	1.23	5.36E+02	4.83E+02	1.11
Helium I 5877Å intensity	9.93E+02	5.98E+02	1.66	2.07E+03	1.79E+03	1.16
Helium I 10833Å intensity	7.47E+03	4.53E+03	1.65	1.53E+04	1.33E+04	1.15